Modélisation de la morphologie et de la distribution des nœuds à l'intérieur des tiges d'espèces résineuses

Thèse

Emmanuel Duchateau

Doctorat en Sciences forestières
Philosophiae Doctor (Ph.D.)

Québec, Canada

Résumé

La présence de nœuds à l'intérieur de la tige est une des caractéristiques internes ayant le plus d'impact sur les propriétés mécaniques du bois. Il existe une grande quantité de modèles décrivant l'impact de la croissance et des stratégies sylvicoles sur le développement des branches et quelques modèles décrivant la géométrie des nœuds. Cependant la difficulté à obtenir des données internes précises explique que très peu d'études se sont intéressées à modéliser les relations entre les caractéristiques morphologiques des nœuds et les caractéristiques externes des branches et de l'arbre. La présente recherche a pour objectif principal d'améliorer nos connaissances de la nature des nœuds (fréquence, répartition, forme et taille) de manière à les intégrer dans des modèles de croissances des arbres.

Dans un premier volet, nous avons mis au point un modèle statique de la géométrie des nœuds utilisant seulement 5 paramètres à partir d'une combinaison de deux équations non linéaires. La grande flexibilité de ces équations nous a permis de décrire des nœuds de morphologies très variables. Les paramètres obtenus ont ensuite été exprimés en fonction de caractéristiques externes facilement mesurables, afin d'être intégrables dans un modèle de croissance. Dans un second volet, nous avons analysé le ratio d'allocation de matière entre les nœuds et la tige au cours du développement de l'arbre, puis élaboré un modèle linéaire mixte qui se veut dynamique dans le temps. Ce dernier décrit l'évolution de la morphologie d'un nœud en fonction de la croissance secondaire de la tige. Finalement, par une méthode empirique basée sur deux filtres successifs tenant compte du diamètre des branches et de leur espacement, nous avons pu améliorer le positionnement des unités de croissance le long de tiges d'épinette. Cette délimitation nous a permis de modéliser le nombre de branches dans les unités de croissance ainsi que leurs positions autour et au long du tronc. L'intégration de ces modèles de nœuds couplés à une distribution plus réaliste des nœuds dans le tronc permettra de développer un simulateur de la croissance des arbres capable de représenter la morphogénèse des nœuds à l'intérieur de la tige.

Abstract

The presence of knots is one of the internal characteristics with the greatest impact on the mechanical properties of wood. Several models describe the impact of tree growth and of silvicultural strategies on the development of branches but fewer models describe the geometry of knots. However, the difficulties to obtain accurate internal data may explain that very few studies have focused on modelling the relationship between the knot morphology and tree and branch characteristics. The main objective of this study was to improve our knowledge of knottiness (frequency, distribution, shape and size) for integration into existing growth models.

In a first stage, we developed a static model of knot geometry using only 5 parameters from a combination of two nonlinear equations. The flexibility of these equations allowed us to describe a wide range of knot types. The parameters obtained were then modelled as functions of measurable tree and branch characteristics, to facilitate the integration into a growth model. In a second stage, we analysed the ratio of knot to stem allocation over the tree development, and then developed a mixed effect model that was dynamic in time. The latter describes the evolution of knot morphology as a function of the stem's secondary growth. Finally, through an empirical method based on two successive filters and using the branches diameter and the distance between them, we were able to improve the positioning of the growth units along black spruce stems. This allowed us to model the number of branches within growth units and their positions along and around the stem. The integration of these knot models coupled to a more realistic distribution of the knots along the trunk will allow the development of a tree growth simulator capable to represent the knot morphogenesis inside the stem.

Table des matières

Listes des tableaux

Listes des figures

Remerciements

Ce projet de recherche a été financé par le conseil de recherches en sciences naturelles et en génie du Canada (CRSNG) et s'intègre dans le réseau stratégique Forêt Valeur. Je tiens à remercier cet organisme pour sa confiance et son appui.

J'aimerais remercier mon directeur Alexis Achim pour m'avoir donné la chance de travailler sur ce projet, m'avoir guidé et avec qui ce fut un plaisir de travailler au cours de ces années. Merci à Chhun Huor Ung et David Auty pour leur aide et leurs conseils tout au long de ce projet. Je tiens également à remercier David Pothier, Alain Cloutier et Aaron Weiskittel pour avoir accepté d'agir en tant que membres du jury.

Mes remerciements s'étendent à toutes les personnes m'ayant assisté lors de la prise de données sur le terrain ainsi qu'à celles ayant participé de près ou de loin aux traitements et à l'analyse des nombreuses données issues du tomographe à rayons-X; Amélie Denoncourt, Fabien Lanteigne, Louis Gauthier, Vanessa Joly, Alice Bernier-Banville, Caroline Hamelin et Eugénie Arsenault.

J'ai eu la chance d'effectuer plusieurs voyages durant ce projet. J'aimerais notamment remercier le laboratoire du LERFoB de l'INRA de Nancy en France pour m'avoir accueilli à deux reprises. Merci particulièrement à Frédéric Mothe et Fleur Longuetaud pour leur accueil. Avec vous j'ai pu développer une collaboration très efficace qui a débouché sur la rédaction de deux articles scientifiques. Vos conseils et vos expertises dans l'analyse des images du tomographe à rayons X ont été des éléments déterminants ayant fait avancer le projet de manière significative. Merci également à Frank Berninger et Anniki Mäkelä pour m'avoir accueilli à l'Université d'Helsinki, à Thierry Fourcaud pour m'avoir accueilli au CIRAD de Montpellier, ainsi qu'à Aaron Weiskittel pour m'avoir reçu à l'Université du Maine. Ces différents séjours m'ont permis de me former aux différentes analyses que j'ai utilisées dans mon projet et m'ont également permis de rencontrer et de discuter avec des chercheurs de différents milieux.

Merci à tous mes collègues de bureau, notamment Sébastien Lavoie, Kaysandra Waldron, Filip Havreljuk et Juliette Boiffin pour tous les bons moments passés en votre compagnie qui ont grandement contribué à rendre cette aventure très agréable. Et finalement, merci à

Paméla pour tous ces bons moments à deux ainsi qu'à ma famille qui, malgré la distance, m'a toujours soutenu et appuyé dans mon projet.

Avant-Propos

Ce document est présenté sous la forme d'une thèse par article. Celle-ci a été conçue selon les critères de présentation adoptés par le comité de programme de 2e et 3e cycle en sciences forestières de l'Université Laval. Les articles suivants, rédigés en langue anglaise, sont inclus dans cet ouvrage.

Chapitre 1*:* E. Duchateau, F. Longuetaud, F. Mothe, C. Ung, D. Auty, and A. Achim (2013) *Modelling knot morphology as a function of external tree and branch attributes*. Can. J. For. Res. 43: 1–12

Chapitre 2: E. Duchateau, D. Auty, F. Mothe, F. Longuetaud, C. Ung and A. Achim (2013) *Modelling knot morphogenesis in trees*. Sur le point d'être soumis à Annals of Botany.

Chapitre 3: E. Duchateau E, Auty D, Mothe F, Achim A (2013) *Improving branch distribution models in trees using X-ray computed tomogrpahy*.

Une partie des résultats du chapitre 3 a été publié dans les travaux de la 7ème conférence sur les modèles structure-fonction des plantes en Finlande (Cf. Annexe). Le reste des résultats sera soumis sous peu pour fin de publication dans la revue scientifique PeerJ.

En tant que candidat au doctorat et premier auteur de ces articles, j'ai effectué la revue de littérature sur le sujet de recherche, la planification du travail, l'analyse des images à rayons-X, l'analyse statistique des données ainsi que la rédaction des différentes publications. Les professeurs Alexis Achim et Chhun Huor Ung, respectivement directeur et co-directeur de ce projet de doctorat et co-auteurs des articles, m'ont conseillé judicieusement durant tout mon cheminement et ont corrigé les articles scientifiques. Fleur Longuetaud, Fédéric Mothe et David Auty ont aussi contribué significativement à l'élaboration des modèles et à la révision des textes.

Il est à noter que les résultats exposés dans ces chapitres ont été présentés lors des congrès suivants :

- Duchateau, E., Ung, C., Achim, A. *Modeling the branch and knot characteristics of black spruce and jack pine*. University of Maine. Orono, USA. Septembre 2009.

- Duchateau, E., Ung, C., Achim, A. *Modélisation des caractéristiques des branches d'épinette noire et de pin gris*. Chaire de sylviculture. Baie-Comeau, Canada. Avril 2010.

- Duchateau, E., Mothe, F., Ung, C., Achim, A. *Modeling the branch and knot characteristics of black spruce and jack pine*. Annual ForValueNet Meeting. Vancouver, Canada. Juin 2010.

- Duchateau, E., Mothe, F., Ung, C., Achim, A. *Modeling the branch and knot characteristics of black spruce and jack pine.* ECANUSA conference. Edmundston, Canada. Octobre 2010.

- Duchateau, E., Ung, C., Achim, A. *Modélisation des caractéristiques des branches d'épinette noire et de pin gris.* Centre INRA - LERFoB. Nancy, France. Decembre 2010.

- Duchateau, E., Mothe, F., Ung, C., Achim, A. *Modeling the branch and knot characteristics of black spruce and jack pine.* University of Helsinki. Helsinki, Finland. Janvier 2011.

- Duchateau, E., Mothe, F., Ung, C., Achim, A. *Modeling the branch and knot characteristics of black spruce and jack pine*. Annual ForValueNet Meeting. Edmonton, Canada. Juin 2011.

- Duchateau, E., Mothe, F., Longuetaud, F., Ung, C., Auty, D., Achim, A. *Modélisation des caractéristiques des branches et de leurs effets sur la qualité du bois d'épinette noire et de pin gris.* CIRAD – UMR AMAP. Montpellier, France. Decembre 2011.

- Duchateau, E., Mothe, F., Longuetaud, F., Ung, C., Achim, A. *Modeling the branch and knot characteristics of black spruce and jack pine*. Division 5 IUFRO Conference. Estoril, Portugal. Juillet 2012.

Ces travaux ont également été présentés sous forme d'affiches scientifiques lors des congrès suivants:

- Duchateau, E., Ung, C., Achim, A. *Modélisation des caractéristiques des branches et de leurs effets sur la qualité du bois d'épinette noire et de pin gris*. Conférence du centre de recherche sur le bois (CRB-université Laval) (Poster). Québec, Canada. October 2009.

- Duchateau, E., Mothe, F., Longuetaud, F., Ung, C., Auty, D., Achim, A. *Knot morphology and distribution in black spruce.* Annual ForValueNet Meeting (Poster). Montréal, Canada. November 2012.

- Duchateau, E., Mothe, F., Longuetaud, F., Ung, C., Auty, D., Achim, A. *Modelling knot morphology as a function of external tree and branch attributes.* FIBRE meeting (Poster). Cornwall, Canada. May 2013.

Introduction

Le secteur forestier québécois a traversé une période difficile au cours de ces dernières années. D'une part, le ralentissement de l'économie américaine qui a directement affecté l'économie canadienne et les industries du bois; d'autre part, les calculs de la possibilité annuelle de coupe à rendement soutenu pour la période 2008-2013 qui ont été annoncés par le Forestier en Chef et revus à la baisse. À l'échelle provinciale, cette refonte du calcul de la possibilité forestière a entrainé une diminution de 22 % par rapport à la période 2000-2008 (Bureau du Forestier en chef 2006). Par conséquent, cela a entrainé aussi une réduction des attributions de volume en provenance de la forêt publique à l'industrie qui ne peut opérer à pleine capacité.

Historiquement, la stratégie provinciale pour faire face à cette situation a notamment visé une réduction des coûts d'opération des scieries afin qu'elles restent compétitives (Ministère des ressources naturelles 1996) et une augmentation de la production forestière. Cette intensification est susceptible d'entrainer une baisse de la qualité des productions futures (Bruchert et al. 2000; Hein et al. 2007).

Cette situation porte donc à s'interroger sur les pratiques sylvicoles actuelles et sur la nécessité d'avoir à disposition des modèles de croissance adaptés, couplés à des modèles de qualité du bois, de manière à constituer un outil intéressant pour étudier l'impact de différents scénarios sylvicoles sur la productivité et la qualité. La poursuite des recherches en sylviculture et l'amélioration des modèles actuels s'avèrent donc essentielles.

Il serait notamment intéressant d'intensifier certaines pratiques de manière à accélérer la croissance des arbres, ce qui permettrait d'obtenir des révolutions de coupes plus courtes. Or, de telles pratiques sylvicoles peuvent influencer significativement la fréquence, la taille et l'angle des branches et donc la qualité du bois. En effet, l'utilisation de techniques sylvicoles qui augmentent la croissance et la productivité provoque en contrepartie une augmentation de la taille des branches (Perstorper et al. 1995; Väisänen et al. 1989). Celle-ci entraine alors directement une augmentation de la taille des nœuds qui peut entrainer une diminution de la qualité des bois (Jäghagen and Albrektson 1996; Makela et al. 2000; Mäkelä et al. 1997; Väisänen et al. 1989).

Le concept de qualité du bois est lié à la productivité forestière, et une bonne connaissance des facteurs influençant cette qualité permet d'orienter la sylviculture. Les propriétés mécaniques du bois qui sont importantes pour l'utilisation du bois comme élément de structure sont les propriétés élastiques, qui indiquent la rigidité, et les propriétés de résistance, qui reflètent la capacité portante du bois. Les propriétés élastiques sont exprimées généralement par le module d'élasticité (MOE). Plus un bois aura un MOE élevé, plus il sera rigide et aura une petite déformation sur la charge. Les propriétés de résistance mécanique sont exprimées généralement par le module de rupture (MOR) qui représente la charge maximale qu'une poutre peut supporter avant la rupture (Zink-Sharp 2003). Il existe de nombreux facteurs qui peuvent affecter ces propriétés mécaniques. Parmi les plus importants, on compte la densité du bois, les nœuds et le bois juvénile. Ces trois facteurs ont été très étudiés et peuvent être chacun influencés par les pratiques sylvicoles.

La densité du bois est la caractéristique qui a l'impact le plus significatif sur les propriétés mécaniques (Zink-Sharp 2003). Cette propriété est en corrélation étroite avec les propriétés de résistance du bois, ainsi qu'avec les caractéristiques d'usinage, de collage et de finition. Il s'agit en fait d'une propriété complexe qui dépend d'un grand nombre de variables anatomiques (Nylinder 1965).

Le bois ayant un pourcentage important de bois juvénile présente de faibles propriétés mécaniques (Shi et al. 2005; Zobel and Van Buijtenen 1989; Zobel and Sprague 1998). Il est également caractérisé par un angle élevé des microfibrilles qui engendre une faible stabilité dimensionnelle et, ainsi, pose beaucoup de problèmes à son utilisation comme élément de structure ou à la fabrication des panneaux (Bao et al. 2001).

Les nœuds ont également un impact négatif sur la qualité du bois (Bowyer et al. 2007; Jozsa and Middleton 1994; Zhang et al. 1998). Ils affectent les propriétés mécaniques du bois parce qu'ils provoquent la discontinuité et la déviation du fil (Dinwoodie 2000). Cela crée donc des zones de faiblesse où sont concentrés les contraintes mécaniques (Bodig and Jayne 1982), ce qui provoque des pertes de résistance pouvant aller jusqu'à 80 % (American Society for Testing and Materials 1992). Les dimensions critiques des nœuds varie avec la dimension de la pièce et avec la position du nœud dans la section de la pièce (Zhang et al. 1998). La grosseur des nœuds est donc un facteur qui affecte grandement la

résistance mécanique du bois (Tustin and Wilcox 1978), diminue le classement des poutres de structure (Middleton et al. 1996) et des bois de menuiserie (Pellicane et al. 1987) et, par conséquent, la valeur des produits de sciage (Zhang and Chauret 2001). Les nœuds affectent aussi négativement d'autres propriétés du bois comme les qualités esthétiques et l'usinabilité.

Actuellement, en Amérique du nord, les méthodes de classification visuelle du bois d'œuvre sont fortement utilisées. Ces méthodes sont basées sur la localisation et la dimension des défauts dans la pièce. La fréquence, la taille et la distribution des nœuds sont parmi les paramètres les plus importants à être considérés lors d'évaluations visuelles. Pour le pin gris (*Pinus banksiana* Lamb.), si l'on ne tient pas compte des dommages provoqués lors des opérations de sciage, les nœuds sont responsables d'environ 90 % des défauts (Zhang et al. 2006).

Les nœuds sont l'attachement interne des branches au tronc (Lemieux et al. 2001). Ils sont donc directement liés à la branchaison et, à fortiori, aux conditions de croissance de l'arbre, puisqu'ils sont affectés par la taille et l'angle des branches (Fisher and Honda 1979). Il est donc fondamental de connaitre le développement des branches pour connaitre la qualité des bois (Persson 1976) et prédire l'impact de la sylviculture sur les nœuds.

Les arbres sont soumis à de fortes compétitions pour l'accès à la lumière et aux ressources nutritives. Dès leur jeune âge, ils sont en concurrence avec des espèces annuelles souvent très compétitrices, puis avec des arbustes et d'autres arbres. Pour accéder à ces ressources, l'arbre doit développer son tronc et son houppier; la structure de la branchaison a donc une importance première pour les fonctions physiologiques (Fisher and Honda 1979; Horn 1971). Les dimensions du houppier sont considérées comme de bons indicateurs de la vigueur de l'arbre et de la capacité photosynthétique de celui-ci, et donc de la qualité du bois produit (Bravo et al. 2001). Ces dimensions sont en grande partie conditionnées par le besoin d'accéder aux ressources lumineuses ainsi que par la compétition avec les arbres voisins et entre les branches d'un même arbre (Franco 1986; Rouvinen and Kuuluvainen 1997). L'architecture du houppier est donc l'expression d'un équilibre entre les processus endogènes propre à l'espèce et les contraintes exercées par l'environnement (Barthelemy and Caraglio 2007). Les branches sous le houppier ont été affectées par les conditions de

croissance passées, alors que celles dans le houppier ont un fort lien avec aux conditions actuelles (Colin and Houllier 1991; Moberg 2000). Le diamètre des branches, leur angle d'insertion, leur statut (vivant, mort), leur fréquence et leur orientation autour et le long du tronc sont autant de paramètres caractérisant la branchaison.

D'un point de vue biologique, l'agencement des branches et de leurs ramifications via l'étude de la phyllotaxie est étudié depuis de très nombreuses années (Jean 1994). Pont (2001) a étudié l'agencement des branches de Pin de Monterey (*Pinus radiata)* dans le but de faire apparaitre une séquence ontogénique de formation. De nombreuses études portant notamment sur les arbres tropicaux se sont intéressées aux ramifications des branches et aux structures adoptées pour optimiser l'accès à la lumière et limiter la compétition entre les branches (Barthelemy and Caraglio 2007). La ramification des branches d'épinette noire a également été étudiée par Bégin et Filion (1999) et par Laberge et al. (2001). On constate souvent une certaine régularité dans les structures du monde végétal et parfois animal. De nombreuses études ont d'ailleurs montré que ces structures possèdent des propriétés mathématiques bien connues (Séquence de Fibonacci, Nombre d'Or…) (Bailly 2004; Boissiere 2003; Couder and Douady 2000; Pont 2001).

D'un point de vue forestier, si on souhaite améliorer la qualité des bois produits, il convient de comprendre les mécanismes ayant une influence sur le développement de l'arbre et de la branchaison et de décrire les schémas de développements existants. Ainsi, en faisant varier l'espacement lors de la plantation ou lors d'éclaircie on a une influence directe sur le développement du houppier. On permet aux arbres d'accéder à plus de lumière, favorisant ainsi leur développement dans le but de produire un bois de meilleure qualité (Grace et al. 1999; Hein 2008; Weiskittel et al. 2007; Zhang et al. 2006). Cependant, en accélérant la croissance et la productivité, on peut provoquer en parallèle une augmentation de la taille des branches (Väisänen et al. 1989). Le diamètre des branches augmente avec l'augmentation de la longueur de la couronne et, par le même fait, de l'âge des branches (Mäkinen 1996). En maintenant une densité élevée des peuplements, on peut donc limiter l'augmentation de la fréquence et de la taille des branches (Zhang and Chauret 2001). On a également une forte corrélation positive entre le diamètre à 1,30 m (DHP) et la taille des branches (Colin and Houllier 1991; Maguire 1994; Persson 1976). Le diamètre des branches augmente avec le DHP, qui lui augmente avec l'intensité des

éclaircies. Des études ont montré cette relation chez l'épinette noire (Zhang and Chauret 2001), l'épinette de Norvège (*Picea abies*) (Johansson 1993) et le pin gris (Buckman 1964). De même, l'inclinaison des branches augmente avec l'augmentation du diamètre des branches et est affectée par la compétition avec les arbres voisins qui augmente les contacts entre branches (Deleuze et al. 1996). Il s'avère donc essentiel d'avoir des modèles précis pour prédire l'impact de décisions sylvicoles sur la branchaison et améliorer les pratiques actuelles. La compréhension des règles de développement de l'évolution de la branchaison permet de modéliser le développement de l'arbre et de prédire d'éventuels effets de pratiques sylvicoles sur celui-ci (Peltola et al. 2002; Zhang et al. 2006).

L'étude du développement des branches, notamment celles de 1er ordre directement attachées au tronc, se fait de deux façons, soit par la distribution verticale le long de l'arbre et la distribution horizontale (circulaire) autour du tronc (Pont 2001). De nombreuses approches ont été mises au point pour prédire la distribution verticale. Il existe des modèles linéaires simples (Doruska and Burkhart 1994; Drolet et al. 1972; Lejeune 2004; Maguire et al. 1994; Maguire et al. 1991), des modèles polynomiaux plus complexes (Björklund 1997; Colin and Houllier 1991; Maguire et al. 1999; Maguire 1994), des modèles non linéaires (Benjamin et al. 2007; Mäkinen and Colin 1999), et des modèles mixtes non linéaires (Garber and Maguire 2005; Garber and Maguire 2003). La distribution circulaire, en revanche, a été beaucoup moins étudiée. Il existe donc peu de modèles visant à prédire l'azimut des branches. Pourtant, il s'agit d'un paramètre important pour la simulation de la qualité du bois, puisqu'il détermine en partie la possibilité d'optimiser le débitage en fonction des caractéristiques internes de la tige (Lemieux et al. 2000; Tong et al. 2013). De nombreuses études considèrent que la répartition est uniforme autour du tronc (Cochrane and Ford 1978). Doruska et Burkhart (1994) ont également montré, à l'aide de statistiques circulaires que les branches du pin à encens (*Pinus taeda* L.) sont uniformément distribuées. Grace et al. (1999), en revanche, ont montré qu'en tenant compte du diamètre des branches, la répartition n'est plus uniforme et que les plus grosses branches se situent dans la direction nord. Lemieux et al. (2001) indiquent également que pour l'épinette noire, la répartition en fréquence et en diamètre des branches n'est pas uniforme. Ces résultats sont appuyés par Benjamin et al. (2009) qui ont pu démontrer cette tendance à l'aide de statistiques circulaires. La principale raison à ce manque

d'information plus précise sur la répartition circulaire des branches provient de la difficulté à obtenir une mesure précise de l'azimut. Ces modèles nécessitent des mesures précises des angles des branches, or les mesures externes généralement utilisées sont souvent imprécises (Duchateau et al. 2013c).

En parallèle à l'étude de la branchaison, de nombreuses recherches portent directement sur la modélisation des nœuds. De la même manière que l'étude de la branchaison, l'étude des nœuds se fait sur plusieurs points : d'une part, la géométrie même du nœud et, d'autre part, la répartition de ces nœuds le long du tronc. Les nœuds ont normalement leur origine sur la moelle de l'arbre et leur diamètre augmente progressivement avec la distance radiale. La collecte des données internes permet de décrire la forme d'un nœud et de modéliser cette géométrie. Cette approche a subi des améliorations successives. Le modèle initial représentait le nœud comme un cône à axe droit perpendiculaire à la moelle (Richards et al. 1979). Cependant, comme le modèle ne correspondant pas à la réalité, un angle d'inclinaison fut ajouté. Le nœud est toujours représenté par un cône, mais le modèle utilise l'angle d'inclinaison de la branche pour décrire celui du nœud (Leban and Duchanois 1990; Samson 1993a).
L'axe du nœud étant rarement linéaire, mais plutôt courbe (Pietilä 1989; Samson 1993a; Shigo 1986), l'hypothèse de l'axe droit fut rapidement abandonnée. Cette courbure s'explique par le fait que la branche fait au début de sa formation un angle positif par rapport à l'horizontal puis cet angle diminue progressivement avec l'augmentation du volume et de la masse de la de la branche au cours de sa croissance (Wilson and Archer 1979; Zimmerman and Brown 1971). Un modèle encore utilisé actuellement est représenté par une juxtaposition continue de 3 zones, soit : un tronc de cône elliptique à axe défini par une courbe cubique paramétrique de type Hermite, un tronc de cône elliptique à axe droit et une moitié d'ellipsoïde de révolution symbolisant la fermeture d'un nœud mort (Samson et al. 1996). Les équations du modèle ont été modifiées et simplifiées par les travaux de (Lemieux et al. 1997a, 2001). Ce modèle permet de s'ajuster aux formes les plus courantes de nœuds présentées dans la littérature.
La principale difficulté liée à l'étude des nœuds réside dans l'obtention des données internes. En effet, contrairement aux données externes facilement mesurables, les données

internes sont difficilement accessibles. Habituellement, la description et l'analyse des caractéristiques internes des billons implique de procéder de manière destructive, notamment par une méthode manuelle qui consiste à découper précisément le nœud. Harless et al. (1991) ont découpé leurs billons en rondelles sur lesquelles ils ont détouré les défauts afin de simuler des sciages tenant compte de la position de ces derniers. Lemieux et al. (1997a) ont utilisé des déroulages pour caractériser les nœuds dans des billons d'Épinette de Norvège. La répartition des nœuds et de l'aubier/duramen ont été analysés dans des billons de pin maritime (*Pinus pinaster*) à partir de l'analyse de la surface de planches (Pinto et al. 2003). On obtient alors un ensemble de paramètres (angles, statut…) qui décrivent le nœud (Björklund and Petersson 1999; Trincado and Burkhart 2008). Ces méthodes sont couteuses en temps et en main d'œuvre, et le risque d'erreur est assez élevé. De plus, ce type d'étude limite le nombre de nœuds à analyser par verticille, car de nombreux nœuds sont trop proches l'un de l'autre pour tous être découpés et analysés. Il existe d'autres méthodes qualifiées de non destructives. Elles sont de plus en plus utilisées car elles sont beaucoup plus efficaces et offrent un gain de précision et de temps important (Moberg 2000). À l'aide de balayeurs optiques qui numérisent la surface de la bille, des scientifiques ont élaboré des modèles reliant la forme externe des billons à leurs caractéristiques internes, de manière à prédire la qualité interne à partir de mesures de la surface externe. Cependant, les modèles actuels ne reflètent pas suffisamment bien la réalité des défauts internes et le processus d'analyse peut être long et donc difficilement applicable pour le travail à la chaine de l'industrie qui utilise principalement ces scanners pour des mesures de volumes et de défilement (Samson 1993b; Thomas et al. 2003; Zhang and Que-Ju 2005).

Il existe également d'autres procédés qui en plus de l'information sur la forme externe des billons peuvent accéder directement à leur structure interne. Les principaux sont les tomographes à rayons X ou gamma et l'imagerie par résonance magnétique (IRM). Les améliorations constantes des outils informatiques et des scanners permettent d'affiner de plus en plus cette technique. La tomographie à rayons X est l'une des plus utilisées. Il s'agit d'une méthode permettant d'obtenir des images de coupes d'un objet de façon non destructive. Les images sont reconstruites à partir de l'atténuation de faisceaux de rayons X lancés selon différentes orientations dans un plan de coupe passant au travers du volume

étudié. Le principe général de fonctionnement du scanner est d'effectuer de multiples projections sous différents angles. À partir de l'information acquise lors des différentes projections, il est possible de calculer les coefficients d'atténuation de chaque voxel (désigne un pixel en 3D, contraction de « volumetric pixel ») traversé afin de reconstruire une image de la section. Au final, cela permet une reconstruction de certaines propriétés de l'intérieur de l'objet scanné (Longuetaud et al. 2005).

La modélisation des nœuds a deux applications principales, l'une dédiée à l'impact des décisions sylvicoles, l'autre dédiée à l'amélioration des procédés de sciage. En effet, en plus d'améliorer la qualité des bois en évaluant à l'avance l'impact des stratégies sylvicoles à travers des modèles de croissance couplés à des modèles de qualité, il est également possible d'influencer cette qualité et de minimiser l'effet des nœuds au moment de la transformation du bois. Il est nécessaire pour ce faire d'avoir une bonne connaissance du profil géométrique et de la distribution spatiale des nœuds. Ce type d'étude est justifié par une distribution souvent non uniforme des nœuds autour du tronc (Björklund and Petersson 1999; Samson 1993a). Puisque la dimension critique des nœuds varie avec la dimension de la pièce et avec la position du nœud dans la section de la pièce, il y a plusieurs façons de limiter l'effet des nœuds sur le bois de structure; soit, entre autres, en produisant des pièces de grandes dimensions et en adaptant la technique du sciage à la morphologie et à la répartition des nœuds (Zhang et al. 1998).
Un modèle de qualité intégrant une représentation de la géométrie des nœuds couplé à un logiciel de sciage peut augmenter la qualité des produits transformés (Harless et al. 1991; Hodges et al. 1990; Leban and Duchanois 1990). On peut également lier ce logiciel de sciage à un logiciel de classement de qualité pour connaitre directement le classement des produits finis (Steele et al. 1994). On constate dans une étude de Lemieux et al. (1997a) qu'un sciage tenant compte de la position des nœuds permet une augmentation des classements des poutres. Le développement de plus en plus important de la technologie des scanners permet de mettre en application cette approche (Schajer and An 2012; Wagner et al. 1989). Cela permet de détecter rapidement la localisation des défauts et de positionner la bille pour limiter l'impact de ces défauts et, ainsi, augmenter la qualité. La précision obtenue dépendra alors du scanner et du modèle de simulation (Bhandarkar et al. 1999).

Notre étude porte sur deux espèces parmi les plus importantes commercialement pour le Québec : l'épinette noire et le pin gris (Ministère des ressources naturelles 1996). Ces deux espèces font partie du groupe SEPM (sapin, épinettes, pin gris et mélèzes). Au Québec, les forêts continues dominées par l'épinette noire, appelées pessières à mousses, couvrent 412 400 km^2 (MRN 2001). Le bois de l'épinette noire a été utilisé principalement pour la construction d'habitations et la fabrication de la pâte et du papier. Ses longues fibres permettent la fabrication de papiers minces tout en étant très solides. Comme bois d'œuvre, sa très grande résistance à la rupture en fait un des bois de structure des plus recherchés dans la construction d'habitations en Amérique du Nord. Le pin gris est un conifère dont l'aire de répartition couvre une grande partie du Canada. Il s'agit d'une essence indigène résineuse disponible au Québec en abondance. Plus de 2,5 millions de mètre cubes de bois rond sont transformés chaque année dans la province (MRNF 2008). Sa croissance lente et ses nœuds sains lui permettent d'être valorisé aussi bien pour des usages structuraux que pour des usages d'apparence. Le pin gris a aussi d'excellentes propriétés d'usinage et de collage.

Le choix de ces deux espèces, outre leur importance commerciale, est également motivé par les nombreuses différences liées au développement de leur branchaison. En effet, l'épinette noire est une espèce tolérante à l'ombre et possède plutôt de petites branches, nombreuses, de nombreuses branches d'inter-verticille et souvent présentes jusqu'à la base du tronc. Le pin gris est une espèce intolérante avec des branches généralement plus grosses et s'élaguant assez rapidement. Ces deux espèces nous permettront de comparer et d'adapter les modèles à des développements de branchaison contrastés.

Le présent projet vise à l'intégration de modèles précis de la géométrie des nœuds couplés à une distribution plus réaliste de ces nœuds dans le tronc afin d'améliorer les simulateurs de croissances d'arbres existants.

Chapitre 1: Modelling knot morphology as a function of external tree and branch attributes

1.1. Résumé

Les modèles utilisés actuellement pour décrire la morphologie des nœuds sont généralement basés sur des fonctions polynomiales dont les paramètres sont difficilement interprétables. Ainsi, ils sont difficiles à intégrer dans les simulateurs de croissance en raison de la difficulté à relier la forme des nœuds et les caractéristiques externes des branches et des arbres. Des images de tomographie à rayons-X le long des tiges de 16 pins gris (*Pinus banksiana Lamb.)* et de 32 épinettes noires (*Picea mariana (Mill.) BSP*) ont été utilisées pour extraire, respectivement pour chaque espèce, la forme 3D de 3450 et 11 276 nœuds. Dans un premier temps, nous avons utilisé une approche de modélisation non linéaire basée sur une fonction de Weibull afin de décrire la géométrie de chaque nœud. Des équations distinctes ont été utilisées afin de décrire à la fois l'évolution de la courbure et du diamètre du nœud de la moelle à l'écorce. Cette combinaison de deux équations a permis une représentation exacte de la forme du nœud en utilisant seulement cinq paramètres. Dans un second temps, les paramètres obtenus pour chacun des nœuds ont été extraits et modélisés en fonction des caractéristiques externes de la branche et de l'arbre (p. ex. le diamètre de la branche, l'angle d'inclinaison, la position dans la tige, la hauteur et le diamètre de la tige). Lors de l'ajustement du modèle à un jeu de données séparé, les résidus de l'équation de courbure de l'épinette noire étaient inférieurs à 2,9 mm le long du profil de nœud dans 75 % des cas. Cette valeur était de 2,8 mm pour les résidus de l'équation du diamètre. Chez le pin gris, ces valeurs étaient respectivement de 5,4 mm et 3,2 mm. Globalement, l'aptitude à prédire les attributs des nœuds à partir des données externes de branches et d'arbre offrent le potentiel d'améliorer la simulation des propriétés internes du bois.

1.2. Abstract

Existing models for describing knot morphology are typically based on polynomial functions with parameters that are often not biologically interpretable. Hence, they are difficult to integrate into tree growth simulators due to the limited possibilities for linking knot shape to external branch and tree characteristics. X-ray computed tomography (CT) images taken along the stems of 16 jack pine (*Pinus banksiana Lamb*.) trees and 32 black spruce (Picea mariana (Mill.) B.S.P.) trees were used to extract the three-dimensional shape of 3450 and 11 276 knots from each species, respectively. Using a nonlinear approach, we firstly fitted a model of knot geometry adapted from a Weibull function. Separate equations were used to describe both the curvature and the diameter of the knot along its pith. Combining these two equations gave an accurate representation of knot shape using only five parameters. Secondly, to facilitate the integration of the resulting model into a tree growth simulator, we extracted the parameters obtained for each knot and modelled them as functions of external branch and tree characteristics (e.g., branch diameter, insertion angle, position in the stem, tree height, and stem diameter). When fitted to a separate data set, the model residuals of the black spruce knot curvature equation were less than 2.9 mm in any part of the knot profile for 75% of the observations. The corresponding value from the diameter equation was 2.8 mm. In jack pine, these statistics increased to 5.4 mm and 3.2 mm, respectively. Overall, the ability to predict knot attributes from external tree- and branch-level variables has the potential to improve the simulation of internal stem properties.

1.3. Introduction

The size and distribution of knots within trees are among the most important factors affecting the quality of end-use products (Buksnowitz et al. 2010; Zink-Sharp 2003). Mechanistically, they cause discontinuities and deviations of the grain (Dinwoodie 2000), which create zones of weakness due to stress concentrations.

They also have a potential impact on the suitability of sawn boards for appearance-grade products, where the presence of defects can affect value (Macdonald and Hubert 2002).

For these reasons, silviculturists have tried to obtain a better understanding of the trade-offs between radial growth rate and knot size (Hein et al. 2008; Weiskittel et al. 2007), while wood scientists have investigated ways to optimize processing by taking into account the location and size of knots during sawing (Lemieux et al. 2002; Moberg and Nordmark 2006).

In recent years there has been increasing interest in the development of computer-based systems that are capable of simulating tree growth and structure, which can be used to predict the effects of forest management decisions on wood end-use properties (Houllier et al. 1995). This approach is useful for synthesizing the complex interactions between silviculture (Auty et al. 2012; Mäkinen 1999a; Mäkinen 1999b) and wood properties (Gardiner et al. 2011). An important component of such simulators is a module capable of describing the distribution, size, and shape of knots within a tree.

As knots are the internal continuation of branches in the tree stem, previous modelling efforts have mainly focused on describing external branch characteristics, which are easier to measure. Colin and Houllier (1991) elaborated a branch analysis protocol that was subsequently used and refined by several other studies (Auty et al. 2012; Mäkinen and Mäkelä 2003). This approach consists of simulating the dynamic processes of tree and branch growth through static (in time) measurements of the location and size of branches on trees of different ages. The branching variables of interest can then be expressed as age- or size-dependent functions at any position along the tree stem. Such an approach assumes that knots can be represented by joining the portions of the branch included in the stem at each successive year of growth. An advantage is that data acquisition is relatively simple and can be accomplished with limited equipment. However, this simplicity comes at the expense of reduced accuracy for certain measurements such as branch inclination or azimuthal orientation around the stem. As long as the correspondence between simulated and observed knot shapes remains largely unexplored, it is unlikely that we can realistically simulate internal knot structure precisely from external branch models.

Another possible approach is to directly develop internal knot shape models (Samson et al. 1996; Trincado and Burkhart 2008). Fewer studies have used this approach due to the difficulties of obtaining internal data using destructive methods. For example, Harless et al. (1991) cut logs into transverse disks to reconstruct knot shape, while Lemieux et al.

(1997b) used rotary cutting and Pinto et al. (2003) examined the surfaces of boards. More recently, non-destructive techniques have been developed that can generate high resolution data much more rapidly than destructive methods, e.g., infrared imaging, optical scanning, computed tomography using X-rays or gamma rays, and magnetic resonance imaging (MRI) (Longuetaud et al. 2012; Moberg 2001). Parallel developments in modelling techniques have also led to a series of successive improvements in knot shape models. For instance, early knot models represented the knot as a circular cone perpendicular to the longitudinal axis of the stem (Richards et al. 1979). An angle of inclination was later added (Leban and Duchanois 1990), although it was known that the axis of a knot is rarely straight (Samson et al. 1996). At its initiation point, the angle of insertion of a knot relative to the horizontal is generally positive (i.e., oriented upwards from the horizontal plane), and the curvature is due to the gradual decrease of this angle over time. To account for this phenomenon, Björklund (1997), Lemieux et al. (2001), and Moberg (2001) developed segmented models in which each knot consists of two different zones: the sound knot formed by the live branch, which is generally represented by a cone shape, and the loose (or dead) knot, which is represented by a cylinder. These models are capable of describing a wide variety of sizes and shapes, but the shape equations or the equations that identify the location of cut points of the segmented models are generally based on polynomial functions. This complicates the biological interpretation of the parameters and limits the possibilities for linking knot shape to branch and tree characteristics (Pinheiro and Bates 2009).

This study used empirical data on knot shape and distribution in two commercially important species in eastern Canada: black spruce (*Picea mariana (Mill.) B.S.P.)* and jack pine (*Pinus banksiana Lamb.*). Although both species are highly valued for their lumber sold in the same SPF (spruce–pine–fir) group on the North American market (McKenney et al. 1992), they show contrasting knottiness patterns. Black spruce produces numerous small branches that rapidly bend towards the ground as their diameter increases (Bégin and Filion 1999), whereas jack pine produces fewer but larger branches that maintain a more vertical orientation over a longer period of time (Plourde et al. 2009). In addition, black spruce produces several nodal and internodal branches (Benjamin et al. 2009a), whereas

jack pine produces fewer but larger nodal branches and only a limited number of internodal branches (Beaulieu et al. 2011).

Our main objective was to develop equations that describe knot morphology in black spruce and jack pine using a limited number of interpretable parameters. Specifically, we aimed to develop models describing knot size and curvature that could be linked with the characteristics of the tree and branch to which they are attached. Models are intended for integration into a tree growth simulation system to quantify the effects of silvicultural treatments on knot morphology and inform future forest management decisions.

1.4. Materials and methods

1.4.1. Data collection

The trees were sampled from unmanaged stands in the boreal forest of Quebec, Canada. In total, 32 jack pine trees were harvested in the Lac St-Jean region, and 64 black spruce trees were taken from the North Shore region. To obtain a wide range of knot sizes and shapes, we sampled trees along a chronosequence of stand ages over which we imposed a variation in stand densities. The jack pine chronosequence was selected using forest fire maps from the Quebec Ministry of Natural Resources. We chose a relatively small area where several fires had occurred in consecutive decades. Two black spruce chronosequences were sampled, one near the town of Baie-Comeau, hereafter referred to as South, and one 200 km further north (the North chronosequence). Further details of how these chronosequences were established can be found in Bouchard et al. (2008). Four trees per stand were randomly selected according their social status within the stand, i.e., one dominant, two co-dominant, and one intermediate tree. The only exception was for the oldest black spruce stands (>200 years since the last fire) where the stands had reached an uneven-aged structure (Bouchard et al. 2008). In the latter case, tree selection was made to obtain the largest possible range of tree ages. The jack pine trees ranged from 16 to 91 years of age, whereas the black spruce trees ranged from 9 to 208 years (Table 1-1).

Table 1-1 Mean characteristics of the sample trees, branches, and knots in the data set.

	Black spruce		Jack pine	
	Mean	Range	Mean	Range
Number of stands	16		8	
Number of subject trees	64		32	
Age of the trees (years)	83	9 - 208	50	16 - 91
DBH (cm)	13.5	3.4 - 27.2	14.5	8.5 - 32.8
Height (m)	12.2	2.61 - 23.12	11.7	7.5 - 20.85
Height of the base of the crown (m)	7.3	0 - 16.62	6.1	1.64 - 13.83
Number of measured branches	5114		1852	
Number of measured knots	14343		3450	
Knot diameter at bark	3.47	0.5 - 59	9.84	0.5 - 61.4
Maximum knot diameter	4.69	0.5 - 59	11	0.5 - 61.4
Knot inclination at bark	95	50 - 155	100	46 - 156
Number of occluded branches	302		3538	
Percentage of occluded branches (%)	0.09		0.23	
Percentage of occluded branches (Diameter >=5mm)	0.05		0.02	
Diameter at the extremity of the occluded knots (mm)	3.73	0.02 - 13.35	0.70	0.01 - 21.73
Maximum knot diameter (mm)	5.94	0.03 - 16.73	2.27	0.01 - 21.73
Relative position along the stem	0.33	0.01 - 0.85	0.32	0.01 - 0.98

1.4.2. Tree and branch measurements

External branch measurements were obtained following the protocol established by Colin and Houllier (1991), later refined by other researchers, including Mäkinen and Colin (1998), Kantola and Mäkelä (2004), and Auty et al. (2011). Prior to felling, a line indicating the north-facing part of the stem (azimuth = 0°) was marked with paint, and this line was continued along the length of the stem after felling. The height to the base of the live crown (HBLC, m), defined as the position of the lowest whorl containing at least one live branch and with contiguous live whorls above it, total tree height (H, m), and the height of the first live branch (HFLB, m) were then recorded. For each annual whorl starting from the stem apex, we determined the number of live and dead branches and the diameter of the stem at this position. Due to the large number of branches and the time necessary to measure their characteristics, we did not make further measurements on

internodal branches, while selecting every fourth whorl along the stem for the complete measurements of nodal branches. Branch orientation around the stem (azimuth), angle of insertion relative to the horizontal, vertical diameter, and status (live or dead) were measured for each branch in the whorl. In the remaining annual whorls, only the largest nodal branch was fully measured. A summary of the variables used in this study and their abbreviations can be found in Table 1-2.

1.4.3. Knot measurements

After the field measurements were completed, two trees per stand were randomly selected (i.e., 16 jack pine trees and 32 black spruce trees) and cut into successive 2.5 m logs. The logs were cut so that they included the stem between stump level (0.1 m above ground level) and the level at which stem diameter over bark was at least 9.1 cm (merchantable height). The number of logs per tree varied between one for the youngest tree and seven for the oldest. The logs were then transported to the Institut National de la Recherche Scientifique in Québec City for X-ray computed tomography (CT) scanning using a Somatom Sensation 64 (Siemens Medical Solutions USA, Inc.). This technique provided direct access to the internal characteristics of scanned logs on the basis of density and moisture content variations. Each log was scanned at 2 mm intervals along its longitudinal axis with a 2 mm wide X-ray beam (120 kV, 50 mA) so that the scanned segments were contiguous. The image reconstruction was performed with a pixel size of 0.35 mm × 0.35 mm. As the scanner can only process 2.1 m long pieces, the logs were scanned in two passes.

We obtained an average of 1200 images per log, which were analyzed individually. To perform this task, we used the ImageJ 1.44 freeware (Abramoff et al. 2004) with a Java plug-in (Gourmand, version 1.01) developed at INRA, Nancy, France (Colin et al. 2010) allowing the semimanual extraction of knot geometry. Each knot is attached directly to the pith of the main stem, which is located manually on each image. Then, on several successive images, two points on each side of the knot were added to delineate knot shape from pith to the bark. Finally, a smoothing spline was fitted to these points and the plug-in automatically measured the position and the geometry of each knot. Bild3D, another Java program, was then used to reconstruct the three-dimensional (3D) shape of the stem and

the position and 3D geometry of each knot using the rectangular Cartesian coordinate axes x, y, and z (Figure 1-1). In total, we obtained the geometric profiles of 3450 knots for jack pine and 11 276 knots for black spruce.

Table 1-2 Definitions and abbreviations of the variables used in this paper.

	Description
Tree-level variable	
H	Total tree height (m)
HBLC	Height of the base of the crown (m)
HFLB	Height of the first live branch (m)
DBH	Diameter at breast height (cm)
HD	H to DBH ratio (dimensionless)
Branch/knot-level variable	
I_{bark}	Angle of insertion relative of the horizontal (degrees)
D_{bark}	Diameter of the knot at stem bark/Diameter of the branch (without bark) at stem bark (mm)
R_{max}	Stem radius at the knot position (mm)
Z_H	Distance between the vertical position of the knot at the pith and at the bark (mm)
Z_{rel}	Relative position of the branch along the stem (dimensionless)
Model parameters	
A, B, C	Parameters of Eq. 2 (vertical position)
E, F, G	Parameters of Eq. 3 (diameter)

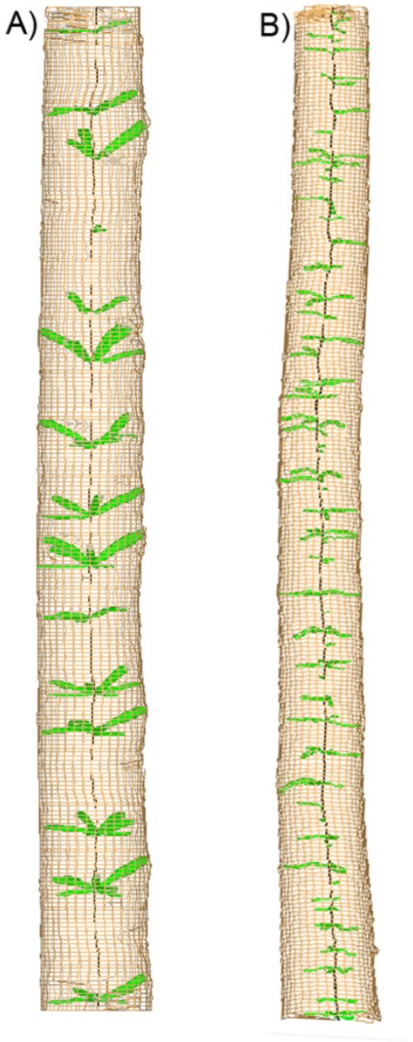

Figure 1-1 Visualization of the knot information extracted from 2.5 m logs located at the base of **(A)** a jack pine stem and **(B)** a black spruce stem. The three-dimensional reconstruction of stem shape and of the geometry of each knot was done using the "Bil3D" Java software.

1.5. Model development

1.5.1. Knot profiles

Previous studies by Samson (1993) and Lemieux et al. (1997a) reported some ovality in knot cross sections in black spruce, with the vertical diameter approximately 10% to 15% greater than the horizontal diameter. However, because external branch diameter was only

recorded in the vertical direction, we chose to model the knot profile along the same axis. Because it was not always possible to locate the pith, knot profiles were described relative to their geometrical centre. In addition, as knot radial direction was generally constant, only the dimensions in a two-dimensional (2D) plane were modelled. The z axis was defined as the longitudinal axis of the main stem, and the x axis was oriented perpendicular to the z axis along a plane formed by the azimuthal orientation of each knot. Fifty points were extracted along the x axis of each knot to describe (i) the location along the z axis of its geometrical centre, hereafter referred to as the vertical position, and (ii) knot diameter (Figure 1-2).

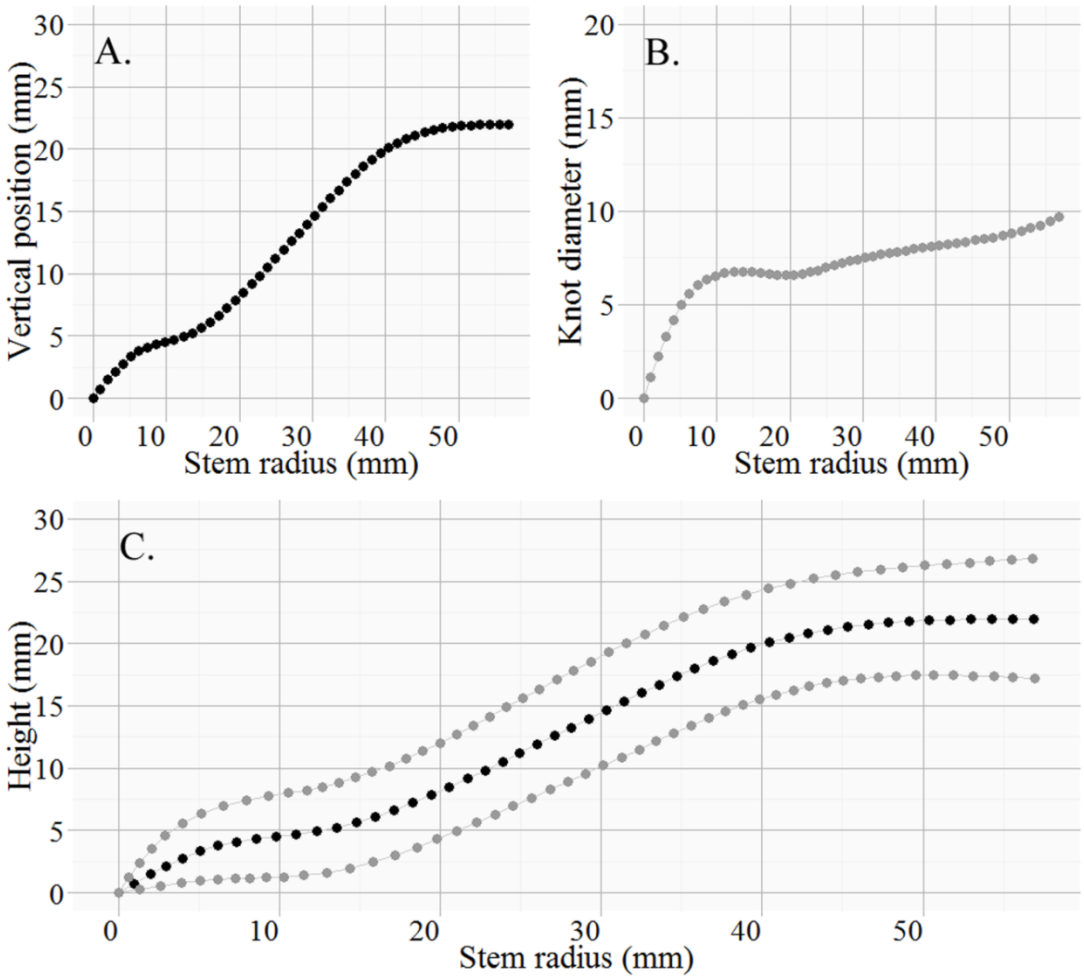

Figure 1-2 (A) Pith-to-bark vertical position of the geometrical center of the knot. **(B)** Evolution of the knot diameter from pith to bark. **(C)** Reconstruction of knot profile from pith to bark combining the position along the z axis and the diameter.

1.5.2. Knot model formulation

Separate models were fitted to describe the evolution of both the diameter and the vertical position of knots. As the profiles of the two curves were similar, they were both represented by the same equation. We chose a nonlinear model based on a combination of a Weibull equation (Zeide 1993) and a linear term, because it was flexible enough to describe the wide variation in observed knot shapes:

[1] $$z = \alpha \times \left(1 - e^{\left(-\beta \times \left(\frac{l}{R_{max} - l}\right)\right)}\right) + \mu \times l \qquad (0 \leq l \leq R_{max})$$

where l is the position along the x axis (distance from the pith of the main stem) and R_{max} is the total length (mm) of the knot along the x axis. Our assumption was that when a knot starts to grow, the rapid increase in branch diameter induces variation in the vertical position that can be described by a curve. Approaching the bark, knot diameter increases constantly but more slowly and with reduced branch curvature. This part of the equation could be described by a straight line ($z = \alpha + \mu \times l$), whereas the β parameter describes the curvature of the knot nearer to the pith (Figure 1-3). The parameters α, β and μ were estimated empirically. In the remainder of the text, we refer to these parameters as A, B, and C for the vertical position equation and E, F, and G for the diameter equation, respectively.

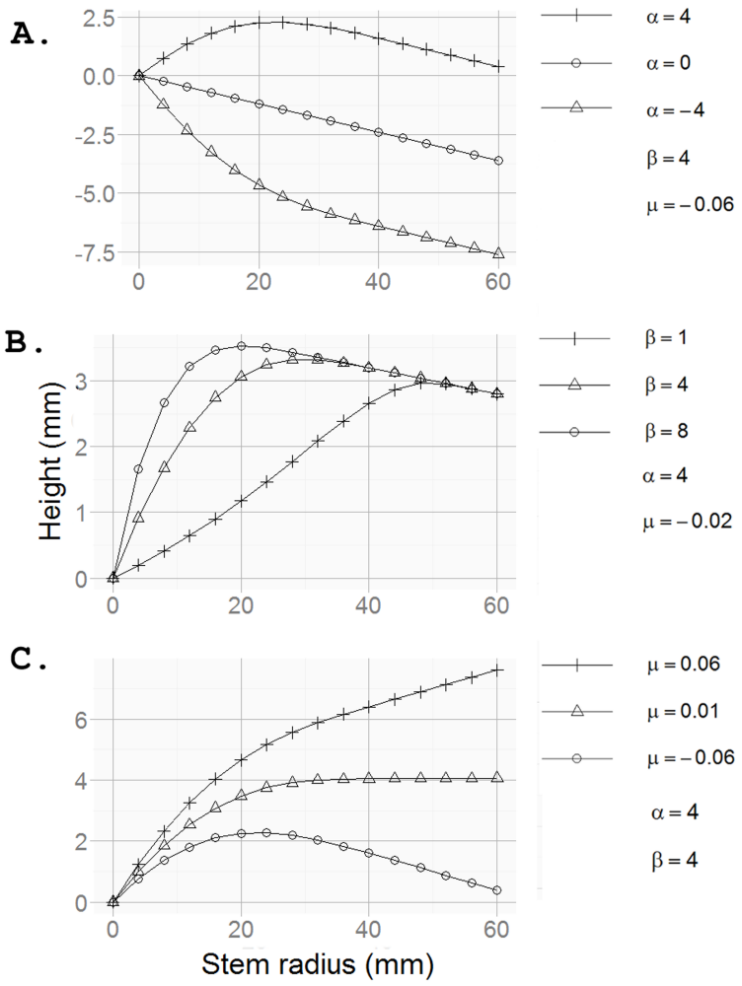

Figure 1-3 Illustration of the behaviour of the curve described by eq. 1and the impact of parameters α, β and μ.

1.5.3. Modelling vertical position

The knot curvature equation must meet two conditions: (i) when l = 0, z = 0, and (ii) when l = R_{max}, z = Z_H, where Z_H is the distance between the vertical position at the pith (Z_{pith}) and at the bark (Z_{bark}), which was obtained from the CT images. The first condition is imposed by the model and the second condition can be met when $A = Z_H - C \times R_{max}$. Therefore, the curvature equation can be expressed as follows:

[2] $$z = (Z_H - C \times R_{max}) * \left(1 - e^{\left(-B \times \left(\frac{l}{R_{max} - l}\right)\right)}\right) + C \times l$$

1.5.4. Modelling knot diameter

Branch diameter tended to increase rapidly during the first few years of growth before a gradual decline in growth rate was observed. In some instances, the maximum diameter was reached before the bark, with a decrease in knot diameter after this point. Such cases were represented in the model by a negative value for the G parameter. The knot diameter model meets two conditions, i.e., when l = 0, z = 0, and when l = R_{max}, z = D_{bark}, where D_{bark} is the knot diameter at the bark. The first condition is imposed by the model, and the second condition can be met when E = D_{bark} − G × R_{max}. The diameter equation can therefore be written as follows:

[3] $$z = (D_{bark} - G \times R_{max}) * \left(1 - e^{\left(-F \times \left(\frac{l}{R_{max} - l}\right)\right)}\right) + G \times l$$

Due to the large variation in knot shapes, the parameters of eqs. [2] and [3] were linked to external tree and branch variables in a two-stage process (Pinheiro and Bates 2009). The first stage was to obtain estimates of the four model parameters for each knot separately, and the second consisted of modelling these parameter estimates as functions of external tree- and branch-level variables.

1.5.5. Stage 1: estimating individual knot parameters

Models were fitted to each knot independently using the "nls" function in the "nlme" library of the R statistical programming environment (R Development Core Team 2012). To determine appropriate starting values for each parameter and for each knot, the diameter profile and the vertical position profile close to the bark were represented as straight lines. The linear regression estimates of the points located within 5 cm of the bark were then used to define the start values of parameters A and C and parameters E and G in the vertical position and diameter profile models, respectively. Using the conditions imposed on each model, parameter B was expressed as a function of parameters A and C, and parameter F was expressed as a function of parameters E and G. This strategy allowed us to obtain a high rate of convergence during parameter estimation (82.9% of jack pine

knots and 88.2% of black spruce knots). Cases in which models failed to converge were mainly due to occluded knots and other knots that had a vertical position curve or a diameter curve very different to those that could be represented with the model (i.e., generally with an S shape). However, for a large majority of knots for which the models converged, we obtained estimates of the parameters B, C, F, and G (Table 1-3).

Table 1-3 Mean and range of parameter estimates from stage 1 of the modelling process and the Pearson's correlation coefficients between each parameter.

	Black spruce		**Jack pine**	
	Mean	Range	Mean	Range
Z_H	4.64	-88 - -120	14.89	-44 - -166
B	2.78	0 - 99.7	5.97	0 - 96.86
C	0.03	-1.43 - 7.42	0.14	-1.13 - 5.9
F	12.33	$8.39.10^{-9}$ - 99.01	9.23	$8.38.10^{-9}$ - 99.41
G	-0.06	-2.11 - 2.11	-0.02	-1.59 - 0.81

	Black spruce \ Jack pine				
	B	C	Z_H	F	G
B	-	0.20	0.02	0.04	0.09
C	0.18	-	0.73	-0.03	0.31
Z_H	0.07	0.59	-	-0.04	0.28
F	0.01	-0.01	0.00	-	0.10
G	0.03	-0.02	0.10	0.09	-

1.5.6. Stage 2: modelling knot parameters as functions of external tree and branch variables

The second stage of the modelling process was to relate the values of the estimates obtained for each knot (B, C, F, and G) to external tree and branch variables. The value of Z_H, which is the (vertical) distance between Z_{pith} and Z_{bark}, was obtained directly from the CT images. However, when working from external data, Z_{bark} was considered known, but we needed to express Z_H as a function of external tree and branch variables. Because the objective of this stage is to enable the integration of the knot models with a tree growth

simulator, accurate measurements of external branch characteristics are desirable. However, these measurements are subject to errors due to factors such as variable bark thickness or branch accessibility. Furthermore, the presence of occluded knots and the fact that only a subsample of branches was measured could cause problems when matching knots to their corresponding branches. To limit problems associated with imprecision in branch measurements and missing data, all occluded branches were omitted from the analysis (Table 1-1). Furthermore, a close relationship was assumed between the knot characteristics at the bark and the measurements on the corresponding branches. This was verified using linear regression using the data from pairs of matching knots and branches.

To ensure continuity, the inclination of each knot close to the bark was required to be the same as that of the corresponding branch. This was achieved by forcing the C parameter to be equal to the inclination of the branch. In the case of knot and branch diameters, the correspondence was already imposed by eq. [3]. The remaining parameters Z_H, B, F, and G were then estimated from branch and tree variables. Several predictor variables and their interactions were screened, as long as the latter were logical and interpretable (Aiken and West 1991). Due to the non-Gaussian distribution of parameters B and F, gamma regression was used in their estimation (Prentice 1974). Because these two parameters must be positive, a log-link was used. The link function provides the relationship between the linear predictor and the mean of the distribution function. We estimated the values of the parameters Z_H and G for each knot using linear mixed-effects models with a random tree effect (Pinheiro and Bates 2009). Model selection was based on Akaike's information criterion (AIC) (Mazerolle 2006), and only significant parameters ($p < 0.05$) were retained in the final models. Two sets of fit indices were also calculated for the chosen models. The predicted values were estimated from the fixed-effects terms of each model in the first set and from both the fixed and random effects in the second set (Gardiner et al. 2011).

Models were fitted to a calibration data set before being tested on a separate evaluation data set (cf., Mäkinen and Song 2002). For the black spruce knots, we used the South chronosequence data (6841 knots) for model fitting and the North chronosequence data (4435 knots) for model evaluation. Because the jack pine data came from a single chronosequence, we randomly selected 770 knots (30% of the total) to evaluate the model that was fitted to the 1796 remaining knots.

1.6. Results

1.6.1. Stage 1

The accuracy of the models fitted to individual knots was assessed by comparing the predicted values with the observed values extracted from the CT images. All curves were relatively unbiased along the length of the pith to bark profiles, indicating that knot shape was represented adequately by the equations. For knot vertical position (eq. [2]), the absolute value of 75% of the residuals was less than 1.6 mm along the black spruce pith-to bark profiles (2.19 mm for jack pine) and the absolute value of 95% of the residuals was less than 2.7 mm (4.7 mm for jack pine) (Figure 1-4).

For knot diameter (eq. [3]), the absolute value of 75% of the residuals was less than 1.4 mm along the black spruce pith-to-bark profiles (1.4 mm for jack pine) and for 95% of the residuals was less than 2.4 mm (2.9 mm for jack pine) (Figure 1-4). Several knots decreased in diameter towards the periphery of the stem, which was indicated by negative values obtained for parameter G. In 59% of black spruce knots and 46% of jack pine knots, the diameter at bark was smaller than the maximum diameter along the knot profile.

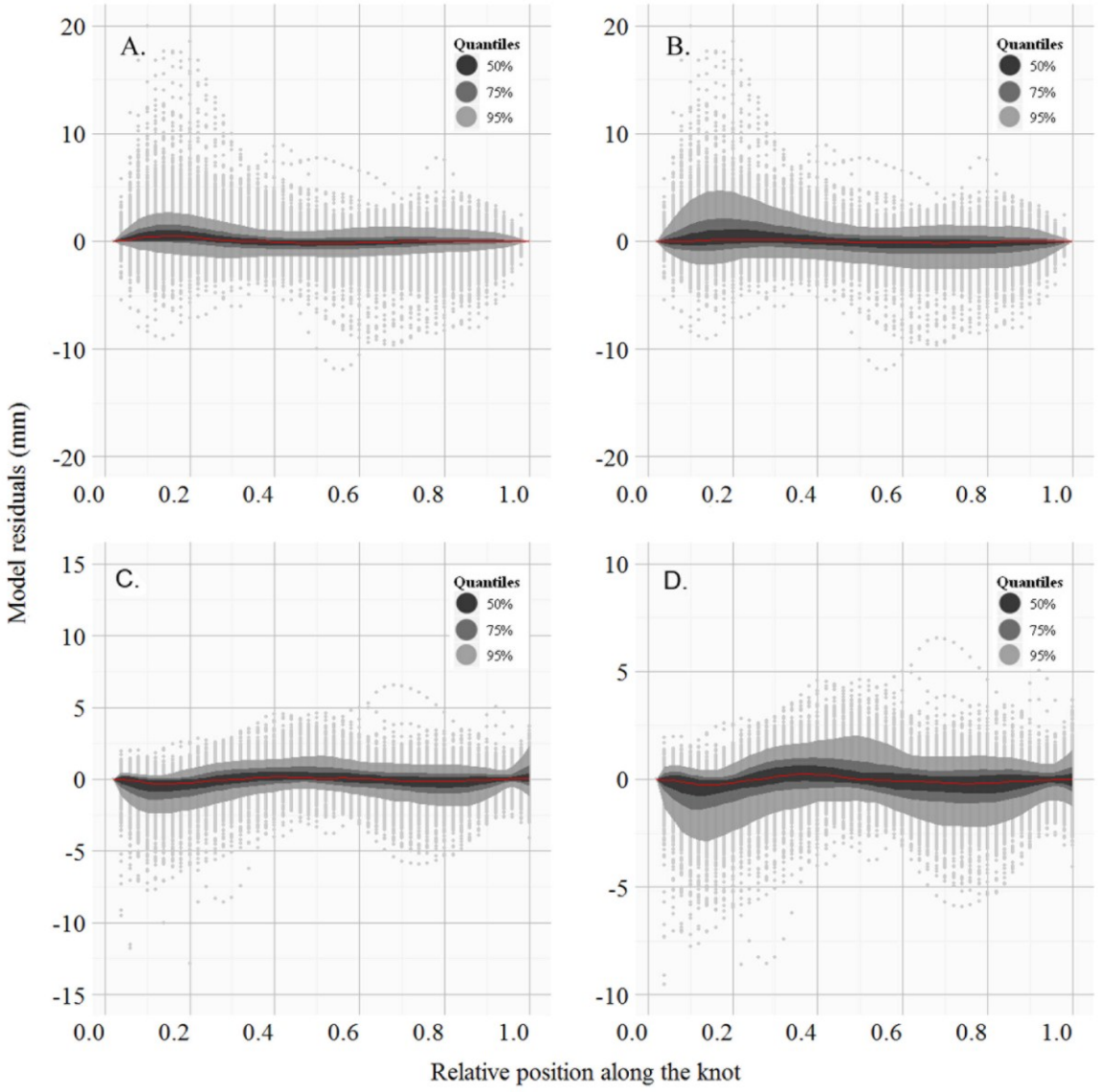

Figure 1-4 Distribution of the model residuals from stage 1 of the modelling process (sorted by quantiles) along the relative position from pith to bark for **A)** vertical position in black spruce knots, **B)** vertical position in jack pine, **C)** knot diameter in black spruce, and **D)** knot diameter in jack pine.

1.6.2. Stage 2

The linear regressions applied to pairs of matching knot and branch diameter measurements gave coefficients of 1.2 ($R^2 = 0.92$) for black spruce and 1.02 ($R^2 = 0.95$) for jack pine. Given these strong correlations, the coefficients close to 1, and the fact that the external branch measurements were inclusive of bark thickness, we considered the knot

diameter at the bark to be a very close approximation of the external branch diameter. In contrast, the correspondence between the inclination of the last 5 cm of each knot and the measured branch inclination was very low, with an average error greater than 20°. The R^2 of the linear regressions between the two measurements was only 0.1 for black spruce and 0.4 for jack pine. Consequently, the inclination of the knot near to the bark was assumed to provide a closer approximation of the true branch insertion angle. For this reason and considering the accuracy of the CT-derived data, the knot measurements at the bark were used as predictor variables in subsequent analyses.

The selection of the final models showed that knot shape can be described using its diameter (D_{bark}, mm) and inclination (I_{bark}, degrees) at the bark, stem radius (R_{max}, mm), and the relative position along the stem (Z_{rel}, dimensionless) (Table 1-4 and Table 1-5). Knot shape was also related to tree-level variables such as height (H, m) and the height to DBH ratio (HD, dimensionless). In both species, the R^2 values were high for Z_H and, to a lesser extent, for G but were much lower for the B and F parameters, which control curvature of the vertical position and the knot diameter near the pith, respectively (Table 1-6). Even though the fit indices for the B and F models were low, the use of the gamma distribution constrained these parameters to vary across the same biological range as the real distribution. This was found to improve the residuals of the models compared with linear mixed-effects models that assumed a normal distribution. Despite being retained in the models on the basis of the AIC criterion, the proportion of the variation that could be attributed to the tree level random effect was very low in all cases (Table 1-6).

Table 1-4 Parameter estimates from stage 2 of the modelling process for black spruce.

	Z_H		B		F		G	
Variables	Estimate	±S.E	Estimate	±S.E	Estimate	±S.E	Estimate	±S.E
$(Intercept)$	-1.0471	0.5231	1.1093	0.1632			-0.3469	0.0387
D_{bark}	-0.1159	0.0364	0.0519	0.0211	0.1368	0.0292	0.0312	0.0022
R_{max}	0.0027	0.0012	0.0026	0.0019	0.0347	0.0011	0.0038	0.0003
I_{bark}	0.1683	0.3712	3.0465	0.2879	0.0528	0.2139	-0.1584	0.0159
Z_{rel}	1.4382	0.2419	-1.1400	0.3455	1.5907	0.2861	0.1452	0.0080
HD	1.1428	0.6584			2.4758	0.1542	0.2627	0.0454
H	-0.0031	0.0163	-0.0143	0.0082	-0.1142	0.0083	-0.0108	0.0013
$D_{bark} \times R_{max}$	0.0099	0.0003	-0.0010	0.0003	-0.0034	0.0003	-0.0004	0.0000
$D_{bark} \times I_{bark}$	0.2204	0.0112			-0.0537	0.0124		
$I_{bark} \times R_{max}$	0.8028	0.0038	-0.0454	0.0044	0.0091	0.0031	0.0014	0.0002
$H \times R_{max}$							-0.0001	0.0000
$D_{bark} \times HD$	-0.6329	0.0460			-0.2031	0.0354	-0.0128	0.0024
$D_{bark} \times H$	0.0223	0.0014			0.0141	0.0013	0.0010	0.0001
$Z_{rel} \times H$	-0.0629	0.0127	0.0593	0.0189	0.0636	0.0192		
$Z_{rel} \times HD$					-2.1148	0.4981		
$I_{bark} \times HD$	3.5130	0.4802						
$I_{bark} \times H$	-0.1733	0.0151						

Note: See Table 1-2 for an explanation of abbreviations. The times sign (×) represents an interaction term.

Table 1-5 Parameter estimates from stage 2 of the modelling process for jack pine.

	Z_H		B		F		G	
Variables	Estimate	±S.E	Estimate	±S.E	Estimate	±S.E	Estimate	±S.E
$(Intercept)$			1.3157	0.2713	1.7000	0.3094	-0.1993	0.0293
D_{bark}	-0.3688	0.0572	0.0003	0.0094	-0.0782	0.0184	0.0156	0.0009
R_{max}	-0.0384	0.0052	-0.0110	0.0025	0.0284	0.0042	0.0014	0.0003
I_{bark}	0.2842	0.1515	2.5874	0.4941	2.3000	0.5739	-0.0375	0.0249
Z_{rel}	1.0865	0.3955	-1.6215	0.4716	0.0052	0.3941	0.1578	0.0091
HD	0.2464	0.1423	-0.4251	0.2673	0.5904	0.1866	0.1516	0.0358
H	-0.0142	0.0090			-0.1178	0.0178	-0.0079	0.0008
$D_{bark} \times R_{max}$	0.0030	0.0004	0.0001	0.0001	-0.0006	0.0001	-0.0001	0.0000
$D_{bark} \times I_{bark}$	-0.0902	0.0274	0.0166	0.0059				
$I_{bark} \times R_{max}$	0.8569	0.0082	-0.0186	0.0032	-0.0131	0.0037		
$R_{max} \times HD$							-0.0008	0.0004
$D_{bark} \times HD$	0.3907	0.0642						
$H \times R_{max}$	0.0028	0.0003	0.0003	0.0001	-0.0006	0.0002		
$H \times D_{bark}$					0.0085	0.0012	0.0002	0.0001
$Z_{rel} \times HD$	-1.4898	0.4389	1.7747	0.5513				
$I_{bark} \times H$					-0.0486	0.0269		
$Z_{rel} \times H$					0.0784	0.0235		
$I_{bark} \times HD$			-2.1835	0.4647	-1.4080	0.5384	-0.0677	0.0310

Note: See Table 1-2 for an explanation of abbreviations. The times sign (×) represents an interaction term.

Table 1-6 Fit indices for the stage 2 models calculated from the fixed and random effects (Parresol 2001).

	Z_H	B	C	F	G
Black spruce models					
Fixed effects	0.9286	0.0099	0.5198	0.0641	0.3499
Tree random effect	0.9299				0.3636
Jack pine models					
Fixed effects	0.9291	0.0398	0.7071	0.0832	0.3248
Tree random effect	0.9296				0.3294

1.6.3. Model evaluation

When fitted to the evaluation data sets, the models developed in stage 2 adequately represented knot morphology. For knot vertical position (eq. [1[2]), the absolute value of 75% of the residuals was less than 2.9 mm along the full length of the pith-to-bark profiles for black spruce (5.4 mm for jack pine) and less than 6.9 mm for 95% of the observations (14.5 mm for jack pine) (Figure 1-5). Model accuracy was lowest near the pith of the main stem, i.e., the point of origin of the knot. This result was expected, as the location of this point was estimated from the known position of the knot at the bark and also because of the low R^2 of the B parameter model. For the knot diameter model (eq. [3]), the absolute value of 75% of the residuals was less than 2.8 mm along the black spruce pith-to bark profiles (3.2 mm for jack pine) and less than 4.5 mm for 95% of the observations (5.1 mm for jack pine) (Figure 1-5). Knot diameter close to the pith was slightly overestimated, which was most likely attributable to the low R^2 of the F parameter model.

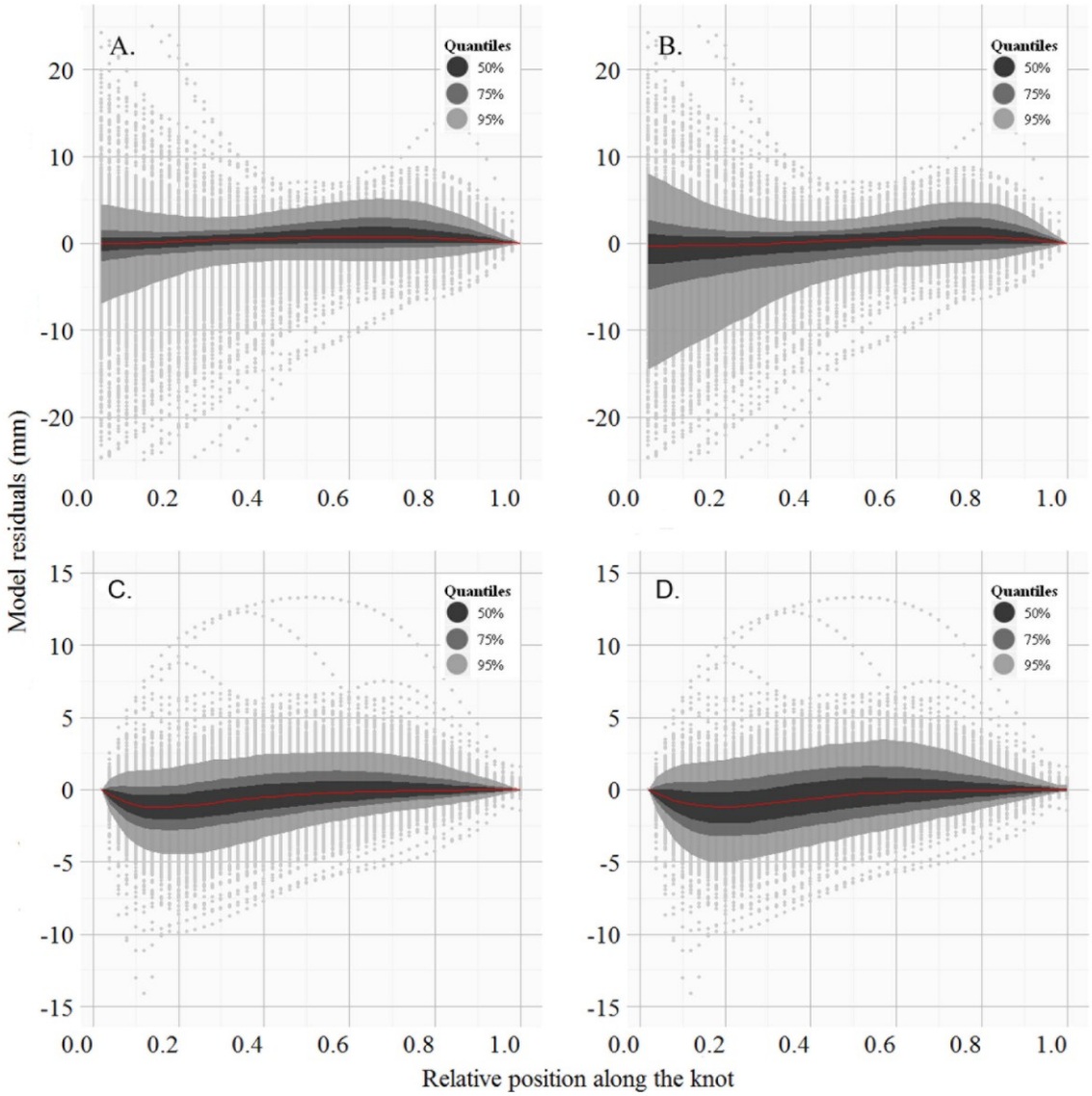

Figure 1-5 Distribution of the model residuals from stage 2 of the modelling process (sorted by quantiles) along the relative position from pith to bark for **(A)** vertical position in black spruce knots, **(B)** vertical position in jack pine, **(C)** knot diameter in black spruce, and **(D)** knot diameter in jack pine.

1.6.4. Simulations

To analyse the influence of external tree and branch parameters on knot shape, we created a series of simulated knots using the model predictions (Figure 1-6). Firstly, parameters were allowed to vary while all others were set to their mean values. We observed that the

youngest knots near the top of the tree, which are very likely to be alive, were almost linear in shape, whereas knots further down the stem showed a higher degree of curvature. Close to the pith, the inclination was steep and tended progressively towards a more horizontal orientation (Figure 1-6). This variation in the inclination was predicted to be greater in larger knots. Although this approach gave a visual representation of the effect of a selected variable, it is potentially problematic as the variations in external parameters are, in reality, not completely independent. This can lead to improbable scenarios in the simulations. For example, 5 mm knots (Figure 1-6, 3A) located at the base of a mature tree were impossible to simulate because eq. [2] gave negative values for knot diameter.

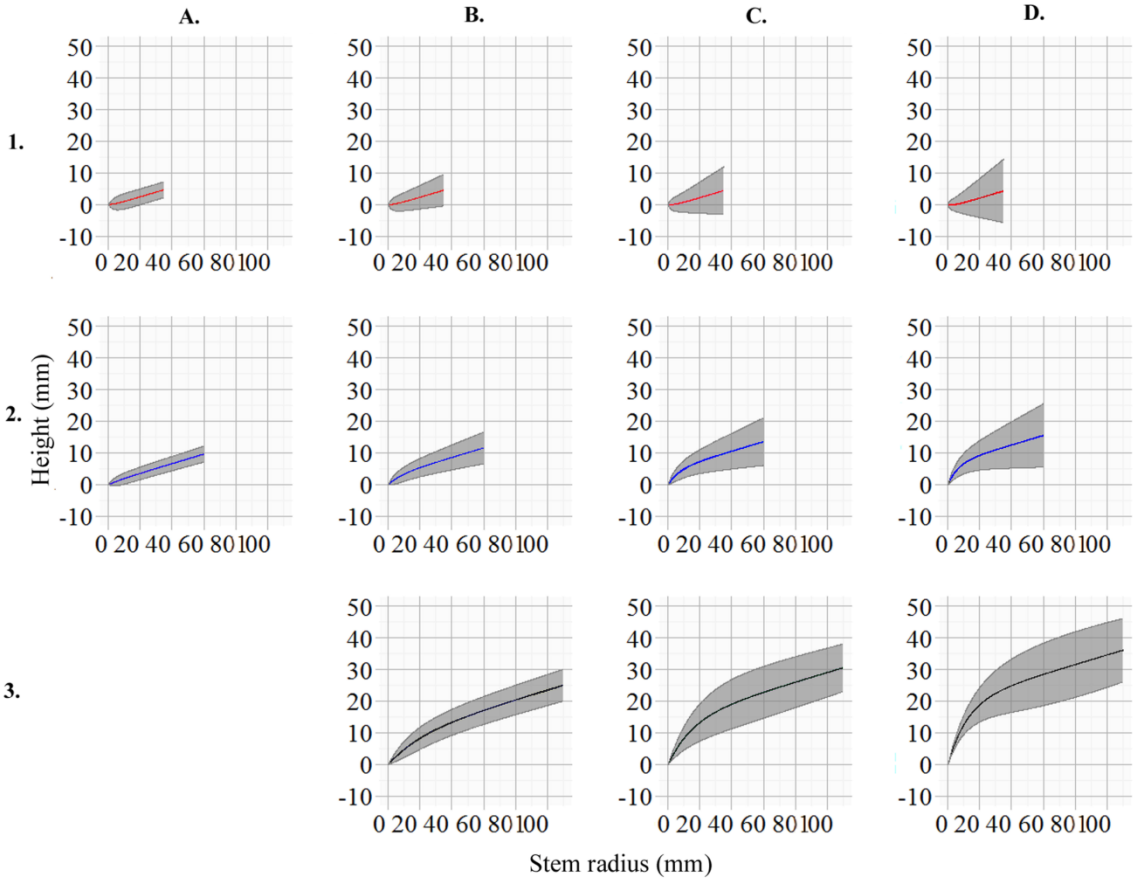

Figure 1-6 Knot shape simulations for different branch diameter values (**A**, 5 mm; **B**, 10 mm; **C**, 15 mm; **D**, 20 mm) and different relative positions along the tree (**1**, 0.8; **2**, 0.5; **3**, 0.2) in black spruce, with all other parameters fixed at their overall mean values. The shaded area represents the vertical diameter of the knot.

Therefore, in a second simulation, knot shapes were simulated at three different positions along the tree using the mean observed parameter estimates (i.e., those obtained in stage 1) at these positions. This showed that knot angle tended to be steeper at a higher position along the stem and that the conditions for a declining knot diameter towards the periphery of the stem most commonly occurred in the lower stem (Figure 1-7).

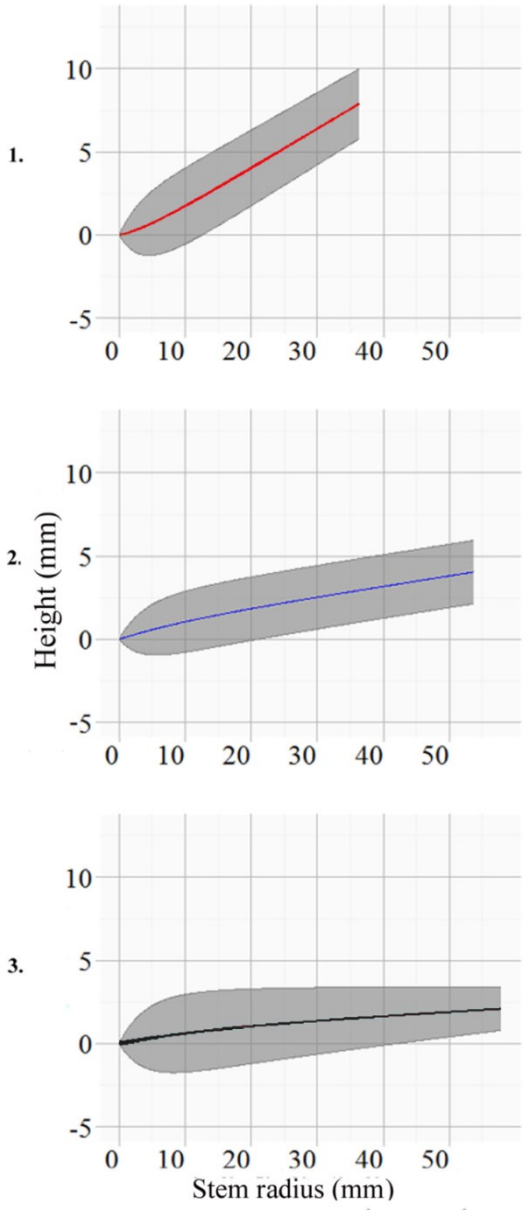

Figure 1-7 Effect of three different relative positions along the stem (1, 0.8; 2, 0.5; 3, 0.2) on the black spruce knot shape, with all other parameters fixed at their mean values at each position. The shaded area represents the vertical diameter of the knot.

1.7. Discussion

The utilization of the CT scanning technology produced a large amount of data with very high precision. However, there were some slight inaccuracies in the knot diameter measurements close to the bark, thought to be due to the high moisture content of sapwood, which made it difficult to differentiate between a knot and the surrounding wood. Nevertheless, we consider this a minor limitation compared with the numerous advantages of the method. In addition to the determination of the precise location of the knot within the stem, CT scanning offers greater accuracy for the inclination, azimuth, and to a lesser extent, diameter measurements compared with the laborious methods used to measure external branch characteristics (Colin et al. 1993). Thus, the precision of our knot simulation models is mainly limited by the capacity of existing growth models to provide accurate input data.

A disadvantage of the two-stage modelling approach is that errors propagate from one stage to the next. Although attempts were made to fit single-step models, the wide diversity of knot shapes meant that the models did not converge. One advantage of our models is the flexibility of the equations, which allow a representation of many possible knot shapes using only five parameters. Previously published knot models were generally based on polynomial equations or on segmented linear equations (Lemieux et al. 1997a), but such models do not allow for the interpretation of the parameters. Trincado and Burkart (2008) developed a system of equations for loblolly pine based on nonlinear functions, but these models were developed for young trees in fast-growing plantations, which exhibit very little knot curvature. However, the presence of mature trees in our data meant that knot curvature had to be accounted for in the development of the models. The slight sigmoidal trend in the residuals of the vertical position model (

Figure **1-4**A and B) was due to some knots forming an S shape along their profile. However, this small trend was present in only 25% of the residuals, and in any case, the degree of curvature was small. For simplicity and model parsimony, therefore, this tendency was ignored in the final choice of functional form.

The equations developed in this study were flexible enough to be fitted to two species with contrasting branching patterns. In addition, we were able to link the parameters of the knot

models to external branch and tree characteristics, which are themselves influenced by site factors and local growing conditions. The integration of the developed models with a growth model capable of simulating the impact of different silvicultural treatments on tree and branch characteristics should therefore lead to a more accurate assessment of knot size and distribution along the stem. Once achieved, links with a sawing simulator could help improve the estimation of end-use properties and the value of wood products.

The high level of accuracy of the Z_H and G parameter predictions was probably due to the fact these parameters describe the part of the knot close to the bark, which is expected to be more closely related to the external branch characteristics than the parts of the knot further into the stem. Conversely, the external data were not as well related to the B and F parameters, which describe how the curvature evolves along the pith-to-bark profile of each knot. These parameters are likely to have been affected by the history of branch growth, which was not accounted for in our models. Only current tree and branch characteristics were used rather than repeated measurements through time. Further research should focus on the development of dynamic models using data from stands with a known history of natural disturbances and (or) silvicultural treatments.

Lemieux et al. (2001) had little success linking knot shape with external branch attributed due to the large variation in knot shapes along the stem. One exception was external branch diameter, which was found to be a good predictor of internal knot diameter. Our simulations showed that for a given branch diameter, knot shape varies significantly as functions of position along the stem and the inclination of knot near the bark. Using branch diameter alone would have made it impossible to induce variability in our knot shape simulations. The addition of inclination, knot length, relative position along the tree, total height, and the height to DBH ratio allowed such variability. The knots near the top of the tree, being attached to younger branches, were more likely to be live and growing, which explains their steeper inclination angles. The effect of the height to diameter ratio suggests that knot shape is not only modulated by the vigour of the branch, but also by the vigor and social status of the tree within the stand.

A potential drawback of our study is that in some cases, it was possible for the knot diameter model to predict negative values. However, this was a rare occurrence affecting only 4% of the black spruce knots, mainly the smallest ones, and none of the jack pine

knots. Further problems might arise due to the exclusion of occluded branches. However, this was a necessary step as the purpose of the study was to link internal knot attributes with their external characteristic. Although 23% of black spruce branches in this study were occluded (and 9% of jack pine branches), these were also generally restricted to the smaller branches, which have a limited impact on wood quality. In addition to the dynamic nature of branch growth, future modelling efforts need to account for their mortality and subsequent occlusion for a more accurate prediction of knot development over the life of the tree.

A potentially significant disadvantage of this study is the inability to distinguish between the sound and dead sections of individual knots. This is important because dead knots can have a detrimental effect on end-use properties and therefore are an important wood quality parameter (Vestol and Hoibo 2000). To account for the presence of dead knots, previous models have considered the live portion of a knot as being conical in shape and the dead portion as being cylindrical (Samson 1993a; Trincado and Burkhart 2008). This implied that once the maximum diameter was reached, the branch died and the diameter remained constant until self-pruning occurred. However, an analysis of our database showed that around 50% of the knots, more commonly the smaller ones, showed a peak in branch diameter along the pith-to-bark profile. Although it was not possible determine precisely from the CT images whether sections of a knot were alive or dead, we hypothesize that the point at which the maximum knot diameter is reached could correspond to the boundary between the sound and dead segments. Our knot diameter model (eq. [2]) was able to describe this peaking behaviour. One possible explanation for the decline in knot diameter beyond this point is shrinkage associated with branch mortality. Mäkinen (1999a; 1999b) reported that, on average, Scots pine branches died 7 years after diameter growth ceased. Following branch death, the growing stem slowly incorporates sections of the dead branches. Bark loss and gradual deterioration of the dead branch might result in a decline in knot diameter.

1.8. Conclusion

This study showed that it is possible to model knot shape accurately using a total of only five parameters from a combination of two nonlinear equations. The advantage of using our approach is its flexibility in describing a wide variety of knot shapes in two species with very different branching patterns, while still providing interpretable parameters. These parameters can, in turn, be modelled using a limited number of external branch and tree variables. The fact that knot properties can be predicted from current external data and without prior knowledge of the past tree and stand growth history allows for integration of the models into tree growth simulators for the prediction of end-use properties.

Chapitre 2: Annual development of knot morphology in Picea mariana: a modelling approach

2.1. Résumé

Le développement d'un arbre est un processus dynamique dans le temps et celui-ci est affecté par les contraintes liées à l'arbre et à son environnement. Il existe de nombreux modèles de la croissance annuelle de la tige des arbres. En revanche, l'intégration des nœuds dans ces modèles est beaucoup plus difficile en raison de la difficulté à obtenir des données internes, et en particulier à une échelle annuelle. La plupart des modèles existants représentent la géométrie du nœud à un temps donné. L'utilisation d'images de tomographie à rayons-X prises le long des tiges de 11 épinettes noires (Picea mariana (Mill.) BSP) et couplé à une analyse des cernes avec le logiciel Windendro^{TM} nous a permis d'extraire la forme 3D et la position de 5377 nœuds, et ce, pour chaque année de développement.

Cela nous a permis dans un premier temps d'analyser le ratio d'allocation de matière entre les nœuds et la tige au cours du développement de l'arbre, puis de développer un modèle linéaire mixte qui se veut dynamique dans le temps et qui décrit l'évolution de la morphologie d'un nœud (courbure et diamètre) en fonction de la croissance secondaire de la tige (largeurs de cernes) et d'autres caractéristiques externes de l'arbre (diamètre à hauteur de poitrine, hauteur, position dans l'unité de croissance). Le modèle de diamètre est segmenté en trois parties continues représentant l'initiation du nœud, sa croissance et sa mort. La courbure, étant influencée par le diamètre, n'a été segmentée en qu'en deux parties représentant une phase ascendante suivie d'une phase descendante. Lors d'une validation croisée de l'ajustement du modèle, les résidus de l'équation de courbure de l'épinette noire étaient inférieurs à 36.7 mm le long du profil de nœud dans 90 % des cas. Cette valeur était de 9.7 mm pour les résidus de l'équation du diamètre. De manière générale, les modèles de courbure et de diamètre se sont avérés non biaisés. Le modèle peut être intégré à des simulateurs de croissance des arbres capables de prédire l'évolution annuelle des largeurs de cernes, ce qui permettrait une représentation améliorée de la structure interne de la tige.

2.2. Abstract

Tree development is a dynamic process in time, which is affected by the constraints of the tree and its environment. It exist many models of the annual tree growth. However, the integration of knots in these models is complicated by the difficulties in obtaining internal data, particularly at an annual level. Most existing knot models represent geometry at a given time. The use of X-ray computed tomography images taken along the stem of 11 black spruce trees (Picea mariana (Mill.) BSP) coupled with a stem analysis using the Windendro^{TM} software allowed us to extract the three-dimensional shape and position of 5377 knots, for each year of development.

This allowed us first to analyze the ratio of knot to stem allocation during tree development and then, to develop a linear mixed model which was dynamic in time. The model describes the evolution of knot morphology (curvature and diameter) as a function of the stem's secondary growth (ring widths) and of other external tree characteristics (diameter at breast height, height, position along the growth unit). The diameter model was segmented into three contiguous parts representing the initiation of the knot, its growth and its death. As it was influenced by diameter, the curvature model only had to be segmented into 2 parts representing an upward phase followed by a downward phase. A cross-validation exercise was run to evaluate the accuracy of the model. The model residuals of the black spruce knot curvature equation were less than 36.7 mm in any part of the knot profile for 90% of the observations. The corresponding value from the diameter equation was 9.7 mm. Generally, the curvature and diameter models were found to be unbiased. The model can be integrated into a tree growth simulator capable to predict the annual ring width development, which would lead to an improved representation of the stem's internal structure.

2.3. Introduction

Knots are formed when branches are incorporated into growing tree stems. They are among the most important factors affecting the end-use characteristics of forest products (Buksnowitz et al. 2010), affecting both visual and mechanical properties (Dinwoodie 2000), and consequently lumber value (Macdonald and Hubert 2002). For these reasons, silviculturists are interested in understanding the trade-offs between stem radial growth rate and branch size (Hein et al. 2008; Weiskittel et al. 2007), while wood scientists have attempted to optimize lumber production by accounting for the location and size of knots within a log (Lemieux et al. 2002; Moberg and Nordmark 2006).

Early studies of knot development used time-consuming destructive methods, which tended to limit sample size (Harless et al. 1991; Lemieux et al. 1997b). In early models, knots were represented as a circular cone perpendicular to the longitudinal axis of the stem (Richards et al. 1979). An angle of inclination was later added, and further refinements led to the mathematical representation of knot curvature using segmented or polynomial equations (Leban and Duchanois 1990; Lemieux et al. 2001; Samson et al. 1996). However, complex knot models have rarely been integrated into computer-based systems capable of simulating tree growth and structure (Houllier et al. 1995; Mäkelä 2002; Perttunen et al. 1996). Duchateau et al. (2013c) developed a nonlinear model capable of representing a wide variety of knot shapes using external tree and branch characteristics, which can be integrated into a growth simulator. However, as this model provides a static representation of knot shape at a given point in time, it cannot take into account the full history of tree growth. There is, therefore, a need for models of knot morphogenesis that are capable of synthesizing the complex spatiotemporal interactions between a tree and its environment. For this purpose, functional-structural plant models (de Reffye et al. 1997) offer an interesting development framework, since they are dedicated to linking growth-driven processes with plant morphogenesis (Fourcaud et al. 2008).

Tree and branch ontogeny can be studied by conducting long-term experiments (Pretzsch 2005), but repeated observations are time-consuming and costly. To overcome this problem, Colin and Houllier (1991) elaborated a branch analysis protocol that has been subsequently applied and refined by several other authors (e.g. Achim et al. 2006; Mäkinen

and Mäkelä 2003; Weiskittel et al. 2007). The approach consists of simulating the dynamic processes of tree and branch growth through field measurements of the location and size of branches on trees of different ages. However, the simplicity of the approach comes at the expense of reduced accuracy for some attribute measurements, such as branch inclination or azimuthal orientation around the stem (Duchateau et al. 2013b). In addition, the resulting models cannot be truly dynamic since they are not parameterized using repeated measures on the same trees over time.

More recently, non-destructive techniques capable of rapidly generating high-resolution data have been developed, such as infrared imaging, optical scanning, computed tomography (CT) using X-rays or gamma rays, and magnetic resonance imaging (MRI) (Longuetaud et al. 2012; Moberg 2001). These innovations have enabled the parallel development of an alternative modelling approach that focuses on reconstructing the internal history of stem and knot growth. Using data acquired by CT and optical scanning, the aim of this study was to relate knot morphogenesis to the secondary growth of the main stem in black spruce (Picea mariana), a dominant species in the North American boreal forest. Specific objectives were therefore 1) to examine variation in the ratio of knot to stem allocation over time and 2) to derive empirical relationships describing the evolution of knot morphology as a function of secondary stem growth. Our intention was to describe these relationships in a way that facilitates integration of the models in FSPMs (de Reffye et al. 1997).

2.4. Materials and methods

2.4.1. Tree and knot measurements

A sample of 10 trees was collected from unmanaged stands in the North-Shore region of Québec, Canada. The selected stands covered a wide range of ages and stem densities, which induced some variation in terms of branch and knot development (Table 2-1). After felling, each tree was cut into 2.5 m logs, for a total of 41 logs. One-cm-thick discs were taken at the base and the top of each log. The sample material was then transported to the Institut National de la Recherche Scientifique in Québec City for CT scanning using a Somatom Sensation 64 (Siemens Medical Solutions USA, Inc.)

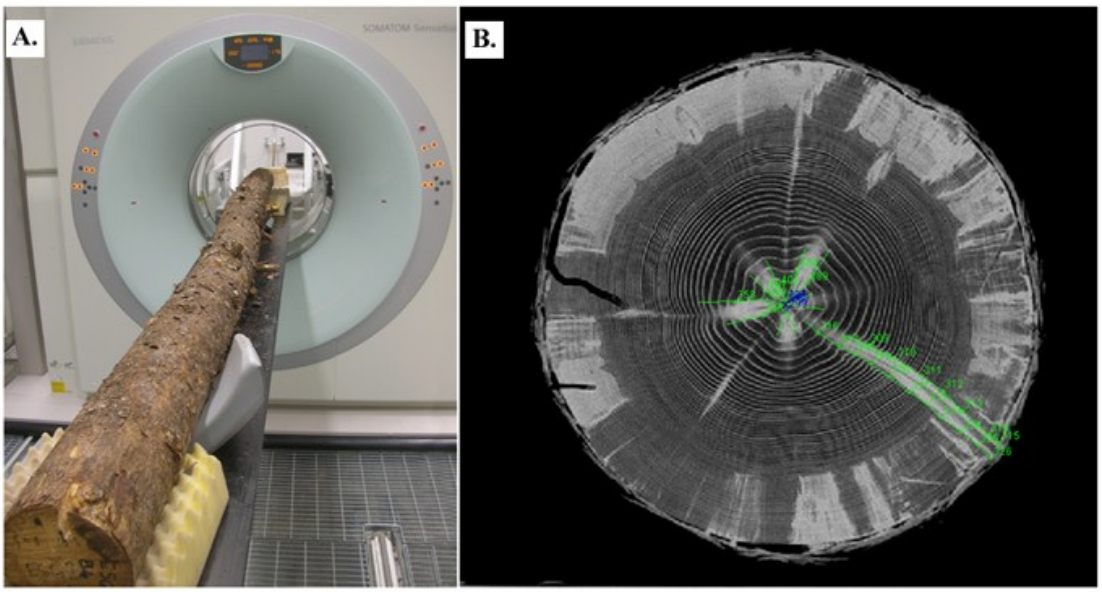

Figure 2-1A).This technique provided direct access to the internal characteristics of the scanned logs on the basis of wood density and moisture content variations. Each log was scanned at 2 mm intervals along the longitudinal axis with a 2-mm-wide X-ray beam (120 kV–50 mA), so that the scanned segments were contiguous. A notch was made using a chainsaw to indicate the north direction (azimuth = 0°) at the base of each log. This allowed for consistent image alignment to obtain accurate azimuthal information along the stem. Knot geometry was extracted using the ImageJ 1.44 free software (Abramoff et al. 2004), with a Java plug-in ('Gourmand', version 1.01) developed at INRA, Nancy, France (Longuetaud et al. 2012). Each knot was attached directly to the pith of the main stem, which was located manually on each image (

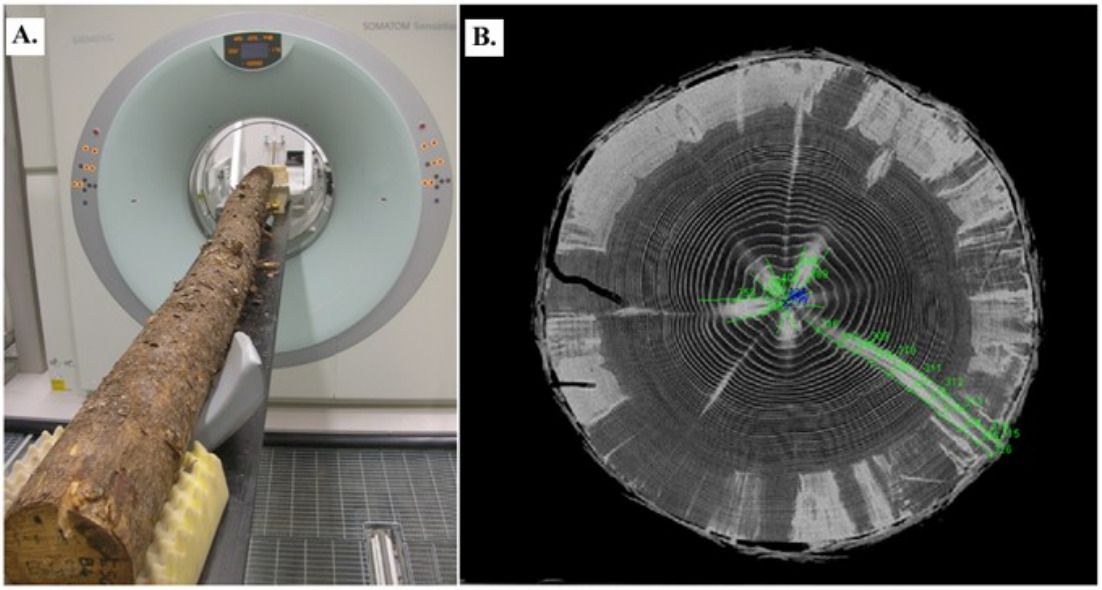

Figure 2-1B). Knot shape was then delineated from pith to bark on successive images. Following this step, the3D shape was reconstructed by fitting nonlinear equations describing the evolution along the radial profile of both the curvature (i.e. the vertical position of the central axis of the knot relative to its insertion point at the pith) and the diameter of each knot. Duchateau et al. (2013c) provided full details of the method.

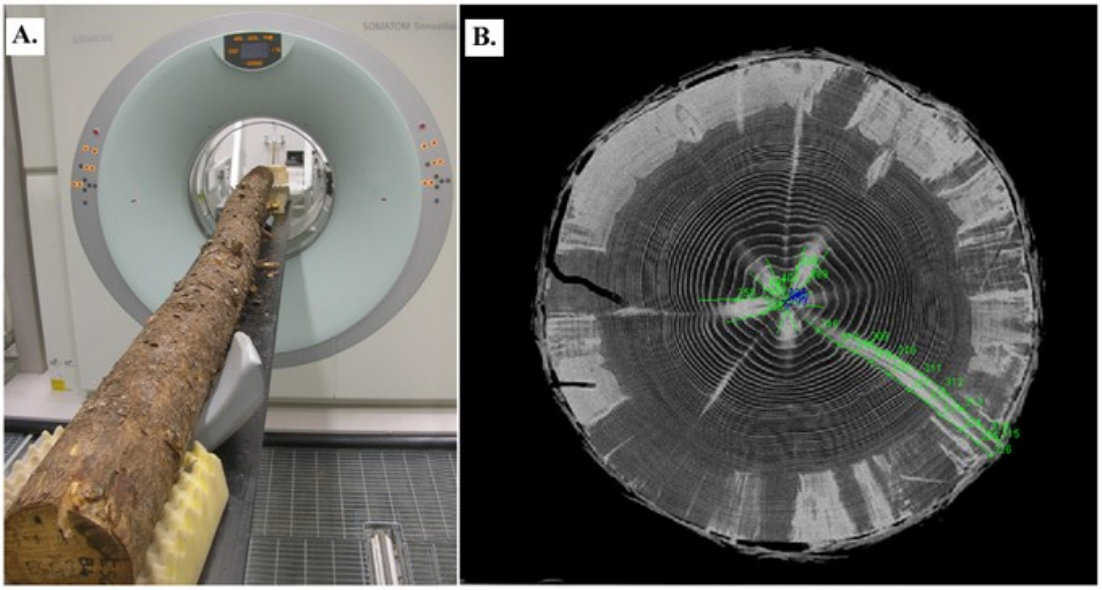

Figure 2-1 A) CT Scanning a 2.5 m log using a Somatom Sensation 64, **B)** Extraction of the position and diameter of each knot profile on CT scanning images using the ImageJ Java plug-in 'Gourmand'.

Table 2-1 Mean characteristics of the 10 sample trees in the dataset.

	Min	Max	Mean	SD
Age of the trees (years)	29	152	100	32
DBH (cm)	8	22.4	17.2	4.48
Height (m)	6.3	20.8	15.3	4.1
Knot diameter at bark (mm)	0.1	45.9	8.69	5.66
Maximum knot diameter (mm)	0.1	47	9.02	5.62
Relative position along the stem	0.01	0.93	0.39	0.23
Number of annual rings along the knot	6	140	60	27
Annual ring width (mm)	0.007	4.875	0.96	0.54

2.4.2. Annual ring data reconstruction

Annual ring data were not easily obtainable from the CT images, except close to the pith, due to factors such as narrow rings and the higher moisture content of the sapwood (Fig.2-1B). Therefore, each disc was optically scanned and annual ring boundaries were delineated with a semi-automatic image analysis algorithm (WinDENDRO^{TM}; Régent Instruments, Québec, 2005). Then, annual radial increments were calculated in the four cardinal directions. To link rings between two successive discs, all the ring-width series were cross-dated with the help of 'pointer years' (Guay et al. 1992). In total, 57 discs were analysed to reconstruct 41 logs containing the geometric profiles of 5377 knots.

To link the annual knot geometry to the annual radial stem increments, it was necessary to reconstruct the ring widths at the position of each knot. We used the discs taken from the end of each log (Figure 2-2A) and linked the rings dating from the same year of growth. This way, the radial growth of the stem was retraced from pith to bark in the four main cardinal directions. In each direction, a linear interpolation between the ring width values measured at the top and at the bottom of the log was used to estimate the ring widths at any longitudinal position along the log (Figure 2-2B). For the rings close to the pith on the

lower disc that were not present on the upper disc, the mean value of the coefficient of interpolation of the first five rings present on both discs was used as a good approximation. Because of ring deformity and deviations around the knots (Figure 2-3A), it was impossible to obtain precise annual ring data at the exact location of each knot. Therefore, annual ring increments were calculated using a linear interpolation between the two series of ring widths along the measured radii on each side of the knot (Figure 2-2C). This way, we obtained a vector of ring width values along the radial profile of each knot. Because the knot data obtained from the CT images gave us the precise radius of the stem at this location, a correction factor was applied to ensure that the end of the knot at the bark matched the position of last annual ring. For each knot, the observed stem radius was compared to the value estimated by linear interpolation and the percentage difference between these two values was applied as a correction factor for each annual ring width along the knot.

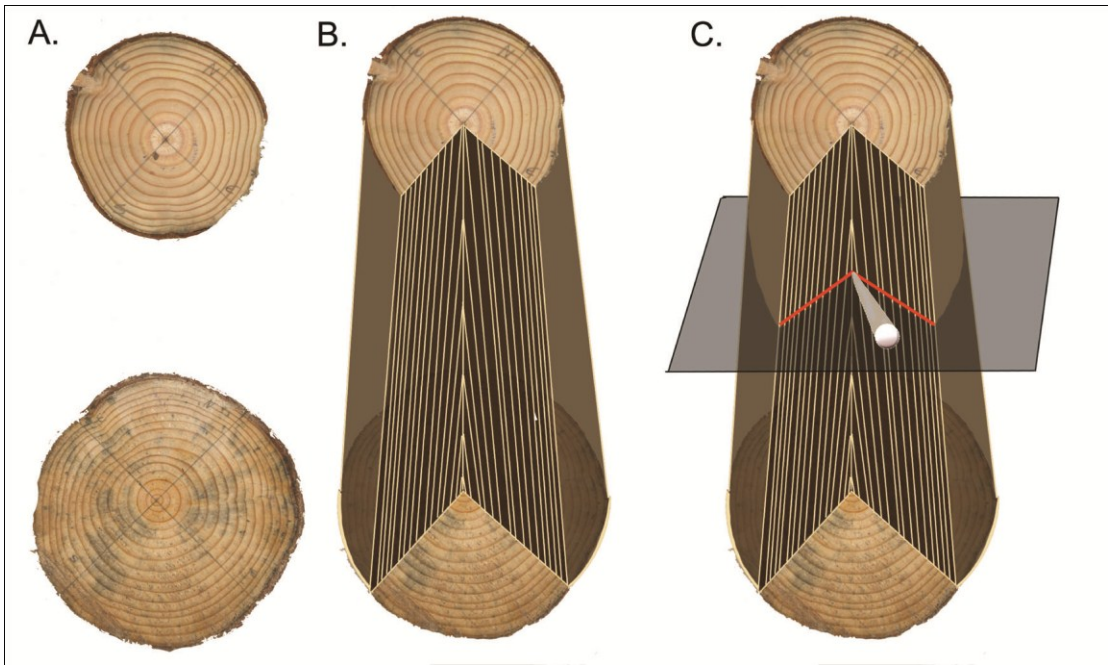

Figure 2-2 A) Annual ring width reconstruction process using two discs, **B)** interpolation of the rings between the two discs to reconstruct the log and **C)** selection of the two cardinal directions bordering the knot to reconstruct the ring widths along the knot profile.

2.4.3. Annual knot data

Knot geometry was characterized by the vertical position (Z) and diameter (D). The nonlinear equation used to reconstruct this knot geometry was a function of the position along the stem radius (Duchateau et al. 2013c). Therefore, using the position along the stem radius of each ring (Figure 2-3B), we were able to estimate the diameter (D_t) and the vertical position (Z_t) of the knot at ring t and, in turn, the annual increments in knot diameter (ΔD_t) and vertical position (ΔZ_t). Values of Z_t were obtained by locating the intersection of the geometrical center of the knot with the limits of the stem's annual rings. The D_t values correspond to the diameter of the knot perpendicular to the knot axis at each intersection point (Figure 2-3C). A full list of the variables and abbreviations used in this study is presented in Table 2-2.

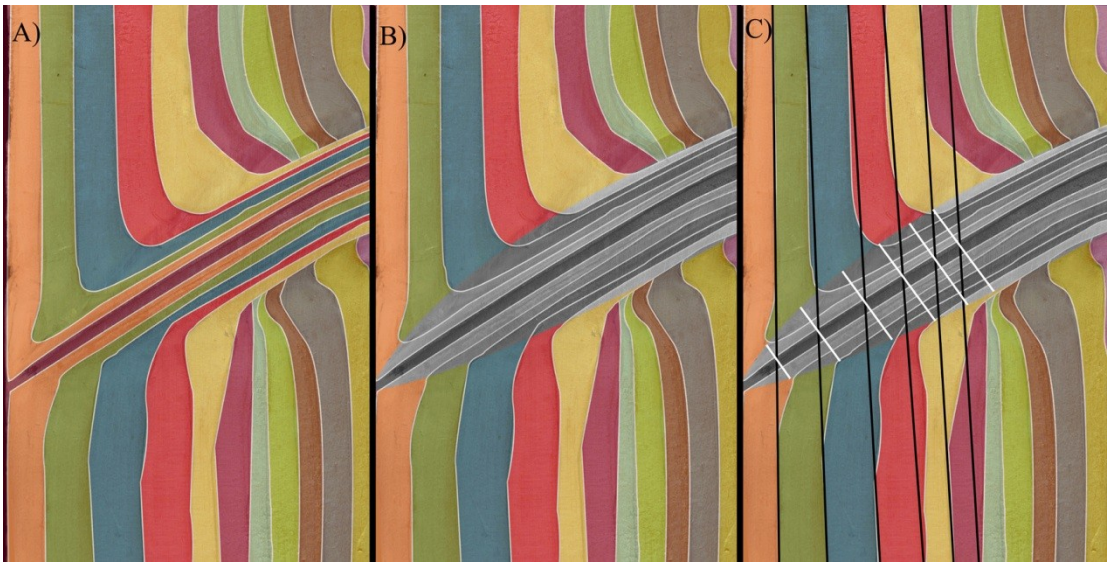

Figure 2-3 A) Example of ring width deformations around a knot, **B)** Description of the knot contour using the knot shape model of Duchateau et al. (2013c) and **C)** extraction of the annual knot data.

To examine the ratio of knot to stem allocation over time, we compared the annual basal area increments of the stem with those of the knots at the stem surface. For a given year of growth, the basal area (at 1.3 m) increment of the stem was first calculated. Then, the sum of all knot increments was calculated and the process was repeated for every year of growth for which we had complete annual growth along the stem (corresponding to the age

of the tree when it reached the height of the top log). Knots with a constant or decreasing diameter were considered dead and were therefore omitted from the analysis.

2.4.4. Knot model development

A statistical modelling approach was used to describe the temporal evolution of knot shape using annual ring- and tree-level characteristics as independent variables. The covariates were selected after calculating the variance inflation factors (VIF) for all potential explanatory variables, to address any potential multicollinearity issues. Variables that were highly correlated (VIF>4) were excluded from the models (O'brien 2007). Because of a high degree of collinearity between successive years, ΔD_t and ΔZ_t were selected as explanatory variables rather than the direct values of D_t and Z_t. In addition, since knot shape did not exhibit large annual variability, knot characteristics at time t-1 were used as independent variables to predict knot data at time t.

To account for the hierarchical structure of the data, we fitted linear mixed-effects models with tree, log and individual knot random effects (Pinheiro and Bates 2009). This was done using the nlme library of the R statistical programming environment (R Core Team 2013). Because heteroscedasticity (non-constant error variance) was detected in the plots of the model residuals, a power variance function of the annual ring number from the pith of the main stem was added to account for this. A continuous first-order auto-regressive term was added to account for any remaining autocorrelation between successive measurements.

Model selection was based on Akaike's information criterion (AIC) (Akaike 1974).

The final model used both the diameter and the annual radial increment of the stem at the location of the knot as predictor variables. To analyse the influence of the tree- and ring-level parameters on knot shape, we created a series of simulated knots using the model predictions. The first simulation tested the influence of the knot position along the tree stem (H_k), holding all other parameters at their mean values. We then examined the influence of various stem growth patterns by varying annual ring increments and again keeping the other parameters constant. A third simulation tested the influence of the relative position of the knot within the annual growth unit. Duchateau et al. (2013b) described the method used to identify the limits of each annual growth unit along the stem.

Table 2-2 Definitions and abbreviations of the variables used in this paper

	Description
Tree-level variables	
DBH_t	Diameter of the tree at breast height at time t (mm)
Age	Age of the tree at the time of knot initiation
H_k	Position of the initiation point of the knot along the stem (ground level = 0) (m)
GU_{pos}	Relative position of the knot initiation point along the annual growth unit (varies from 0 to 1)
GU_{len}	Length of the annual growth unit (m)
Ring-level variables	
RN	Annual ring number from the pith of the main stem
RW_t	Annual ring width at time t (mm)
RW_{tsum}	Sum of successive ring widths from the pith to the position at the time t (mm)
Knot variables	
ΔD_t	Annual increment of the knot diameter from time t-1 to t (mm)
ΔD_{t-1}	Annual increment of the knot diameter from time t-2 to t-1 (mm)
D_t	Predicted knot diameter at time t (mm)
D_{t-1}	Predicted knot diameter at time t-1 (mm)
ΔZ_t	Annual increment of the vertical position of the knot from time t-1 to t (mm)
ΔZ_{t-1}	Annual increment of the vertical position of the knot from time t-2 to t-1 (mm)

2.5. Results

2.5.1. Knot growth in relation to stem growth

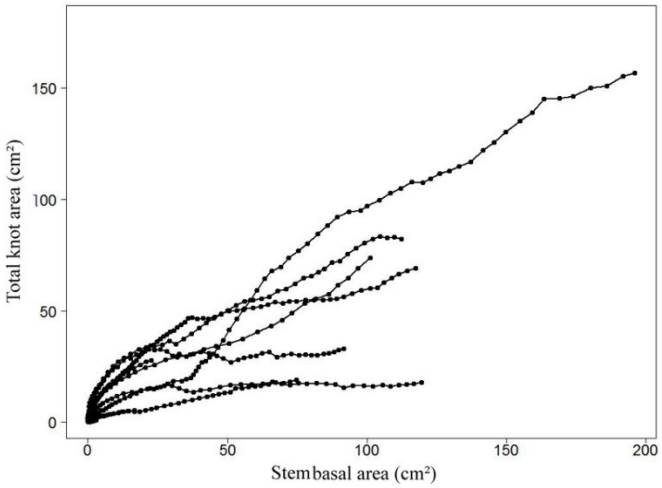

Figure 2-4 Evolution of total knot area at bark versus stem basal area at breast height (1.3 m) for each tree

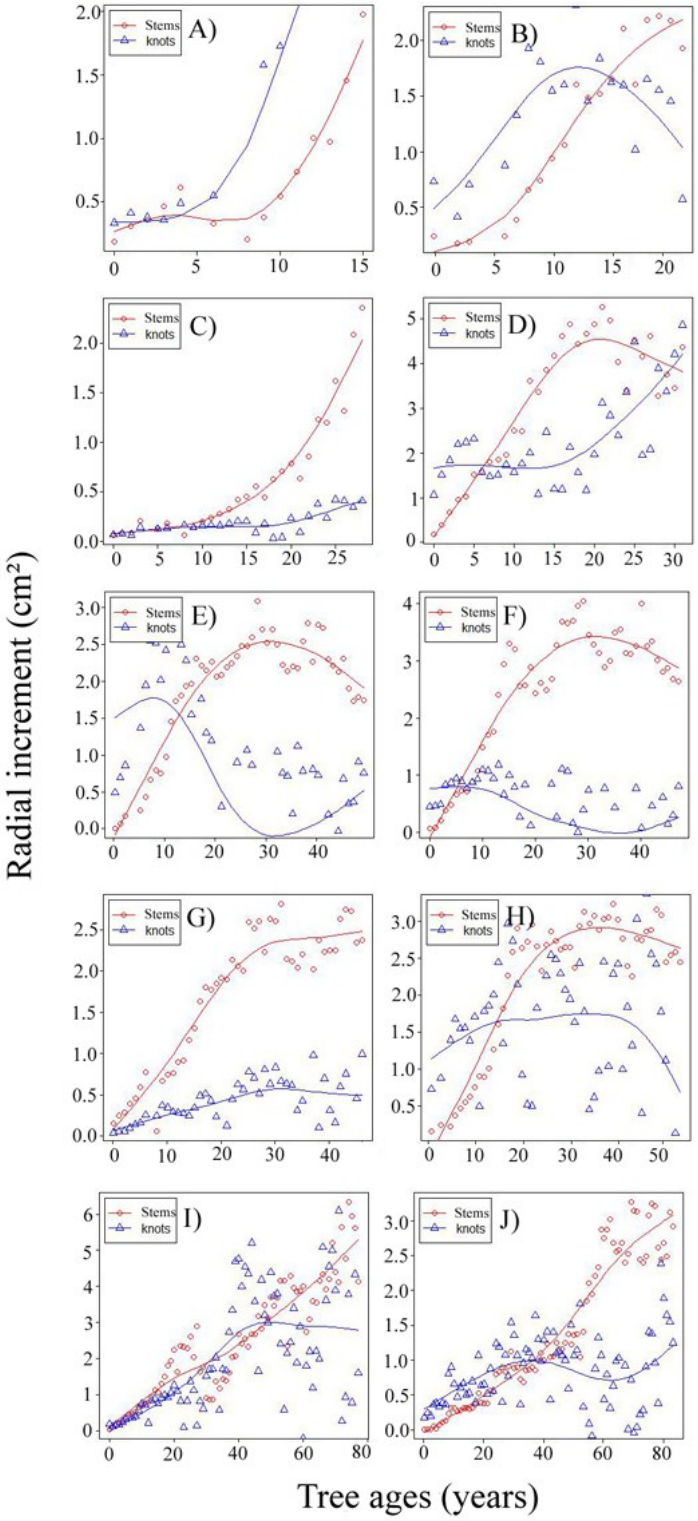

Figure 2-5 Simultaneous evolution of annual basal area increment for the trees (at 1.3 m) and the total knot area at bark. Note that different scales were used in each graph

Initially, total knot area increased rapidly in relation to stem basal area, before slowing down (Figure 2-4). The average ratio of knot to stem area was about 0.7, although there was substantial variation between trees. Annual growth increment was also highly variable between individual trees, suggesting that knot development could not be modelled using simple allometric functions of stem growth (Figure 2-5). In some cases, however, changes in stem area increments lagged behind increases or decreases in knot area increments (Figure 2-5A, B, C, E). In addition, some trees tended to favor stem development (Figure 2-5C, F, G), while others favored knot development (Figure 2-5A, D). In other trees, the relationship between the two variables was more balanced (Fig. 2-5I, J). In any case, for a given stem basal area increment, there was a large variation in knot area increment. We therefore determined that it was not possible to include allometric rules of knot versus stem area in the subsequent development of the overall knot model.

2.5.2. Models of knot development

An initial attempt was made to fit a single model describing both diameter and vertical position, and thereby reconstruct the entire knot in a single step. However, since knot diameter was strongly underestimated in the single model, we decomposed knot shape into separate models for diameter and vertical position.

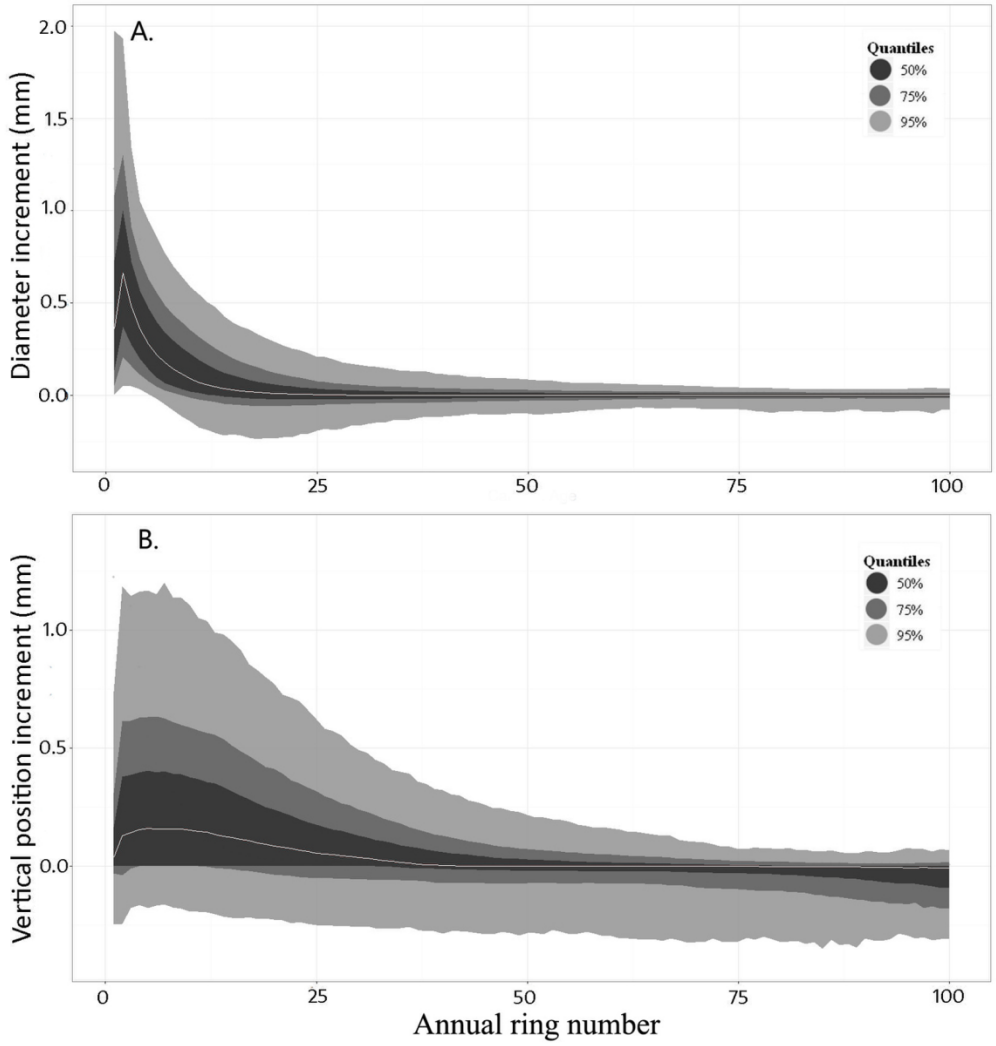

Figure 2-6 Distributions of **A)** annual diameter increment (ΔD_t) values and **B)** annual vertical position increments (ΔZ_t) as functions of the annual ring number from the stem's pith. The grey line indicates the median of all observations for a given ring number. Contours provide the distribution quantiles around the median

Values of ΔD_t typically increased rapidly close to the pith before declining. On average, the increment was largest in the first four years, before gradually decreasing until around year 25 (Figure 2-6A). These patterns of variation suggested that the knot diameter model could be separated into three sections. Firstly, the initiation phase was defined as the first four years of knot development, where the diameter increment was generally greatest. Because ΔD_t values did not follow a Gaussian distribution, D_t was modelled directly in this section. The second section corresponded to the remaining part of the active growth phase up to ring 25, where the increments were positive, but typically lower than in the first

section. The final section of the model represented the portion of the knot where variation in diameter increment was small. Table 2-3 shows the parameter estimates of the fixed effects for each section of the model. The annual diameter increment was influenced by the position of the knot along the stem (H_k, m) as well as its relative position within an annual growth unit (GU_{pos}). In addition, ΔD_t was found to be related to the DBH of the stem in the year of knot formation (DBH_t, m) and to ring characteristics of the main stem, such as annual ring width (RW_t, mm) and the distance from the pith (RW_{tsum}, mm). To evaluate model accuracy, knots were reconstructed using data estimated in the previous year as input (ΔD_{t-1}, D_{t-1}), and compared to the observed knot shape. Plots of the model residuals (observed minus predicted values) showed that, on average, knot diameter was slightly underestimated in the middle section of the knot profiles, but overall the model was unbiased (Figure 2-7A). The absolute value of 50% of the residuals was less than 2.6 mm along the pith-to-bark profiles and the absolute value of 90% of the residuals was less than 9.7 mm.

Table 2-3 Fixed effects parameter estimates and standard errors for each section of the knot diameter model. Section 1: knot initiation (years 1 to 4), Section 2: growth phase (years 5 to 25), Section 3: stabilisation and death (years 26 and over). Fixed effects terms are additive and × represents an interaction term. Abbreviations: see Table 2-2

	Section 1			Section 2			Section 3		
Variable	**Estimate**	**S.E**	***P*-value**	**Estimate**	**S.E**	***P*-value**	**Estimate**	**S.E**	***P*-value**
(Intercept)							0.0106	0.0010	<0.0001
ΔD_{t-1}				0.7862	0.0017	<0.0001	0.9183	0.0013	<0.0001
D_{t-1}	0.6827	0.0094	<0.0001	-0.0312	0.0004	<0.0001	-0.0009	0.0000	<0.0001
GU_{pos}	0.4153	0.0223	<0.0001	0.0172	0.0028	<0.0001	0.0053	0.0003	<0.0001
RW_{tsum}	0.0419	0.0060	<0.0001	0.0030	0.0001	<0.0001	0.0001	0.0000	0.0203
RW_t	0.4225	0.0149	<0.0001	0.0473	0.0011	<0.0001	-0.0085	0.0005	<0.0001
DBH_t	-0.0028	0.0005	<0.0001	-0.0008	0.0000	<0.0001	-0.0001	0.0000	<0.0001
H_k	0.0108	0.0045	0.0171				0.0003	0.0001	<0.0001
D_{t-1} x GU_{pos}	0.0834	0.0102	<0.0001	0.0146	0.0004	<0.0001			
RW_{tsum} x RW_t	-0.0269	0.0026	<0.0001	-0.0006	0.0000	<0.0001	0.0001	0.0000	<0.0001
ΔD_{t-1} x D_{t-1}				-0.0044	0.0003	<0.0001	0.0029	0.0002	<0.0001

The average annual variation of ΔZ_t was typically greater than zero until ring 40. Beyond this point the vertical position stabilized, before decreasing after ring 60 (Figure 2-6B). The knot vertical position profile was therefore separated into two sections delineated at ring number 50. The predictor variables were the same as for the diameter increment model, with the addition of D_t. The parameter estimates for the vertical position model are given in Table 2-4. Knots were again simulated using the predicted data from the previous year as input (Z_{t-1}). The model remained unbiased along the knot profile up to ring 75, with a slight overestimation beyond this point (Figure 2-7B). The absolute value of 50% of the residuals was less than 11.9 mm along the entire pith-to-bark profiles, while the absolute value of 90% of the residuals was less than 36.7 mm.

Table 2-4 Fixed effects parameter estimates and standard errors for each section of the knot vertical position model. Section 1: typically upward (years 0 to 50), Section 2: typically downward (years 51 and over). Fixed effects terms are additive and × represents an interaction term. Abbreviations: see Table 2-2

	Section 1			**Section 2**		
Variables	**Estimate**	**S.E**	***P*-value**	**Estimate**	**S.E**	***P*-value**
(Intercept)	-0.1443	0.0049	<0.0001			
D_t	0.0014	0.0003	<0.0001	-0.0001	0.0000	<0.0001
RW_{tsum}	0.0019	0.0000	<0.0001	0.0001	0.0000	0.0020
ΔZ_{t-1}	0.8411	0.0009	<0.0001	0.9651	0.0008	<0.0001
RW_t	0.0944	0.0008	<0.0001	-0.0031	0.0010	0.0018
GU_{pos}	0.0755	0.0021	<0.0001			
GU_{len}				0.0016	0.0009	0.0667
DBH_t	0.0001	0.0000	0.0118	0.0001	0.0000	0.0360
H_k	0.0025	0.0005	<0.0001	0.0001	0.0001	0.0501
D_t x RW_{tsum}	-0.0001	0.0000	<0.0001			
RW_{tsum} x RW_t	-0.0014	0.0000	<0.0001	-0.0001	0.0000	0.0001
D_t x GU_{pos}	-0.0084	0.0004	<0.0001			

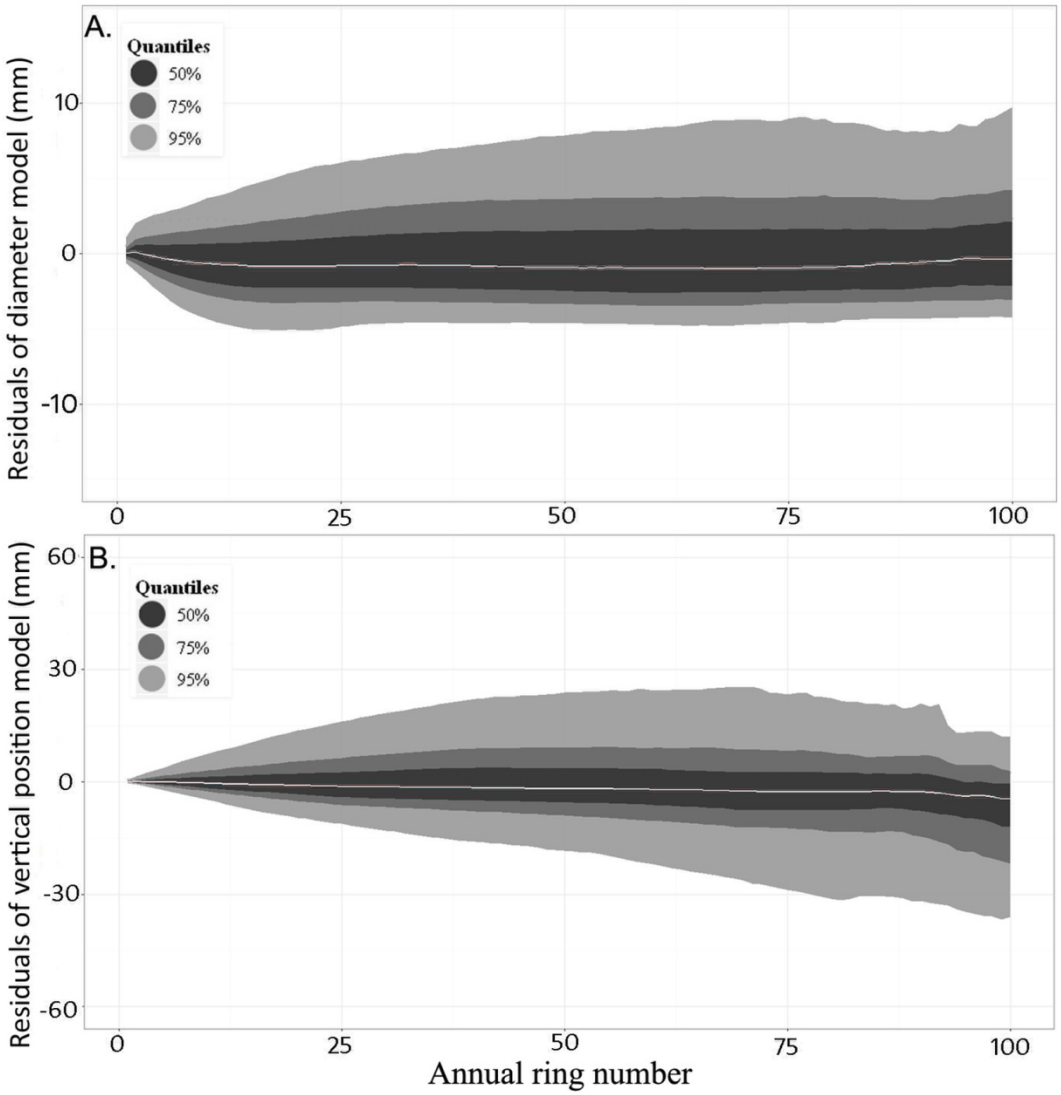

Figure 2-7 Distribution of the model residuals (sorted by quantiles) along the evolution of the ring number for **A)** knot diameter and **B)** knot vertical position. The grey line indicates the median of all observations for a given ring number. Contours provide the distribution around the median.

2.5.3. Simulations

The simulations indicated a relationship between the location of the knot along the stem and knot inclination, which increased towards the stem apex. In addition, knot diameter increment close to the pith was greater in the upper stem (Figure 2-8). Faster growth was associated with an excurrent (i.e. upwards) branch habit, while slower growth showed the opposite trend (Figure 2-9). This remained the case even for a scenario where initial

growth was slow but later increased. The model was also able to describe the variations in the knot profile from the base to the top of an annual growth unit, with knots located nearer the top having a larger diameter and a more upright orientation (Figure 2-10).

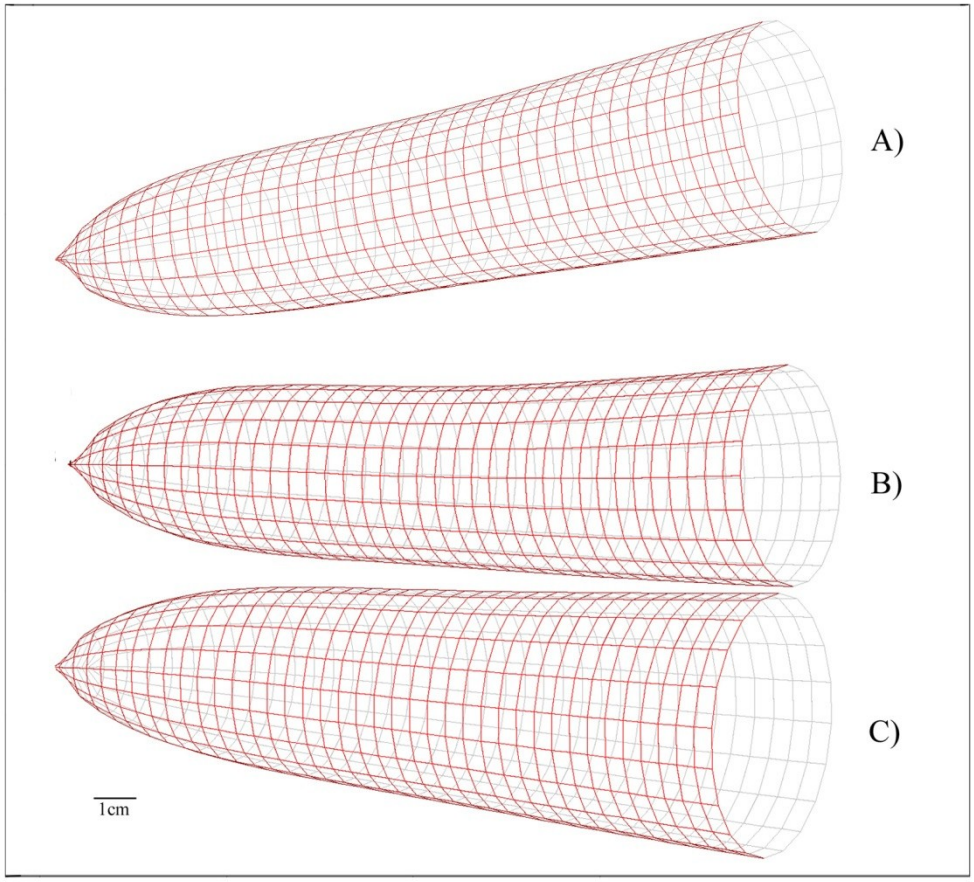

Figure 2-8 Effect of three different relative positions along the tree stem (**A**, 0.7; **B**, 0.4; **C**, 0.1) on the knot shape, with all other parameters held to their mean values. The segmentation on the knot profile corresponds to the annual growth rings of the main stem. The values 0.7, 0.4 and 0.1 indicate 70%, 40% and 10% of the tree height.

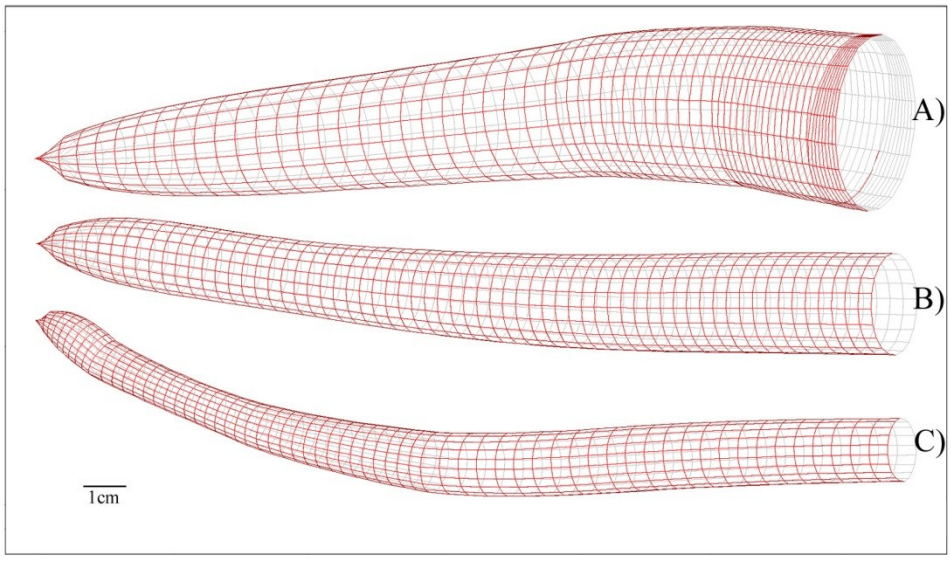

Figure 2-9 Simulated knots showing the effect of different growth patterns with age. **A)** Decreasing ring width, **B)** constant ring width and **C)** increasing ring width with small variations. All other parameters were held at their mean values. The segmentation on the knot profile corresponds to the annual growth increments of the main stem.

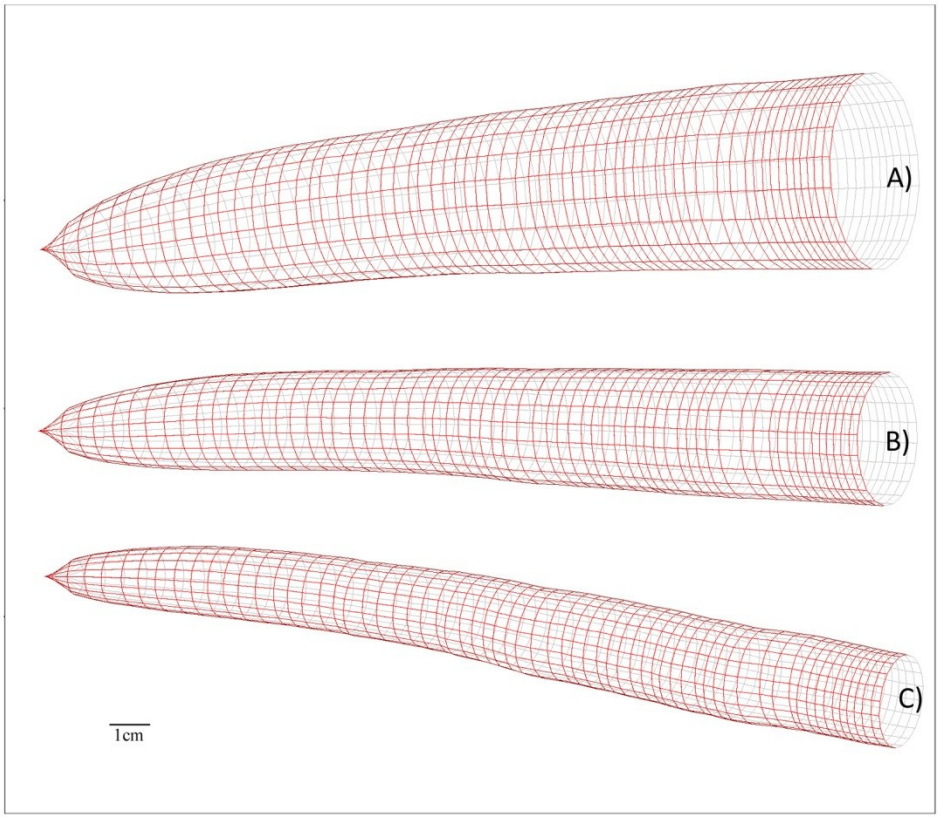

Figure 2-10 Simulated knots showing the effect of the relative position within an annual growth unit (**A**, 0.9; **B**, 0.45; **C**, 0.1) on knot shape. All other parameters were held to their mean values. The segmentation on the knot profile corresponds to the annual growth increments of the main stem. The values 0.9, 0.45 and 0.1 indicate 90%, 45% and 10% of the annual growth unit.

2.6. Discussion

This study provided new knowledge of the simultaneous annual development of knots and tree stems. We observed large variation in the knot area at the stem surface, even between trees with a similar stem basal area. This was surprising, as we expected knot growth to be closely linked with stem basal area increments. Although they were correlated to some extent, there were important variations around the general relationship. This could be a reflection of the limited pool of photosynthates available for tree growth. Since annual biomass production must be allocated to the needles, branches, reproductive organs, roots and stem (Kellomäki et al. 1999; de Reffye et al. 1997), a higher annual allocation to one component may affect the allocation to other parts of the tree. In a given year, it is therefore possible that a higher allocation to the stem might affect the allocation to branches. Over a period of years, this could affect crown size and in turn the overall production of photosynthates. This may explain the asynchronous growth patterns in Figure 2-5. However, more data will be necessary to fully understand these allometric relationships and include them in models of knot development.

Reconstructions of annual growth using stem taper equations (Garber and Maguire 2003; Mäkelä 2002; Sharma and Zhang 2004) are commonly used to create 'maps' of the internal structure of tree stems (Courbet and Houllier 2002; Ikonen et al. 2008; Pinto et al. 2003). However, to our knowledge very few studies have considered the behaviour of growth rings around knots (Pellicane and Franco 1994). In this study, the linear interpolation of annual ring width variation along the stems was a simplification, since in reality growth rings deviate around knots. However, because it was impossible to obtain exact information for each knot, this simplification proved to be the most efficient method of automating the analysis for a large number of observations. Although the use of the CT scanning technology produced a large amount of high-precision data, the extraction of the

diameter and position information for each knot had to be performed manually. This process resulted in some local deformations that did not reflect the true shape of the knots. For this reason, we chose to reproduce knot shape using the nonlinear equations developed by Duchateau et al. (2013c), which can reproduce a wide variety of shapes while maintaining smooth knot profiles.

Even though annual rings can be partially observed on CT images (

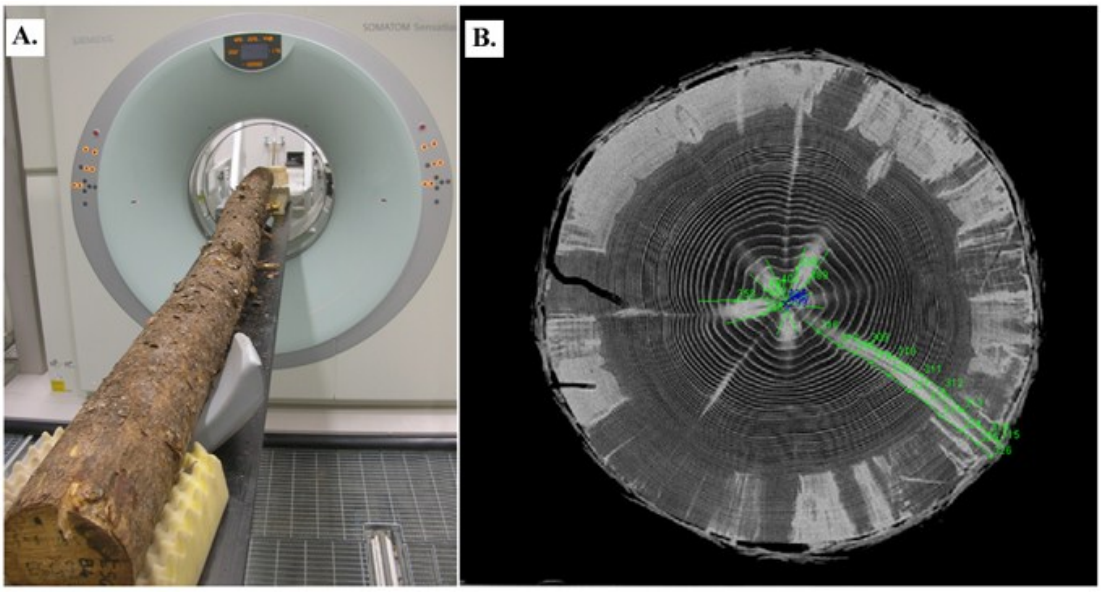

Figure 2-1B), there are no precise methods for detecting them. Jaeger et al. (1999) and Longuetaud et al. (2005) developed algorithms to automatically extract growth information from CT images. However, they had limited success since the algorithms could not detect growth rings inside knot boundaries or in the sapwood. Our results indicate that knot development was most strongly related to stem increments during the first 25 years of tree growth, by which time knots had typically reached their maximum diameter. The automatic detection of annual rings close to the pith of the main stem could therefore lead to further improvements in knot development models.

Previous studies developed segmented models in which each knot consisted of two different zones (Björklund 1997; Lemieux et al. 2001; Moberg 2001). The live section of the knot was represented by a cone and the dead portion by a cylinder, to reflect the cessation of growth. In this study, however, a decline in knot diameter was frequently observed (nearly 40% of cases), presumably as a result of branch deterioration after death. This trend was therefore explicitly included in the knot diameter model. In addition, the inclusion of the diameter and vertical position increments of the previous year as predictor

variables allowed for smooth transitions between the knot sections, and hence more realistic knot shapes.

The simulations under different growth patterns also produced plausible variation in knot shape along the stem and within annual growth units. The inclusion of annual growth unit information allowed the aggregation of nodal and internodal branches in the same model. These are separated in most branch distribution models (Auty et al. 2012; Colin and Houllier 1992; Maguire et al. 1994), since nodal branches tend to grow faster and live longer than internodal branches (Doruska and Burkhart 1994; Moberg 2001). However, analysis of the CT images showed no clear separation between these two groups (Duchateau et al. 2013b). Generally, knot diameter tended to increase progressively from the base to the top of the growth unit, which facilitated the development of a continuous model for all branches.

Simulations also showed that young branches had a typically excurrent habit, but over time the angle progressively decreased until they were oriented downwards. Since branch diameter and branch length are closely correlated (Kenk and Unfried 1980), larger branches generate increased bending moments at the point of intersection with the stem. The influence of snow can amplify this lever effect in boreal forest species such as black spruce (Bégin and Filion 1999). Accordingly, gravitropism has been proposed as a possible explanation for the decurrent growth of large branches (Yamamoto et al. 2002). However, there could also be an effect of vigour, since our simulations suggested that large, vigorous branches tend to have an excurrent habit.

The analysis of the residuals showed that the models were relatively unbiased and generally accurate. To improve accuracy even further, the annual increment model could be linked with a knot mortality model, enabling greater precision in the separation of live and dead knots. However, in this study it was not possible to precisely delineate the boundary between live and dead portions of the knots from the CT images. A further refinement would be the addition of a self-pruning model, so that occluded knots can be represented in the simulations. This might also prevent the simulation of unusual knot profiles, such as that shown in Figure 2-9C. This simulation represented a hypothetical case where stem growth was very slow for the first 20 years, before increasing. While such growth conditions could be generated when the canopy is opened suddenly as a result of

natural disturbances, in reality these branches may die before the end of the simulation period.

The use of CT scanning technology enabled the reconstruction of the simultaneous annual development of knots and tree stems. Although no consistent allometric pattern was found, we were able to produce a dynamic model of knot development as a function of stem radial increments and external tree characteristics. The model has the potential to improve the representation of the internal structure of woody stems in functional-structural models of tree development.

Chapitre 3: Modelling knot distribution in trees using the CT-scanning technology

3.1. Résumé

La modélisation de la croissance des plantes est un domaine de la recherche très important qui a connu un intérêt croissant ces dernières années grâce au développement de systèmes informatiques capable d'intégrer ensemble différents modèles biologiques. Cependant, la plupart des données utilisées pour paramétrer ces modèles sont basées sur des mesures externes qui peuvent être imprécises, notamment dans la description spatiale de la branchaison. Dans les arbres, cela peut induire une sous-estimation du nombre d'unités de croissance ainsi que des erreurs dans la position et la distribution de ces unités le long de la tige. Des images de tomographie à rayons-X prises le long des tiges de 33 épinettes noires (*Picea mariana* (Mill.) BSP) ont été utilisées pour extraire la forme 3D et la position de 23 040 nœuds. À l'aide de ces données précises, nous avons mis au point une méthode empirique basée sur deux filtres successifs pour améliorer le positionnement des unités de croissance et corriger l'importante sous-estimation du nombre d'unités observées lors des mesures externes. La sélection des pseudo-verticilles de branches dont la surface basale était supérieure au 75ème percentile, puis une distance minimale de 0.075 m entre chaque unité de croissance nous a donné le nombre d'unités le plus proche de la réalité. Une fois les unités de croissance décrites, nous avons élaboré une simulation de la distribution des branches le long de ces unités. Le nombre de branches et leurs positions selon leurs diamètres ont été modélisés principalement en fonction de la longueur de l'unité de croissance et de sa position dans la tige. À l'aide de statistiques circulaires et du test de Rayleigh, la distribution des branches a été modélisée autour du tronc. La plus grosse branche de chaque unité suivait une distribution de Von Mises avec une orientation préférentielle au sud-sud-ouest (213°). L'angle entre la 1ère et les 2ème et 3ème plus grosses branches suivait une distribution bimodale. La distribution de l'ensemble des branches restantes peut être considérée comme uniforme. Cette analyse a été rendue possible grâce notamment à la précision obtenue en utilisant la tomographie. Elle permet une amélioration significative des modèles de branchaison de l'épinette noire.

3.2. Abstract

Plant growth modelling is an important field of research and in recent years there has been an increasing interest in the development of computer-based systems capable of integrating different biological models. However, most of the data used to parameterize the existing models are based on external measurements, which can be imprecise, especially in the spatial representation of the branching. In trees, this can induce an important underestimation of the number of growth units and lead to errors with regards to their location and their distribution along the stem. X-ray computed tomography (CT) images taken along the stems of 33 black spruce (*Picea mariana (Mill.) B.S.P.*) trees were used to extract the three-dimensional shape and the position of 23040 knots. With these accurate data, we developed an empirical method based on two successive filters to select the best position of the GU limits and correct the important under-estimation observed with the external measurements. The selection of branch pseudo-whorls with a basal area greater than the 75th percentile and a minimum distance between two units of 0.075 m gave the number of growth units closest to the reality. Once the limits of the growth units were located, we analysed the distribution of branches along these units. The number of branches and their positions according to their diameters were modeled mainly as a function of the length of the growth unit and its position along the stem. Using circular statistics and Rayleigh's test, the distribution of branches was modeled around the stem. The biggest branch of each growth unit followed a Von Mises distribution with a preferential orientation towards a south-southwesterly direction (213°). The angle between the 1st and the 2nd and 3rd largest branches followed a bimodal distribution, while the remaining branches showed a uniform distribution. This analysis was made possible by the accuracy of the data obtained by X-ray tomography. It led to a significant improvement of branch distribution models for black spruce.

3.3. Introduction

Plant growth modelling is a very important field of research and in recent years there has been an increasing interest in the development of computer-based systems that can

integrate both functional and structural aspects. Most relationships between the architectural development of the tree crown, stem growth and internal wood properties have an ecophysiological and/or biomechanical basis (Fourcaud et al. 2008). However, the interactions between plant functions, organogenesis and the environment are complex, and very few models have successfully integrated all aspects (Mathieu et al. 2009). To meet different objectives, plant organisation may be read at different scales, but in order to represent processes with accuracy, it is necessary to study the organization of plant components, their dynamic development and their three-dimensional distributions.

In trees, there is evidence that structure is influenced by the need to optimize the exploitation of resources (Barthelemy and Caraglio 2007). The fact that resources are not distributed equally in all directions and vary over time can lead to a non-homogenous structure of the wood characteristics (density, MOE, microfibril angle, etc.) (Xu and Harrington 1998) and of the branches (Pont 2001). In temperate regions, tree development occurs in an annual cycle and the elongation of a shoot in one year is called a growth unit (GU). This is an important component of existing models of branch distribution in trees (Achim et al. 2006; Auty et al. 2012; Colin and Houllier 1991). Development may vary between successive GUs along the main stem (Auty et al. 2012; Ikonen et al. 2008) as well as within a GU i.e. along and around the axis of the stem in a given GU (Benjamin et al. 2009a; King 1998). Integrating such variations in branch distribution models would allow representing the non-homogeneity of the final tree structure.

Most of the data used to parameterize the existing branch distribution models in trees are based on external measurements (Auty et al. 2012; Mäkinen and Mäkelä 2003). An advantage of this approach is that data acquisition is relatively simple and can be accomplished with limited equipment (Colin and Houllier 1991). However, this simplicity comes at the expense of a reduced accuracy for certain measurements, such as branch inclination or azimuthal orientation around the stem (Duchateau et al. 2013c).

In addition, branch distribution models can be static (Auty et al. 2012) or dynamic in time (Weiskittel et al. 2007). A fully dynamic approach generally requires expensive and time consuming experiments where repeated measurements of tree and branch characteristics are obtained (DeBell et al. 2004). This explains why most studies have used a pseudo-

dynamic approach, which consists of simulating the dynamic processes of tree or branch growth through static measurements on trees of different ages (Achim et al. 2006; Colin and Houllier 1991; Mathieu et al. 2009). More recently, non-destructive techniques, such as infrared imaging, optical scanning, computed tomography using X-rays or gamma rays, and magnetic resonance imaging (MRI) (Longuetaud et al. 2012; Moberg 2001), have been developed that can generate high resolution data much more rapidly than destructive methods. These techniques can be used to reconstruct the internal history of stem and branch growth (Duchateau et al. 2013a). The annual secondary growth can be partially observed on CT images through the identification of annual rings, but methods to precisely detect these rings limits, and hence the limits of the GU, are still under development (Longuetaud et al. 2005). This task is made particularly challenging in the sapwood, where the presence of water in fresh-cut trees decreases the contrast between early- and latewood. However, one aspect where CT scanning can provide precise information is in the distribution of branches (or knots) along the stem, from their origin at the stem's pith to their position at the bark (Duchateau et al. 2013a; Duchateau et al. 2013c).

Black spruce (*Picea mariana* (Mill.) BSP) is the dominant coniferous species in the North American boreal region. Itcovers a large geographical area with a wide range of climatic conditions (Gamache and Payette 2004). It is also one of the most important commercial species in eastern Canada (McKenney et al. 1992). Its architecture follows Rauh's model and has monopodial, orthotropic axes with rhythmic growth (Bégin and Filion 1999). However, its survival in a wide range of climates (including extreme conditions at the limit of the tree line) is facilitated by a high reiterative capacity, which characterises its ontogenic development. This implies a strong capacity of duplicating a vegetative structure through a possible dedifferentiation of the axes and a large number of dormant buds at the bottom of the GUs (Bégin and Filion 1999). In addition, it is a long-lived species with a typical life expectancy of 200 years in large parts of the boreal forest (Farrar 1996) and up to 500 years at the tree line. These characteristics of the species imply that 1) the branches and knots are abundant in mature trees and 2) it is difficult to identify growth units along the stem, and hence the distribution of the branches along and around them. Our aim for this study was to develop a method to locate growth units along the stem and to describe

the distribution of knots within these units in black spruce, using data extracted by X-ray tomography.

3.4. Materials and methods

3.4.1. Plant material

The objective of the sampling was to obtain a wide range of tree and branch development stages, so samples were selected trees along two chronosequence of stand ages, one near the town of Baie-Comeau, Qc, Canada, and one 200 km further north. A total of 33 black spruce trees ranging from 9 to 208 years in age were sampled from unmanaged stands. Each chronosequence was composed of eight sampling sites selected across a range of time since the last stand initiating fire. Two trees per stand were selected randomly according their social status within the stand i.e. one dominant and one co-dominant tree. The only exception was for the oldest stands (> 200 years since the last fire), which had reached an uneven-aged structure (Bouchard et al. 2008). In these cases the selection was based on tree ages using cores samples, a young and an older tree having grown in different competitive environments. At first, external branch and tree measurements were made following the protocol established by Colin and Houllier (1991), later refined by Auty et al. (2012). Prior to felling, a line indicating the north-facing part of the stem (azimuth = 0°) was marked with paint, and this line was continued along the length of the stem after felling. Total tree height (H, m) and diameter at breast height (dbh, cm) were then measured. The positions of the GUs were determined visually, by looking at bark scars in the youngest parts of the tree or otherwise considering that the biggest branches were at the top of the GU (Colin and Houllier 1992). For each annual growth unit starting from the stem's apex, we determined the number of live and dead branches, the position along the stem and the diameter of the stem at the base of the GU. The branch characteristics were also recorded (diameter, inclination and azimuth).

Then, knowing the potential imprecision of the external measurements and the consequent difficulty to find the GU limits, X-ray tomography technology was used to obtain more accurate information, which provided a complete description of the GUs including

occluded knots. After the field measurements were completed, trees were cut into successive 2.5 m logs. Logs were cut so that they included the stem between stump level (0.1 m above ground level) and the level where stem diameter over bark was at least 9.1 cm (merchantable height). For a subsample of 41 logs, we took discs at each ends. Before cross-cutting the stem, longitudinal marks were made with a chainsaw, spanning on both sides of the cuts. Since these marks were visible on the CT-Images, it was possible to precisely orientate the images for all logs within the same tree. The number of logs per tree varied between one for the youngest tree and seven for the oldest. Logs were transported to the Institut National de la Recherche Scientifique in Quebec City for X-ray computed tomography (CT) scanning using a Somatom Sensation 64 (Siemens Medical Solutions USA, Inc.). Each of the 107 logs obtained were scanned at 2 mm intervals along its longitudinal axis with a 2-mm-wide X-ray beam, so that the scanned segments were contiguous. In total, we obtained the internal profiles of 23 040 branches (Figure 3-1). To perform the reconstruction of the knot profile, we used the ImageJ 1.44 freeware (Abramoff et al. 2004), with a Java plug-in ('Gourmand', version 1.01) developed at INRA, Nancy, France (Colin et al. 2010) which allow the semi-manual extraction of knot geometry. Another Java program, 'Bild3D' was then used to reconstruct the 3D shape of the stem, and the position and 3D geometry of each knot using the rectangular Cartesian coordinate axes x,y,z (For more details about the method, see Duchateau et al. 2013c).

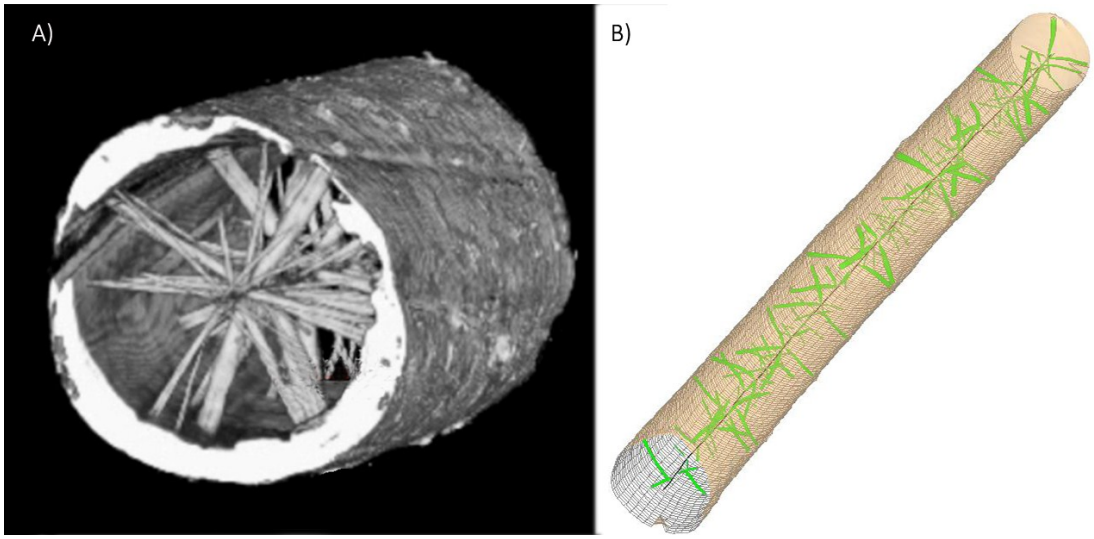

Figure 3-1 A) CT Visualisation of the internal part of the branches from the CT images and **B)** three-dimensional reconstruction of stem shape and of the geometry of each knot using the "Bil3D" Java software

3.4.2. Data analysis

3.4.2.1. Growth unit selection

The selection of the GU limits with the external measurements is generally based on branch diameter, since nodal branches located at the top of the GU are usually bigger than internodal branches. However, in the case of the black spruce trees, the number of branches per GU can be really high and there is no clear difference in the diameter ranges of nodal and internodal branches. In the youngest part of the tree, the presence of scars on the bark can be used as a good indicator of the GU limits, but these scars disappear after a few years. In addition, in the lower part of the stem several branches can have died, broken and been occluded. To verify the accuracy of GU limits selected using external measurements, we used the discs taken between each log to deduce the number of GUs in every 2.5 m log. Since there is a difference of one ring between two annual growth units in a tree stem, we could compare the number of rings at each end of the log and obtain the exact number of GUs within a log.

Different knot parameters at bark were then tested to find the locations of the GU limits. Knot diameter was first considered, but due to the large number of branches with similar diameters, it proved impossible to precisely discriminate the limits. We hence developed a method based on two filters to select the best position of the GU limits using the basal area of branches. Since we had the internal information, it was possible to determine where each branch was initiated (Colin et al. 2010). Despite the fact that it was possible to have big branches at any location along a GU, we expected that they should be concentrated at it top i.e. at the location of the pseudo-whorl (Moberg and Nordmark 2006). Therefore, when branches appeared to on the CT images as being initiated at the same position along the stem's pith, we summed the branch basal areas. This provided a series of peaks in basal area which could potentially represent the location of pseudo-whorls (Figure 3-2). We applied different thresholds to select potential GU limits. Then, minimum distance thresholds were also tested to make sure that GUs of plausible lengths were identified. If the distance between two potential GU limits was under this threshold, we only kept the limit positioned the highest along the tree.

We adjusted these thresholds to our subsample of 44 logs for which we had a disc at each extremity. The final selection was made according to the combination of thresholds that provided the smallest overall bias when compared with the number of GUs in each log measured from growth rings. Once the best combination was established, we applied this empirical method to our complete set of sample logs.

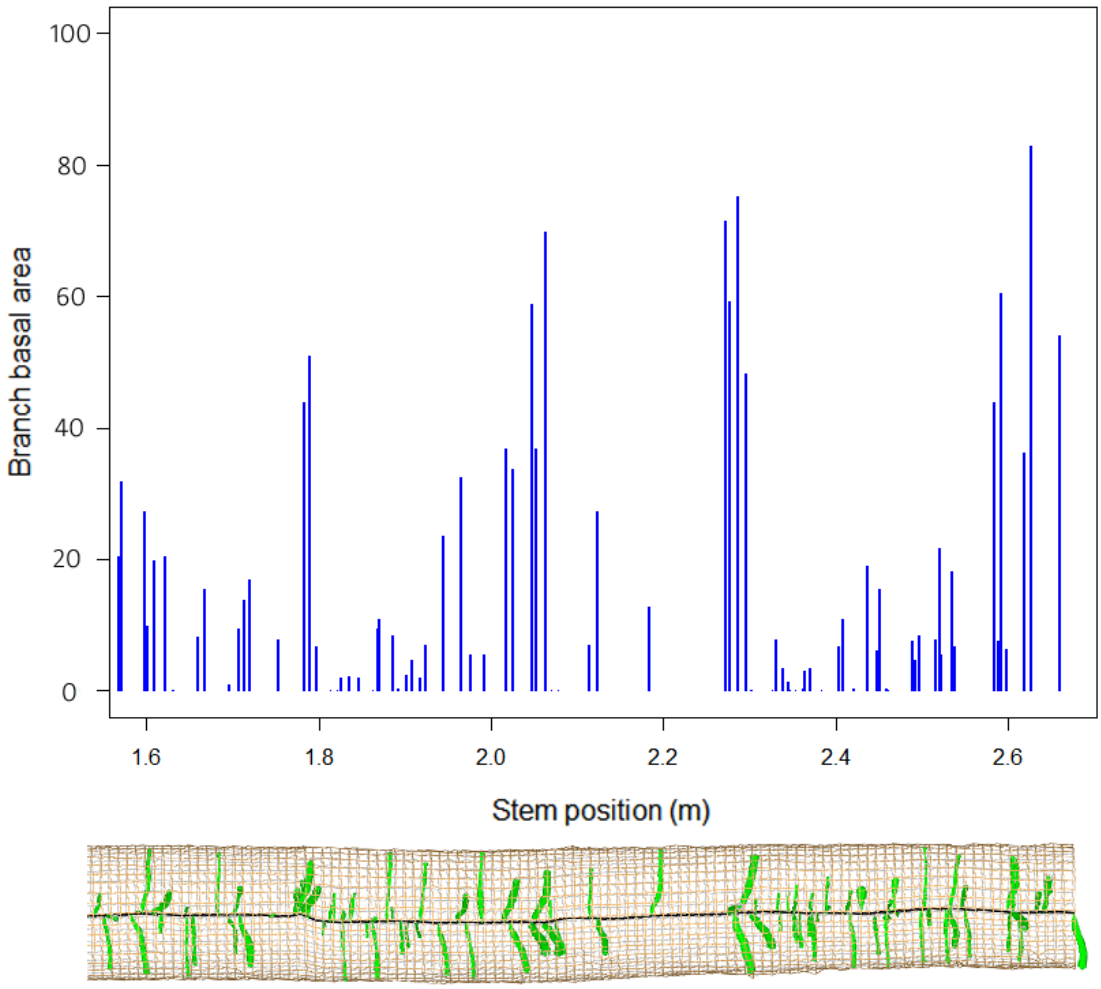

Figure 3-2 Distribution of branch basal area along a stem

3.4.2.2. Distribution and status of branches within a growth unit

To simulate the development of knots on an entire tree, we firstly needed to predict the number of branches in each GU. In the northern spruce species, the buds can be pre-formed or neo-formed (Colombo 1986). Since we did not have the information on the

needles, we tested two empirical predictors i.e. the length of the GU in the previous year and the current one using a Poisson regression. The position along the stem and the DBH of the tree were also added as covariates in the statistical analysis.

Secondly, we studied the position of the branches on the GU. Most branch distribution models separate nodal from internodal branches (Colin and Houllier 1991; Weiskittel et al. 2007), as the latter are typically much smaller, have a shorter lifetime and exert a much smaller influence on plant development and on wood properties. However, unlike for other species, it was difficult to clearly delineate nodal and internodal branches in black spruce. Each branch was thus ordered by diameter ranks, as proposed by Benjamin et al. (2009b) and their relative vertical positions were calculated. Then, a stochastic distribution was simulated to obtain a realistic positioning of the branches along the stem according to their rank. We analysed the location of four of the biggest branches in each GU to determine a section at the top of the growth unit that could be considered as the nodal zone for the purposes of our following analyses.

Finally, we studied the position of the branches around the longitudinal axis of the stem. For this purpose, we had to use statistical methods capable of taking into account the circular distribution of the branches around the stem. We used the 'CircStats' package (version 0.2-4) in the R statistical programming environment (version 2.15.1) (R Development Core Team 2012). The distribution of branch azimuths at the tree or at the GU level was characterised by two parameters. A circular mean, which is a resultant vector direction for all the data, and a resultant vector length, which describes the dispersion around this mean. The larger the value of this vector, the more concentrated are the data around the mean direction (Jammalamadaka and Sengupta 2001). We used Rayleigh's test to determine if a distribution was significantly different to a uniform (random) distribution (Batschelet 1981). We studied the distribution of the biggest branches both at the tree and the GU levels, and attempted to generate datasets with the same distributions. For this purpose, the von Mises distribution was used as it provides a continuous probability distribution around the circle (also known as the circular normal distribution) (Best and Fisher 1979). This distribution is characterized by two parameters, the mean azimuth (mean) and a parameter (k) describing the concentration of the data around the mean azimuth. The closer k is to zero, the more concentrated are the data around the mean. To

refine the branch model and adjust the simulation for each tree, we analysed the distribution at the tree and at the GU levels and tested for the influence of tree characteristics on both.

We then supposed that the branches located in the same GU can have an influence on each other, and that this influence increases with the diameter of the branch and with the proximity between them. This analysis was only performed on the biggest three branches in each GU. The angles between the first and the second and between the first and the third branches were calculated. An attempt was made to model their distributions as functions of GU or tree characteristics.

In order to obtain realistic simulations, it was necessary to integrate branch mortality and self-pruning models. Each knot profile was reconstituted year by year using the method developed by Duchateau et al. (2013a), so that annual knot diameter increments were obtained. Once this increment became equal to or smaller than zero, we considered that the branch was dead. Once the branch was classified as dead, we calculated the probability that it remained present or that it was self-pruned. This way, both the mortality and the self-pruning models gave an annual time series of probabilities. The time series were generated using generalized mixed models (GLMM) (Koper and Manseau 2009). The status of the branch was treated as an annually-assessed binary variable. A logit-link function with a binomial distribution was used to model the probability that a branch remained alive first, and then pruned.

3.5. Results

3.5.1. Growth unit selection

We observed that the external measurement induced an important underestimation of the total number of GUs in logs. On average, we missed 2.4 GUs per 2.5m log (15% of the GUs) and the standard deviation was equal to 3.7 (Figure 3-3A).

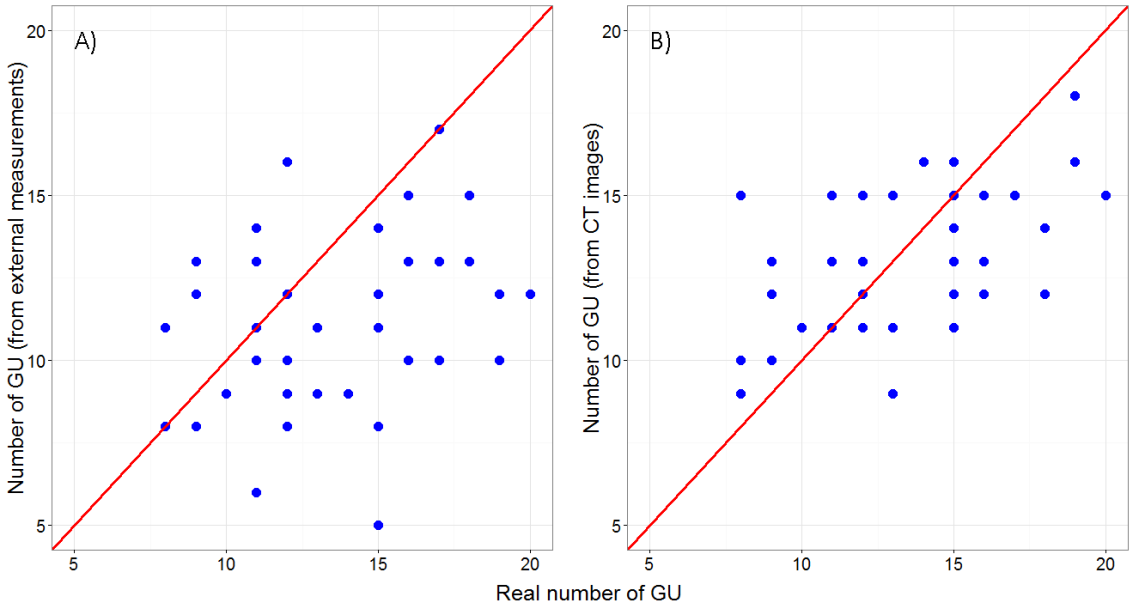

Figure 3-3 Comparison between real (measured using growth rings) and **A)** external estimations of the number of GUs and **B)** the estimations from the CT images

Results from the CT data revealed that any peaks greater than the 75th percentile on the branch basal area graphs (see Figure 3-2) was could be considered as a potential GU limit (Figure 3-4A). Then, a minimum distance equal to 0.075 m gave the number of GUs closest to the reality (Figure 3-4B, Table 3-1). The standard deviation was still rather high (2.8), but the mean value of the residuals approached 0 (0.195).

Table 3-1 Selection of the best thresholds to improve the identification of GU limits

Distance selection (m)	50th percentile		75th percentile		90th percentile	
	Mean	sd	Mean	sd	Mean	Sd
0.02	-22.09	5.15	-9.59	5.10	1.37	3.84
0.06	-0.49	4.14	-1.56	2.67	3.19	3.30
0.075	3.34	4.14	**0.19**	**2.82**	3.44	3.33
0.01	9.5	2.59	2.54	3.56	4.05	3.28

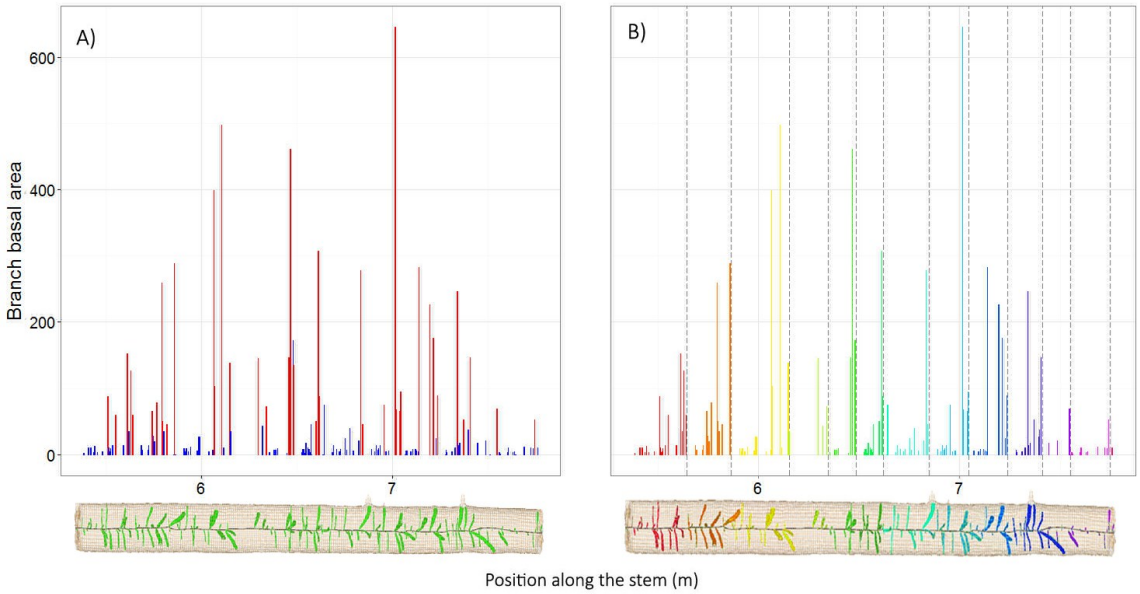

Figure 3-4 Distribution of the branch basal areas along the stem from data extracted using the ImageJ Java plug-in 'Gourmand; **A)** selection of the biggest branch basal areas as a potential GU limit; **B)** selection of the different growth unit using our two filters method

There was no significant effect of tree age on the difference between the number of GUs measured using ring counts and that obtained by applying the filters. However, we observed a marginally significant negative influence of the position along the tree (p = 0.06). This suggested that the farther from the top of the tree, the more we tended to overestimate the number of GUs.

In order to study the branch distribution in the remaining parts of this study, the thresholds for GU identification were applied to the complete CT scanning dataset. To avoid obtaining incomplete GUs due to the sampling of discs, it was decided to suppress GUs located at the extremities of each log. In total, we retained 1171 GUs (Table 3-2).

Table 3-2 Mean characteristics of the GUs estimated from the internal dataset

		Percentile				
	Mean	0%	25%	50%	75%	100%
Number of GUs per log	13	8	11.5	13	15	18
Number of branches per GU	19	2	11.5	16	24	58
Length of the GU (m)	0.196	0.076	0.136	0.178	0.240	0.614

3.5.2. Distribution of branches within growth units

3.5.2.1. Number of branches per growth unit

The number of branches (NBR) produced on a GU was found to be highly correlated to the length of this GU (GU_{len}) (Figure 3-5). However, there was no correlation with the length of the GU from the previous year. The interaction between GU_{len} and the height of the GU (GU_h, m) also had a significant effect (See Eq. 1 & Table 3-3). The R^2 of the full model was 0.8 (0.6 for the fixed effects only).

[1] $$NBR = a1 + a2 \times GU_{len} + a3 \times GU_h + a4 \times (GU_{len} \times GU_h) + \delta_{tree}$$

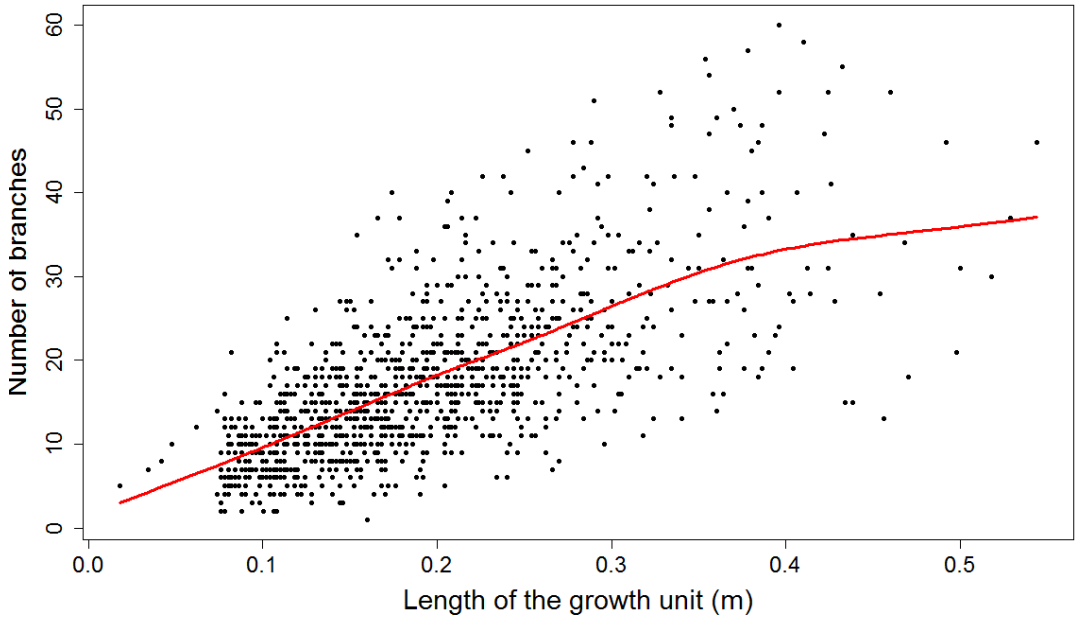

Figure 3-5 Relation between the number of branches per growth unit and its length. The red line represents the relationship

Table 3-3 Parameter estimates for the model predicting the number of branches per GU (See eq.1)**.** × represents an interaction term

Variables	Estimate	S.E	P.value
Intercept	2.24844	1.00403	0.0254
GU_{len}	76.98217	3.13821	<0.0001
GU_h	-0.06696	0.10727	0.5326
$GU_{len} \times GU_h$	2.09422	0.43074	<0.0001

3.5.2.2. Branch rank distribution along the GU

As expected due to our GU selection thresholds, most of the biggest branches were located close to the top of each GU (Figure 3-6). The relative position along the GU (P_{rel}) of the branches according to their rank can be described by a power function $P_{rel} = a\,X^b$ where $a = 1$ and $b = -0.26$ and X the rank of the branch. This function described 26% of the variance in branch positions in the entire dataset. However, the distribution could not be considered as normal around the mean predicted positions for each rank (Figure 3-6). We observed an asymmetry (skewness) of the distributions, which varied with the rank. This skewness was modelled using an exponential function:

[2] $$Y_{skew} = 2 + 2.9 \exp(^{-3.7\times\frac{1}{X}})$$

where X is the diameter rank of the branch. In order to have a more realistic distribution, we simulated a stochastic distribution for each rank using P_{rel} as the mean of this distribution, and Y_{skew} as the skewness. Since the standard deviation of the prediction was rather constant among ranks, we used the mean value of 0.17 in the simulations.

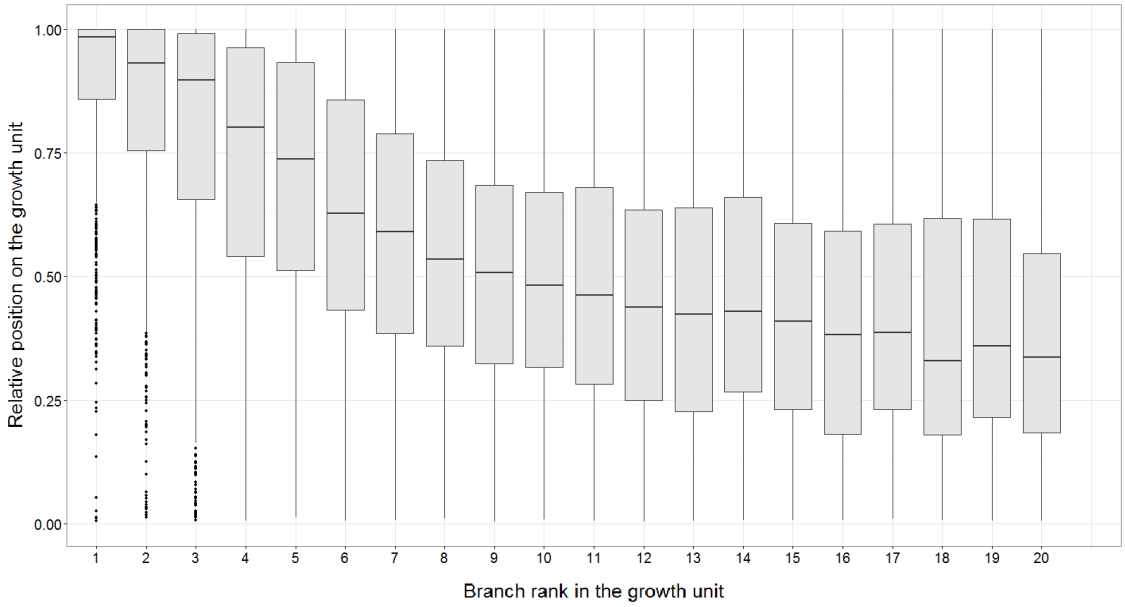

Figure 3-6 Relative position of the branches along the GU according to their diameter rank. Horizontal lines on the boxplots indicate the 25th, 50th and 75th percentiles. The ends of the vertical bars indicate the 5th and 95th percentiles, while dots represent individual observations.

When cumulating the percentage of presence of each branch rank and as a function of the position along the GU, it was observed that from a relative position of 0.6 from the base of the GU, we generally had at least 3 of the four biggest branches (91% of the branches of rank n°1, 88% of the n°2, 81% of the n°3 and 75% of the n°4). For the remaining analyses we considered that all the branches located on the upper 40% of the GU as nodal branches.

3.5.2.3. Circular distribution

The analysis of all the azimuths of all branches (n = 20,562) showed that their overall distribution at the tree level was uniform (Figure 3-7A). However, when considering only the biggest branch of each GU, we observed a preferential orientation towards 213° (Figure 3-7B). This was not the case of the biggest branch of the tree, which showed no significant preferential orientation (Figure 3-7C).

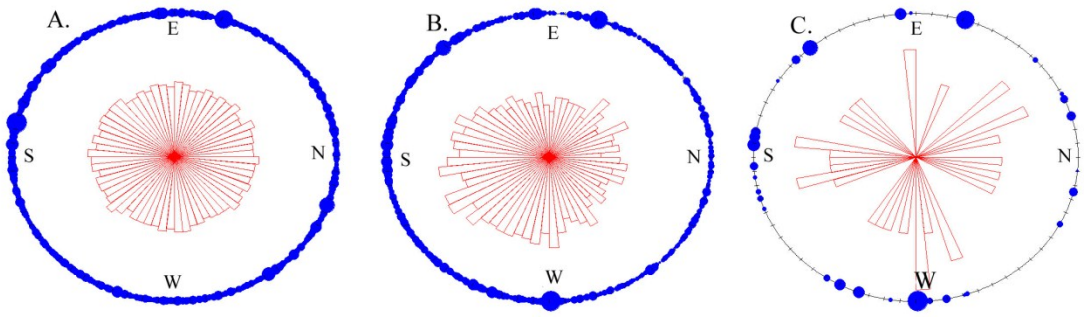

Figure 3-7 Distribution of the branches around the stem by diameter (in blue) and by number (in red) for **A)** all branches in the dataset, **B)** the biggest branch per GU and **C)** the biggest branch per tree

The distribution of the biggest branch per GU was non-uniform (alpha = 0.05) for 22 trees out of a total of 33. The Von Mises distribution used to simulate the position of the biggest branch in each GU had a mean azimuth equal to 213° (SD=5°) and a mean concentration parameter of 0.47 (SD=0.045). After testing for the influence of the age of the tree, the total height, the diameter at breast height and the influence of the between-tree competition, it appeared that no significant relationships could enable predictions of these values for each separate tree.

The distribution of all branches in a GU could be considered as uniform (Figure 3-7A), suggested that it could be simulated using a uniform circular distribution. However, we observed that the angles between the biggest branch and the next two in diameter ranking were very variable but usually larger than 40° (Figure 3-8). Only 8% of the branches ranked 1 and 2 were separated by less than 40°, and 15% for the branches ranked 1 and 3. With a completely random distribution, this percentage would be around 23%.

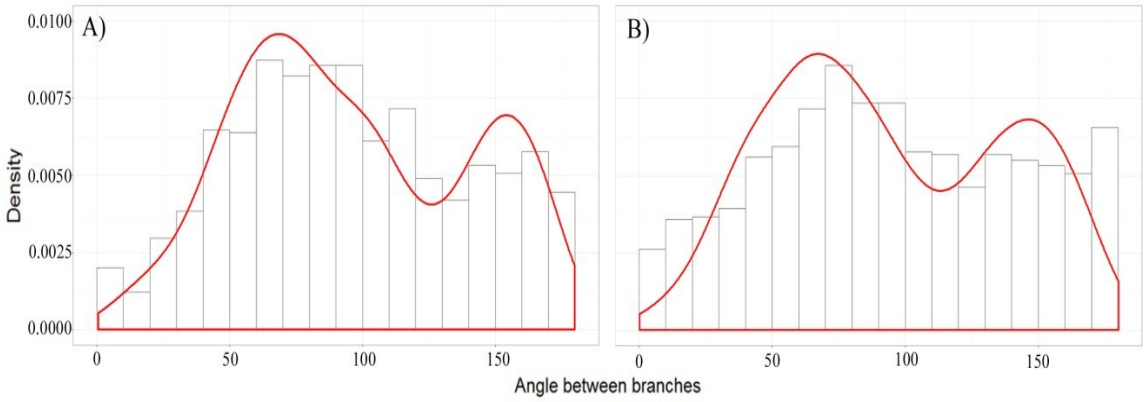

Figure 3-8 Absolute value of the angles measured per pseudo-whorl between **A)** the 1st and the 2nd biggest branches and **B)** the 1st and the 3rd biggest. The red line represents the simulated distribution

The angle between the 1st and the 2nd biggest branches tended to follow a bimodal distribution with a first peak around 76° and a second around 155°. Also, the first peak was the most important (Figure 3-8A). The distribution can be simulated by a combination of two von Mises distributions with mean values at 76° (SD=1°) and 155° (SD=0.8°) and concentration parameters of 3.98 (SD=0.17) and 17.4 (SD=1.43), respectively. The angle between the 1st and the 3rd biggest branches also followed a bimodal distribution with a first peak around 65° and a second around 145°. The first peak was also the most important (Figure 3-8B). Again, the distribution can be simulated by a combination of two von Mises distributions. Mean values were at 65° (SD=1°) and 145° (SD=1°) and concentration parameters at 4.84 (SD=0.22) and 8.19 (SD=0.53), respectively. In these two cases, we could not find any branch characteristics that could help predict whether the angle was located in one peak or the other.

The angles are represented here in absolute value, so the real value can vary between -180° and +180°. After verification, no patterns were found to indicate if the angle was going to be positive or negative. However, we observed that in 60% of cases, when the angle between branches 1 and 2 was oriented in one direction, the angle between branches 1 and 3 was oriented in the other direction.

3.5.2.4. Mortality and self-pruning models

The probability (P_m) that a branch had died was related to the age (Age_t) and diameter of the branch (D_t), the relative position of the branch on the growth unit (P_{rel}), the growth unit length (GU_{len}), height along the tree (GU_h), radial distance to the stem's pith (RW_{sum}) and the diameter at breast height of the tree (DBH) (See Eq. 3 & Table 3-4).

[3] $$\ln\left(\frac{P_m}{1-P_m}\right) = b1 + b2 * Age_t + b3 * P_{rel} + b4 * GU_{len} + b5 * D_t + b6 * RW_{sum} + b7 * DBH + b8 * GU_h + \delta\_tree$$

Table 3-4 : Parameter estimates for the model predicting the annual probability for a branch to remain alive (0: dead; 1: live) (See eq.3)

Variables	Estimate	S.E	P.value
Intercept	3.2064	0.2818	<0.0001
Age_t	0.0033	0.0005	<0.0001
P_{rel}	0.1081	0.0144	<0.0001
GU_{len}	-0.7667	0.0442	<0.0001
D_t	0.1019	0.0017	<0.0001
RW_{sum}	-0.0187	0.0005	<0.0001
DBH	-0.0468	0.0005	<0.0001
GU_h	0.0393	0.0016	<0.0001

Once the branch had died, it could remain present in the next annual ring (1) or be absent (0, self-pruned). The probability (P_{sp}) that a branch remained present was related to the time since the branch had died (T_m), the branch diameter at death (D_m), the relative position on the GU (P_{rel}) and the height on the tree (GU_h) (See Eq. 4 & Table 3-5).

[4] $$\ln\left(\frac{P_{sp}}{1-P_{sp}}\right) = b1 + b2 * T_m + b3 * P_{rel} + b4 * D_m + b5 * GU_h + \delta\_tree$$

Table 3-5 : Parameter estimates for the model predicting the annual probability for a branch remain present if dead (1: present; 2: self-pruned) (See eq.4)

Variables	Estimate	S.E	P.value
Intercept	-4.0743	0.2460	<0.0001
T_m	0.0491	0.0022	<0.0001
P_{rel}	-0.4951	0.1009	<0.0001
D_m	0.0577	0.0185	0.0018
GU_h	0.1341	0.0091	<0.0001

3.6. Discussion

The objective of this study was to refine branch models by adding development functions that initiate branches at plausible positions within a GU. These improvements come with a need for accurate measurements. To obtain branch angles with external measurements, the stem is generally segmented into different circular sections (Colin and Houllier 1991; Moberg 1999). This only provides of rough estimate of the azimuth direction. In addition, measurements in the field can be complicated by the limited accessibility to a proportion of the branches once the tree is felled. The utilization of the CT scanning technology helped obtain a very accurate description of the branches distribution along and around the tree. In addition, it allowed to consider the past branch development through the visualisation of the occluded branches.

The GU information (length, number of branches) is one of the most important parameters in tree growth and branch development models. We observed an important underestimation of the number of GU with the usual external method. The GU length is also one of the most important parameters used to predict the number of branches per GU (Mäkinen and Hein 2006). We noticed an important bias in the GU estimation made from external and, knowing the importance of this information in the development of such models, it seems necessary to take account this information in future studies. Errors appeared both for young and for old trees, and we found that the age of the tree was not significantly linked to the magnitude of such errors in our dataset. However, there was a higher under-estimation at

higher positions along the stem, which was unexpected. Indeed, the presence of several self-pruned branches at the base of the tree suggested that the opposite result would occur. A possible explanation is that in the higher parts of the stem, there were several branches with varied diameters, whereas towards the base of the tree, the only branches still alive were the biggest ones, or if all the branches were occluded, the scar of the biggest ones were still visible. Longuetaud et al. (2005) used CT images and elaborated an approach to locate the pseudo-whorls based on the analysis of the variation of density due to knots. Knots are characterized by high wood density values and they tend to concentrate in pseudo-whorl sections. However, this approach tended to overestimate the number of GUs and had to be coupled with external optical measurements to improve the GU selection. The two filters we applied here were chosen for their simplicity. It allowed eliminating the bias associated with the external measurements. However, our subsample size was rather small (44 2.5m-logs) and a larger, independent dataset should be used to confirm or refine the filters.

The model of the number of branches per GU showed that this variable was mainly dependent on the length of that GU (Harmer 1992; Mäkinen and Colin 1999). Since a proportion of the branches are known to be preformed in black spruce (Bégin and Filion 1999), we expected a significant correlation with the GU information of the previous year. This absence of correlation could indicate that we did not find the real GU limits in several cases. Alternatively, it could be that if the buds were formed during the previous year, their future development the next year (i.e. the observable knots) was influenced by the current annual resources of the tree or its position on the GU (Harmer 1991; Sabatier and Barthelemy 1999).

The longitudinal distribution of the branches along a GU was very variable. However, we observed on average that the diameter of the branch (sorted by rank) increases with the position on the GU. In some cases, we noticed that some of the biggest branches can be located in any part of the GU. This might induce errors in our GU selection. This heterogeneity could be due to the high capacity of dedifferentiation of the axes and of a large number of dormant buds at the bottom of the GUs (Bégin and Filion 1999).The simulated stochastic distribution reproduces the heterogeneity in the branch positioning along a growth unit. This simulation is mainly dependent on the branch rank, since the

addition of tree or branch parameters did not help refine the predictions. Branch location is probably strongly influenced by factors such as competition between trees, between branches on the same trees and by other local effects affecting the branch morphogenesis.

Harless et al. (1991) suggested that sawing patterns affect the lumber grade output. The development of simulators allowed to predict the wood value and to optimize different sawing patterns (Lemieux et al. 2000; Steele et al. 1994). These simulations needed to use a realistic distribution of branches to be realistic. To complete the description of the distribution of branches within a GU, it was necessary to integrate the circular distribution. Most of the existing branch distribution models considered that the distribution is uniform and the angle between branches depends mainly on the number of branches per whorl (Doruska and Burkhart 1994). In black spruce trees, the branches are not distributed in clearly defined pseudo-whorls. Rayleigh's test of uniformity has provided evidence that, in many cases, one can assume that branches are uniformly distributed around the stem. However, we noticed a non-uniform distribution when looking at the biggest branches of each GU. These large branches generally have a larger leaf area, an important light and snow interception so they are of importance for the biological functions of the plant (Hedstrom and Pomeroy 1998). They are also important for wood quality considerations (Buksnowitz et al. 2010). The south–southwesterly direction (213°) was the preferential orientation, which is similar to what was found by Benjamin et al. (2009). This might reflect a preferential allocation to branches that are in a position where they can capture more sunlight. It proved difficult to predict the azimuth of each branches in a GU, but by focusing on the biggest branch per GU, we can first use a random von Mises distribution to approximate the observed distribution. Then, the azimuth of the 2nd and the 3rd biggest branches was found to follow bimodal distributions, which can easily be parameterized. Competition for resources is thought to occur not only between, but also within trees, as a mean to avoid the self-shading and optimize the utilization of the space (Deleuze et al. 1996; Newton and Jolliffe 1998; Sumida et al. 2002). It therefore appears logical that two big branches would typically not grow very close to each other (Osada 2002). This apparent repulsion to limit inter-branch competition should be included in branch distribution models, especially for those used for wood quality simulations as it could provide new insights on the potential gains associated with the optimal log position at

sawing (Lemieux et al. 2000). However, we could not find any influence of the tree or the GU characteristics on the parameters of the distribution. As our dataset was of a limited size, further analyses should be conducted on this topic.

3.7. Conclusion

This study showed that there was an important bias in the estimation of GU limits using the external branch characteristics of mature black spruce trees. This bias could be substantially reduced using two thresholds based on the basal area of pseudo-whorls and on the distance between GUs, which were obtained through CT scanning. Using improved GU selection, we developed a model of the number and the distribution of branches within each GU. The intra-tree and inter-tree variability made it difficult to model the longitudinal and the circular distribution of the branches. However, it was possible to simulate a realistic distribution of the branches around and along the stem, according their diameter ranks. The angles between the three biggest branches of each GU followed bimodal distributions, a fact which suggests that structural rules are involved in branch and knot development. These can have some impact on tree development, but also on the potential to optimise wood processing according to internal tree characteristics. This analysis was made possible by the accuracy obtained using X-ray tomography. The rules we described in this study can be integrated into tree growth and sawing simulators.

Conclusions et perspectives

L'objectif principal de ce travail était d'améliorer les modèles de nœuds pour deux espèces canadiennes, soit l'épinette noire et le pin gris. Cette amélioration passait, d'une part, par un modèle de la géométrie des nœuds et, d'autre part, par une meilleure description des distributions de ces nœuds dans l'arbre. L'analyse des données a été réalisée à partir d'images tomographiques. Cette méthode non destructive nous a permis de visualiser en 3D et de manière précise l'ensemble des nœuds à l'intérieur des billes, et ce, pour un temps d'analyse raisonnable; l'analyse se faisant actuellement de manière semi-manuelle (Colin et al. 2010). Cependant l'amélioration constante des outils d'analyses en fait un outil très performant et précis de plus en plus utilisé dans l'analyse des caractéristiques internes des billes (Longuetaud et al. 2012).

Le premier apport de ce travail a été la mise au point de deux modèles décrivant la géométrie des nœuds. Ces modèles utilisent une approche différente mais ont chacun vocation à être intégrés dans des simulateurs de croissance.

Le modèle élaboré au chapitre 1 est statique dans le temps. À partir de cinq paramètres et de deux équations non linéaires, il est possible de reconstruire la courbure et le diamètre d'un nœud et de décrire une grande diversité de formes (Fig. C-1). Les caractéristiques externes de l'arbre et de la branche attachée au nœud modélisé servent de variables explicatives. Ce modèle s'insère donc dans une simulation capable de faire croître un arbre et de décrire la taille et la position de ses branches.

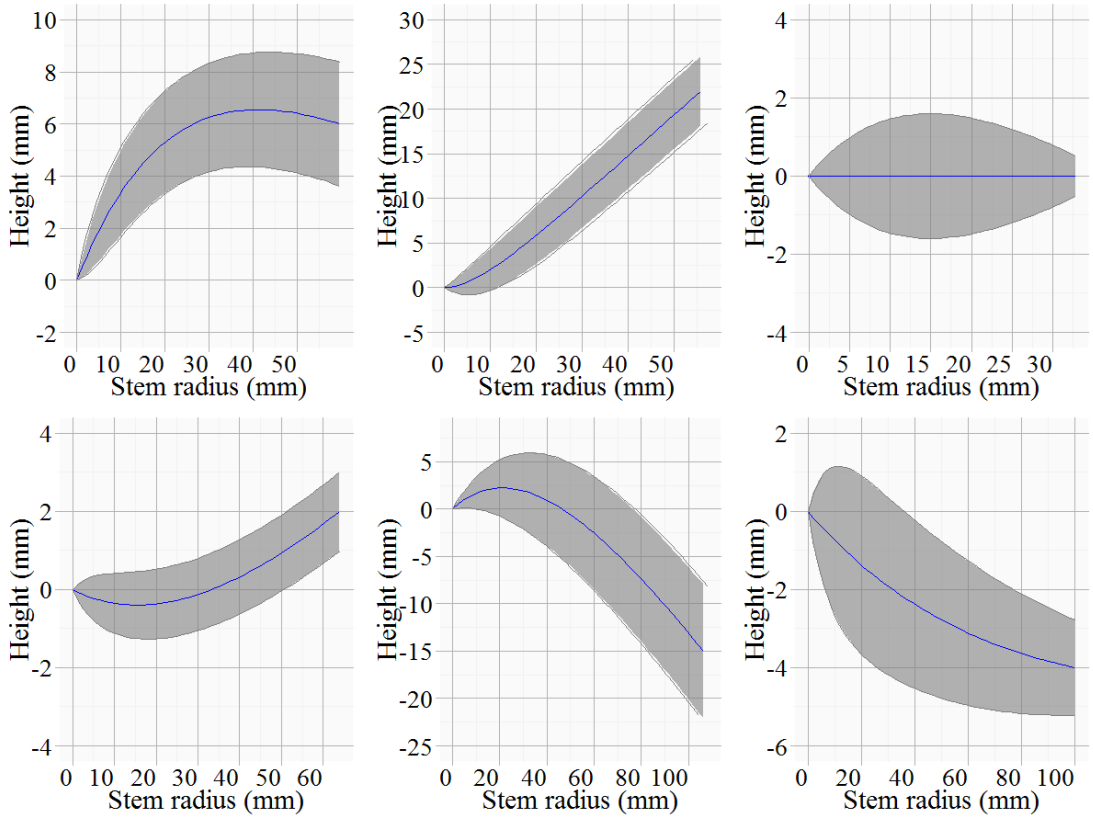

Figure C-4 Illustration de la flexibilité du modèle de nœud développé dans le chapitre

Cependant, ces simulations sont limitées. En effet, ces modèles sont généralement ajustés à partir de données externes qui peuvent être imprécises, notamment pour les données de branches (azimut, inclinaison) (Duchateau et al. 2013c). Cela limite également la précision des distributions de branches ainsi que des unités de croissance (Duchateau et al. 2013b).

Le modèle élaboré dans le chapitre 2 présente une alternative à l'utilisation de ces données externes en se basant uniquement sur la croissance secondaire de la tige. La courbure et le diamètre du nœud sont donc influencés par le développement annuel de l'arbre. Cela nous a aussi permis d'analyser l'allocation de matières entre le tronc et les nœuds. Ce modèle se veut dynamique dans le temps et utilise principalement les données de croissance internes à l'arbre (largeurs de cernes) comme variables explicatives. Ces données sont plus précises et généralement disponibles dans les modèles de croissance existants. Cependant, si les données des largeurs de cernes sont disponibles à l'échelle de l'arbre, peu d'information est disponible sur leur comportement à proximité du nœud et sur la jonction entre ces deux

organes. L'augmentation future de la précision des données internes devrait permettre de combler ce manque.

Avec ces deux modèles, nous sommes donc capables de représenter de manière précise la forme tridimensionnelle d'un nœud (Fig. C-2) et d'intégrer ces modèles dans des simulateurs de croissance. Cependant, afin d'être un outil pertinent permettant de comprendre le développement de l'arbre, le simulateur de croissance doit, en plus d'intégrer un modèle de la géométrie du nœud, être en mesure de simuler une distribution réaliste de ceux-ci dans la tige.

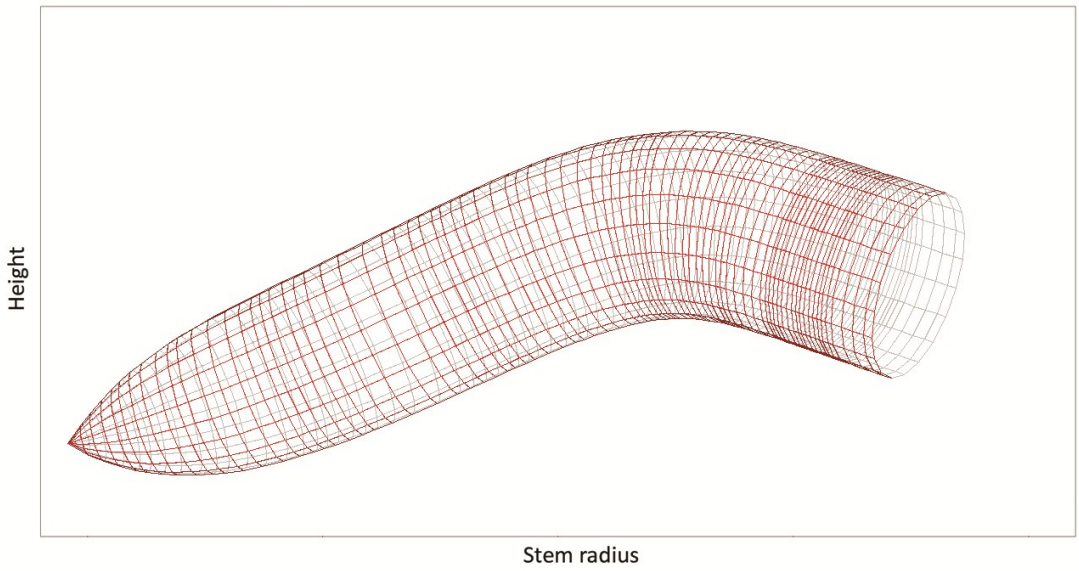

Figure C-5 Simulation tridimensionnelle de la géométrie d'un nœud obtenue par la combinaison d'un modèle de l'évolution de la courbure et du diamètre

Le second apport de ce travail a donc été l'amélioration des connaissances de la distribution des branches autour et le long du tronc, de manière à obtenir des simulations plus réalistes. Les données issues du tomographes à rayons-X nous ont permis d'obtenir une cartographie précise de l'ensemble des branches dans le tronc. Nous avons ainsi amélioré la détection et le positionnement des unités de croissance dans l'épinette noire. D'un point de vue biologique, la délimitation des unités de croissance représente l'un des paramètres fondamentaux de la croissance et de la structure des gymnospermes. La grande variabilité intra- et inter- arbre rend cependant difficile la détection de règles

architecturales de développement chez l'épinette noire. Nous avons donc dû décrire les distributions des branches selon leurs diamètres afin d'obtenir une représentation réaliste de la branchaison.

L'amalgame de tous les modèles présentés dans les trois chapitre de cette thèse nous permet de simuler le développement de la structure interne des nœuds d'une épinette noire à partir uniquement de son historique de croissance radiale et en hauteur. Un exemple pour une bille sélectionnée au hasard parmi nos échantillons est illustré à la Fig. C-3. Les résultats sont encourageants, puisque le degré de réalisme dépasse largement tout ce qui était disponible auparavant. Toutefois, cette simulation met en lumière les ajustements qui permettront de compléter le développement du simulateur. Il sera notamment nécessaire d'affiner encore les paramètres stochastiques définissants le positionnement des branches le long de l'arbre à l'intérieur des unités de croissance afin d'éviter l'absence de branches dans la partie inférieur de ces unités (Figure C-3).

En plus des applications pratiques reliées à la simulation de la qualité du bois, ce volet de l'étude a permis de faire quelques avancées dans des aspects plus fondamentaux reliés aux interactions entre branches d'un même arbre. Les angles entre les branches d'une même unité de croissance peuvent ainsi être modélisés par une distribution bimodale. L'obtention de données de croissance annuelle nous a également permis d'étudier le ratio d'allocation de matière entre les nœuds et la tige au cours du développement de l'arbre et la présence de relation allométrique.

Notre échantillonnage s'étant fait en forêt naturelle, on ne peut affirmer avoir mis au point un outil permettant de prédire l'influence de traitements sylvicoles sur le développement de la nodosité des tiges. Pour ce faire, il sera nécessaire de calibrer nos modèles sur des arbres ayant subi ces traitements. La grande flexibilité des équations et leur ajustement sur deux essences ayant une branchaison très différentes devrait permettre de s'adapter à de nombreuses autres espèces résineuses. Les principes de base du système de simulation étant déjà en place, il suffira de mener des études de calibration dans de nouvelles conditions.

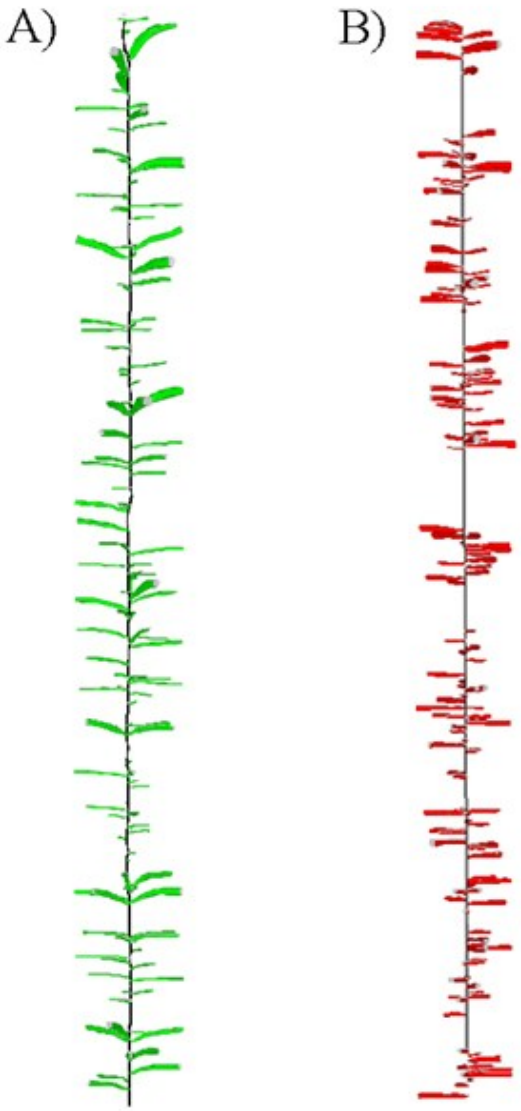

Figure C-6 Comparaison entre A) une bille réelle et B) Simulation d'une bille simulée à partir du modèle de nœud développé dans le chapitre 2 et des distributions de branches décrites dans le chapitre 3.

Références bibliographiques

Abramoff MD, Magalhaes PJ, Ram SJ (2004) Image processing with ImageJ. Biophotonics Int 11:36–43.

Achim A, Gardiner B, Leban J, Daquitaine R (2006) Predicting the branching properties of Sitka spruce grown in Great Britain. New Zeal J For Sci 36:246.

Aiken LS, West SG (1991) Multiple regression: Testing and interpreting interactions. Mult Regres Test Interpret Interact 212.

Akaike H (1974) A new look at the statistical model identification. IEEE Trans Autom Control 19:716–723.

Auty D, Weiskittel AR, Achim A, et al. (2012) Influence of early re-spacing on Sitka spruce branch structure. Ann For Sci 69:1–12.

Bailly R (2004) Première floraison et changement de phyllotaxie chez Fraxinus angustifolia Vahl: Approche architecturale et morphologique.

Bao FC, Jiang ZH, Jiang XM, et al. (2001) Differences in wood properties between juvenile wood and mature wood in 10 species grown in China. Wood Sci Technol 35:363–375.

Barthelemy D, Caraglio Y (2007) Plant architecture: A dynamic, multilevel and comprehensive approach to plant form, structure and ontogeny. Ann Bot 99:375–407. doi: 10.1093/aob/mcl260

Barthélémy D, Edelin C, Hallé F (1989) Architectural concepts for tropical trees. Trop For Bot Dyn Speciat Divers 89–100.

Batschelet E (1981) Circular Statistics in Biology. Technometrics 24:52–83. doi: 10.2307/1267831

Beaulieu E, Schneider R, Berninger F, et al. (2011) Modeling jack pine branch characteristics in Eastern Canada. For Ecol Manage 262:1748–1757.

Bégin C, Filion L (1999) Black spruce (Picea marianna) architecture. Botany 77:664–672.

Benjamin J, Chui YH, Zhang SY (2007) A method to assess lumber grade recovery improvement potential for black spruce logs based on branchiness. For Prod J 57:34–41.

Benjamin JG, Chui YH, Kershaw JA (2009a) Circular Distribution of Branches from Plantation Grown Black Spruce in Ontario. North J Appl For 26:15–20.

Benjamin JG, Kershaw JA, Weiskittel AR, et al. (2009b) External knot size and frequency in black spruce trees from an initial spacing trial in Thunder Bay , Ontario. For Chron 85:618–624.

Best DJ, Fisher NI (1979) Efficient simulation of the von Mises distribution. Appl Stat 152–157.

Bhandarkar SM, Faust TD, Tang MJ (1999) CATALOG: a system for detection and rendering of internal log defects using computer tomography. Mach Vis Appl 11:171–190.

Björklund L (1997) The interior knot structure of Pinus sylvestris stems. Scand J For Res 12:403–412.

Björklund L, Petersson H (1999) Predicting knot diameter of Pinus sylvestris in Sweden. Scand J For Res 14:376–384.

Bodig J, Jayne BA (1982) Mechanics of wood composites. Von Nostrand Reinhold Company, New York, Cincinnati, Toronto 712:

Boissiere S (2003) Dynamique de la Phyllotaxie.

Bouchard M, Pothier D, Gauthier S (2008) Fire return intervals and tree species succession in the North Shore region of eastern Quebec. Can J For Res 38:1621–1633.

Bowyer JL, Shmulsky R, Haygreen JG (2007) Forest products and wood science: an introduction. Wiley-Blackwell

Bravo F, Hann DW, Maguire DA (2001) Impact of competitor species composition on predicting diameter growth and survival rates of Douglas-fir trees in southwestern Oregon. Can J For Res 31:2237–2247.

Bruchert F, Becker G, Speck T (2000) The mechanics of Norway spruce [Picea abies (L.) Karst]: mechanical properties of standing trees from different thinning regimes. Elsevier Science Bv, pp 45–62

Buckman RE (1964) Twenty-two-year results of a precommercial thinning experiment in jack pine (Res. Note LS-46). USDA For. Serv.

Buksnowitz C, Hackspiel C, Hofstetter K, et al. (2010) Knots in trees: strain distribution in a naturally optimised structure. Wood Sci Technol 44:389–398.

Cochrane LA, Ford ED (1978) Growth of a Sitka spruce plantation - analysis and stochastic description of development of branching structure. J Appl Ecol 15:227–244.

Colin F, Houllier F (1991) Branchiness of Norway spruce in north-eastern France - Modeling vertical trends in maximum nodal branch size. Ann Des Sci For 48:679–693.

Colin F, Houllier F (1992) Branchiness of Norway Spruce in north-eastern France - Predicting the main crown characteristics from usual tree measurements. Ann Des Sci For 49:511–538.

Colin F, Houllier F, Joannes H, Haddaoui A (1993) Modeling of the vertical profile of diameters, angles and number of branches for three provenances of the common spruce. Silvae Genet 42:206–222.

Colin F, Mothe F, Freyburger C, et al. (2010) Tracking rameal traces in sessile oak trunks with X-ray computer tomography: biological bases, preliminary results and perspectives. Trees 24:953–967.

Colombo SJ (1986) Second-year shoot development in black spruce Picea mariana (Mill.) BSP container seedlings. Can J For Res 16:68–73.

Couder Y, Douady S (2000) Rational and irrational angles in phyllotaxis. Pattern Form Biol Vis Dyn 145.

Courbet F, Houllier F (2002) Modelling the profile and internal structure of tree stem . Application to Cedrus atlantica (Manetti). Ann For Sci 59:63–80. doi: 10.1051/forest

DeBell DS, Singleton R, Gartner BL, Marshall DD (2004) Wood density of young-growth western hemlock: relation to ring age, radial growth, stand density, and site quality. Can J For Res 34:2433–2442.

Deleuze C, Hervé JC, Colin F, Ribeyrolles L (1996) Modelling crown shape of Picea abies: spacing effects. Can J For Res Can Rech For 26:1957–1966.

Dinwoodie JM (2000) Timber: Its nature and behaviour. Taylor & Francis

Doruska PF, Burkhart HE (1994) Modeling the diameter and locational dstribution of branches within the crowns of Loblolly-Pine trees in unthinned plantations. Can J For Res 24:2362–2376.

Drolet JC, Newnham RM, Tsay TB (1972) Branchiness of jack pine, black spruce, and balsam fir in relation to mechanized delimbing. For. Manag. Institute, Ottawa, Canada, Inf. Rep. FMR-S-34

Duchateau E, Auty D, Mothe F, et al. (2013a) Modelling knot morphogenesis in trees. Ann. Bot. (to be Submitt.

Duchateau E, Auty D, Mothe F, Achim A (2013b) Improving branch distribution models in trees using X-ray computed tomography. 7th Int. Conf. Funct. Plant Model. Saariselkä, Finl.

Duchateau E, Longuetaud F, Mothe F, et al. (2013c) Modelling knot morphology as a function of external tree and branch attributes. Can J For Res 43:266–277. doi: dx.doi.org/10.1139/cjfr-2012-0365

Farrar JL (1996) Les arbres du Canada. Les Editions Fides

Fisher JB, Honda H (1979) Branch geometry and effective leaf area: a study of Terminalia-branching pattern. 1. Theoretical trees. Am J Bot 66:633–644.

Fourcaud T, Zhang X, Stokes A, et al. (2008) Plant growth modelling and applications: the increasing importance of plant architecture in growth models. Ann Bot 101:1053–1063.

Franco M (1986) The influences of neighbours on the growth of modular organisms with an example from trees. Philos Trans R Soc Lond B Biol Sci 209–225.

Gamache I, Payette S (2004) Height growth response of tree line black spruce to recent climate warming across the forest-tundra of eastern Canada. J Ecol 92:835–845.

Garber SM, Maguire DA (2005) Vertical trends in maximum branch diameter in two mixed-species spacing trials in the central Oregon Cascades. Can J For Res 35:295–307. doi: 10.1139/x04-164

Garber SM, Maguire DA (2003) Modeling stem taper of three central Oregon species using nonlinear mixed effects models and autoregressive error structures. For Ecol Manage 179:507–522.

Gardiner B, Leban JM, Auty D, Simpson H (2011) Models for predicting wood density of British-grown Sitka spruce. Forestry 84:119–132.

Grace JC, Pont D, Goulding CJ, Rawley B (1999) Modelling branch development for forest management. New Zeal J For Sci 29:391–408.

Guay R, Gagnon R, Morin H (1992) A new automatic and interactive tree ring measurement system based on a line scan camera. For Chron 68:138–141.

Harless TEG, Wagner FG, Steele PH, et al. (1991) Methodology for locating defects within hardwood logs and determinig their impact on lumber-value yield. For Prod J 41:25–30.

Harmer R (1992) Relationships betweenshootlength, bud number and branch production in quercus-petraea (matt.) Liebl. Forestry 65:61–72.

Harmer R (1991) The Effect of Bud Position on Branch Growth and Bud Abscission in Quercus petraea (Matt .) Liebl . Ann Bot 67:463–468.

Hedstrom NR, Pomeroy JW (1998) Measurements and modelling of snow interception in the boreal forest. Hydrol Process 12:1611–1625.

Hein S (2008) Knot attributes and occlusion of naturally pruned branches of Fagus sylvatica. For Ecol Manage 256:2046–2057.

Hein S, Mäkinen H, Yue CF, Kohnle U (2007) Modelling branch characteristics of Norway spruce from wide spacings in Germany. For Ecol Manage 242:155–164. doi: 10.1016/j.foreco.2007.01.014

Hein S, Weiskittel AR, Kohnle U (2008) Effect of wide spacing on tree growth, branch and sapwood properties of young Douglas-fir [Pseudotsuga menziesii (Mirb.) Franco] in south-western Germany. Eur J For Res 127:481–493.

Hodges DG, Anderson WC, McMillin CW (1990) The economic potential of CT scanners for harwood sawmills. For Prod J 40:65–69.

Horn HS (1971) The adaptive geometry of trees. Princeton Univ Pr

Houllier F, Leban JM, Colin F (1995) Linking growth modelling to timber quality assessment for Norway spruce. For Ecol Manage 74:91–102.

Ikonen VP, Peltola H, Wilhelmsson L, et al. (2008) Modelling the distribution of wood properties along the stems of Scots pine (Pinus sylvestris L.) and Norway spruce (Picea abies (L.) Karst.) as affected by silvicultural management. For Ecol Manage 256:1356–1371. doi: 10.1016/j.foreco.2008.06.039

Jaeger M, Leban JM, Borianne P, et al. (1999) 3D stem reconstruction from CT scan exams. From log external shape to internal structures. Connect. between Silvic. wood Qual. through Model. approaches Simul. software, Proc. IUFRO WP S5. 01 4:

Jäghagen K, Albrektson A (1996) Induced competition among Scots pine seedlings and its effect on future timber quality. New For 12:163–174.

Jammalamadaka SR, Sengupta A (2001) Topics in circular statistics. World Scientific Pub Co Inc

Jean R V (1994) Phyllotaxis: a systemic study of plant pattern morphogenesis. Cambridge Univ Pr

Johansson K (1993) Influence of initial spacing and tree class on the basic density of Picea abies. Scand J For Res 8:18–27.

Jozsa LA, Middleton GR (1994) A discussion of wood quality attributes and their practical implications, Forintek Canada Corp. Spec. Publ. No. SP-34

Kantola A, Mäkelä A (2004) Crown development in Norway spruce [Picea abies (L.) Karst.]. Trees-Structure Funct 18:408–421.

Kellomäki S, Ikonen VP, Peltola H, Kolstrom T (1999) Modelling the structural growth of Scots pine with implications for wood quality. Ecol Modell 122:117–134.

Kenk G, Unfried P (1980) Aststärken in Douglasienbeständen. AFJZ 151:201–210.

King DA (1998) Relationship between crown architecture and branch orientation in rain forest trees. Ann Bot 82:1.

Koper N, Manseau M (2009) Generalized estimating equations and generalized linear mixed-effects models for modelling resource selection. J Appl Ecol 46:590–599.

Laberge MJ, Payette S, Pitre N (2001) Development of stunted black spruce (Picea mariana) clones in the subarctic environment: a dendro-architectural analysis. Ecoscience 8:489–498.

Leban JM, Duchanois G (1990) Modeling wood quality - new software - SIMQUA. Ann Des Sci For 47:483–493.

Lejeune (2004) Prédiction du défilement et de la branchaison de l'Épinette noire. (M.Sc.). Fac. For. géomatique, Univ. Laval, Québec, Canada

Lemieux H, Beaudoin M, Grondin F (2000) A model for the sawing and grading of lumber according to knots. Wood Fiber Sci 32:179–188.

Lemieux H, Beaudoin M, Zhang SY (2001) Characterization and modeling of knots in black spruce (Picea mariana) logs. Wood Fiber Sci 33:465–475.

Lemieux H, Beaudoin M, Zhang SY, Grondin F (2002) Improving structural lumber quality in a sample of Picea mariana logs sawn according to the knots. Wood Fiber Sci 34:266–275.

Lemieux H, Samson M, Usenius A (1997a) Shape and distribution of knots in a sample of Picea abies logs. Scand J For Res 12:50–56.

Lemieux H, Usenius A, Samson M (1997b) A method for the characterization of knots in logs. For Prod J 47:57–62.

Longuetaud F, Mothe F, Kerautret B, et al. (2012) Automatic knot detection and measurements from X-ray CT images of wood: A review and validation of an improved algorithm on softwood samples. Comput Electron Agric 85:77–89.

Longuetaud F, Saint-Andre L, Leban JM (2005) Automatic detection of annual growth units on Picea abies logs using optical and x-ray techniques. J Nondestruct Eval 24:29–43.

Macdonald E, Hubert J (2002) A review of the effects of silviculture on timber quality of Sitka spruce. Forestry 75:107–138.

Maguire DA (1994) Branch mortality and potential litterfall from Douglas-Fir trees in stands of varying density. For Ecol Manage 70:41–53.

Maguire DA, Johnston SR, Cahill J (1999) Predicting branch diameters on second-growth Douglas-fir from tree-level descriptors. Can J For Res 29:1829–1840.

Maguire DA, Kershaw JA, Hann DW (1991) Predicting the effects of silvicultural regime on branch size and crown wood core in Douglas-Fir. For Sci 37:1409–1428.

Maguire DA, Moeur M, Bennett WS (1994) Models for describing basal diameter and vertical distribution of primary branches in young Douglas-Fir. For Ecol Manage 63:23–55.

Mäkelä A (2002) Derivation of stem taper from the pipe theory in a carbon balance framework. Tree Physiol 22:891–905.

Makela A, Landsberg J, Ek AR, et al. (2000) Process-based models for forest ecosystem management: current state of the art and challenges for practical implementation. Tree Physiol 20:289.

Mäkelä A, Vanninen P, Ikonen VP, Samfund FF (1997) An application of process-based modelling to the development of branchiness in Scots pine. Silva Fenn 31:369–380.

Mäkinen H (1996) Effect of intertree competition on branch characteristics of Pinus sylvestris families. Scand J For Res 11:129–136.

Mäkinen H (1999a) Growth, suppression, death, and self-pruning of branches of Scots pine in southern and central Finland. Can J For Res 29:585–594.

Mäkinen H (1999b) Effect of stand density on radial growth of branches of Scots pine in southern and central Finland. Can J For Res 29:1216–1224.

Mäkinen H, Colin F (1999) Predicting the number, death, and self-pruning of branches in Scots pine. Can J For Res 29:1225–1236.

Mäkinen H, Colin F (1998) Predicting branch angle and branch diameter of Scots pine from usual tree measurements and stand structural information. Can J For Res 28:1686–1696.

Mäkinen H, Hein S (2006) Effect of wide spacing on increment and branch properties of young Norway spruce. Eur J For Res 125:239–248.

Mäkinen H, Mäkelä A (2003) Predicting basal area of Scots pine branches. For Ecol Manage 179:351–362.

Mäkinen H, Song T (2002) Evaluation of models for branch characteristics of Scots pine in Finland. For Ecol Manage 158:25–39.

Mathieu A, Cournede PH, Letort V, et al. (2009) A dynamic model of plant growth with interactions between development and functional mechanisms to study plant structural plasticity related to trophic competition. Ann Bot 103:1173–1186. doi: 10.1093/aob/mcp054

Mazerolle MJ (2006) Improving data analysis in herpetology: using Akaike's Information Criterion (AIC) to assess the strength of biological hypotheses. Amphibia-Reptilia 27:169–180.

McKenney D, Fox G, van Vuuren W (1992) An economic comparison of black spruce and jack pine tree improvement. For Ecol Manage 50:85–101.

Middleton GR, Jozsa LA, Monro BD, Sen P (1996) Regional comparisons of wood density and knot size in low stand density lodgepole pine. Spec. Publ. Forintek Canada Corp. SP 36. 27pp.

Moberg L (2000) Models of internal knot diameter for Pinus sylvestris. Scand J For Res 15:177–187.

Moberg L (2001) Models of internal knot properties for Picea abies. For Ecol Manage 147:123–138.

Moberg L (1999) Variation in knot size of Pinus sylvestris is in two initial spacing trials. Silva Fenn 33:131–144.

Moberg L, Nordmark U (2006) Predicting lumber volume and grade recovery for Scots pine stems using tree models and sawmill conversion simulation. For Prod J 56:68–74.

Newton PF, Jolliffe PA (1998) Aboveground modular component responses to intraspecific competition within density-stressed black spruce stands. Can J For Res 28:1587–1610.

Nylinder P (1965) Non-destructive field sampling systems for determining the wood density of standing timber over large áreas. 41:

O'brien RM (2007) A Caution Regarding Rules of Thumb for Variance Inflation Factors. Qual Quant 41:673–690. doi: 10.1007/s11135-006-9018-6

Osada N (2002) Branch Architecture, Light Interception and Crown Development in Saplings of a Plagiotropically Branching Tropical Tree, Polyalthia jenkinsii (Annonaceae). Ann Bot 91:55–63. doi: 10.1093/aob/mcg008

Parresol BR (2001) Additivity of nonlinear biomass equations. Can J For Res 31:865–878. doi: 10.1139/cjfr-31-5-865

Pellicane PJ, Franco N (1994) Modeling wood pole failure. Wood Sci Technol 28:261–274.

Pellicane PJ, Stanfill-McMillan K, Tichy RJ (1987) Effects of knots near the finger of finger-jointed dimension lumber. For Prod J 37:13–16.

Peltola H, Miina J, Rouvinen I, Kellomaki S (2002) Effect of early thinning on the diameter growth distribution along the stem of Scots pine. Silva Fenn 36:813–825.

Persson A (1976) The influence of spacing on the quality of sawn timber from Scots pine. Dept For Yield Res, R Coll For Stock Res Notes 42:122.

Perstorper M, Johansson G, Pellicane PJ (1995) Quality of timber products from Norway Spruce. Wood Sci Technol 29:397–410.

Perttunen J, ÄNEN RS, Nikinmaa E, et al. (1996) LIGNUM: a tree model based on simple structural units. Ann Bot 77:87–98.

Pietilä J (1989) Factor affecting the healing-over of pruned Scots pine knots. Silva Fenn.

Pinheiro JC, Bates DM (2009) Mixed-effects models in S and S-PLUS. Springer

Pinto I, Pereira H, Usenius A (2003) Analysis of log shape and internal knots in twenty Maritime pine (Pinus pinaster Ait.) stems based on visual scanning and computer aided reconstruction. Ann For Sci 60:137–144.

Plourde A, Krause C, Lord D (2009) Spatial distribution, architecture, and development of the root system of Pinus banksiana Lamb. in natural and planted stands. For Ecol Manage 258:2143–2152.

Pont D (2001) Use of phyllotaxis to predict arrangement and size of branches in Pinus radiata. New Zeal J For Sci 31:247–262.

Prentice RL (1974) A log gamma model and its maximum likelihood estimation. Biometrika 61:539–544.

Pretzsch H (2005) Diversity and productivity in forests: evidence from long-term experimental plots. For. Divers. Funct. Springer, pp 41–64

R Development Core Team (2012) R: A Language and Environment for Statistical Computing. R Found. Stat. Comput. Vienna, Austria

De Reffye P, Fourcaud T, Blaise F, et al. (1997) A functional model of tree growth and tree architecture. Silva Fenn 31:297–311.

De Reffye P, Houllier F, Blaise F, et al. (1995) A model simulating above-and below-ground tree architecture with agroforestry applications. Agrofor Syst 30:175–197.

Richards DB, Adkins WK, Hallock H, Bulgrin EH (1979) Simulation of hardwood log sawing. USDA For.Serv. Res. Pap. FPL 355. For. Prod. Lab. Madison; Madison; Wis. USA

Rouvinen S, Kuuluvainen T (1997) Structure and asymmetry of tree crowns in relation to local competition in a natural mature Scots pine forest. Can J For Res 27:890–902.

Sabatier S, Barthelemy D (1999) Growth dynamics and morphology of annual shoots, according to their architectural position, in young Cedrus atlantica (Endl.) Manetti ex Carriere (Pinaceae). Ann Bot 84:387–392. doi: 10.1006/anbo.1999.0939

Samson M (1993a) Modeling of knots in logs. Wood Sci Technol 27:429–437.

Samson M (1993b) Method for assessing the effect of knots in the conversion of logs into structural lumber. Wood Fiber Sci 25:298–304.

Samson M, Bindzi I, Kamoso LM (1996) Mathematical representation of knots in tree trunks. Can J For Res 26:159–165.

Schajer GS, An Y (2012) Improvements in Low-Cost Log Scanning using X-Rays. In: ForValueNet Res. note. http://www.forvaluenet-foretvaleur.ca/spaw2/uploads/files/11 - Improvements in Low-Cost Log Scanning using X-Rays.pdf.

Sharma M, Zhang SY (2004) Variable-exponent taper equations for jack pine, black spruce, and balsam fir in eastern Canada. For Ecol Manage 198:39–53.

Shi JL, Zhang SY, Riedl B (2005) Effect of juvenile wood on strength properties and dimensional stability of black spruce medium-density fiberboard panels. Holzforschung 59:1–9.

Shigo AL (1986) A new tree biology. Shigo and Trees Assoc, Durham, NH.

Steele PH, Harless TEG, Wagner FG, et al. (1994) Increased lumber value from optimum orientation of internal defects with respect to sawing pattern in hardwood sawlogs. For Prod J 44:69–72.

Sumida A, Terazawa I, Togashi A, Komiyama A (2002) Spatial arrangement of branches in relation to slope and neighbourhood competition. Ann Bot 89:301–310.

Team RC (2013) R: A Language and Environment for Statistical Computing. R Found. Stat. Comput. Vienna, Austria

Thomas E, Thomas L, Mili L, et al. (2003) Primary detection of hardwood log defects using laser surface scanning. Citeseer, pp 39–49

Tong Q, Duchesne I, Belley D, et al. (2013) Characterization of Knots in Plantation White Spruce. Wood Fiber Sci 45:84–97.

Trincado G, Burkhart HE (2008) A model of knots shape and volume in Loblolly Pine trees. Wood Fiber Sci 40:634–646.

Tustin J, Wilcox M (1978) The relative importance of branch size and wood density to the quality of Douglas fir framing timber. A Rev Douglas fir New Zealand, 16-19 Sept 1974 267.

Väisänen H, Kellomäki S, Oker-Blom P, Valtonen E (1989) Structural development of Pinus sylvestris stands with varying initial density: a preliminary model for quality of sawn timber as affected by silvicultural measures. Scand J For Res 4:223–238.

Vestol GI, Hoibo OA (2000) Internal distribution of sound and dead knots in Picea abies (L.) Karst. Holz Als Roh-Und Werkst 58:107–114.

Wagner FG, Taylor FW, Ladd DS, et al. (1989) Ultrafast CT scanning of an Oak log for internal defects. For Prod J 39:62–64.

Weiskittel AR, Maguire DA, Monserud RA (2007) Response of branch growth and mortality to silvicultural treatments in coastal Douglas-fir plantations: Implications for predicting tree growth. For Ecol Manage 251:182–194.

Wilson BF, Archer RR (1979) Tree design: some biological solutions to mechanical problems. Bioscience 29:293–298.

Xu M, Harrington TB (1998) Foliage biomass distribution of loblolly pine as affected by tree dominance, crown size, and stand characteristics. Can J For Res 28:887–892.

Yamamoto H, Yoshida M, Okuyama T (2002) Growth stress controls negative gravitropism in woody plant stems. Planta 216:280–292.

Zeide B (1993) Analysis of growth equations. For Sci 39:594–616.

Zhang C, Cheng FF, Miura KT (1998) A method for determining knots in parametric curve interpolation. Comput Aided Geom Des 15:399–416.

Zhang SY, Chauret G (2001) Impact of initial spacing on tree and wood characteristics, product quality and value recovery in black spruce (Picea mariana). Proj. Report, Forintek Canada Corp., Sainte-Foy, 47p

Zhang SY, Chauret G, Swift DE, Duchesne I (2006) Effects of precommercial thinning on tree growth and lumber quality in a jack pine stand in New Brunswick, Canada. Can J For Res 36:945–952.

Zhang SY, Que-Ju T (2005) Modeling lumber recovery in relation to selected tree characteristics in jack pine using sawing simulator Optitek. Ann For Sci 62:219–228.

Zimmerman MH, Brown CL (1971) Trees: structure and function. Springer Verlag, New-York

Zink-Sharp A (2003) Mechanical Properties of Wood. Wood Qual. Its Biol. Basis. Blackwell Publishing, Oxfordshire, UK, pp 197–209

Zobel BJ, Van Buijtenen JP (1989) Wood variation: its causes and control. Springer

Zobel BJ, Sprague JR (1998) Juvenile wood in forest trees. Springer

Annexe: Improving branch distribution models in trees using X-ray computed tomography

Emmanuel Duchateau[1]*, David Auty[1], Frédéric Mothe[2] and Alexis Achim[1]

[1] Faculté de foresterie, géographie et géomatiques, Université Laval, 2405 rue de la Terrasse, Québec G1V 0A6, QC, Canada
[2] INRA, UMR1092 LERFoB, 54280 Champenoux, France
*correspondence: emmanuel.duchateau.1@ulaval.ca

Highlights: The use of external measurements to describe the distribution of branches on tree stems can induce imprecision and bias in estimates of both the number of annual growth units and the azimuthal distribution of branches. The scanning of logs using X-ray computed tomography yielded knot data that enabled more accurate identification of the limits of each growth unit. Such information, in conjunction with current models of tree architecture, can be incorporated into functional-structural models describing relationships between tree morphology and biological processes.

Keywords: X-ray computed tomography, tree architecture, black spruce, branch distribution

Introduction

Computer-based systems capable of simulating the 3D structure of plants, their metabolic processes and environmental interactions are increasingly being developed to increase our understanding of how plant architecture and biological processes interact (Fourcaud et al. 2008). In trees, such functional-structural models can be useful tools for understanding and predicting important wood quality attributes such as branch morphology and distribution. An underlying principle of these models is that plant structure can be described in terms of a hierarchical system of replicating 'architectural units' (Barthélémy et al. 1989). In temperate tree species, the 'growth unit' (GU) i.e. the annual elongation of the terminal shoot from the apical meristem (De Reffye et al. 1995), is the single most important component of existing branch distribution models (e.g. Colin and Houllier 1991). Such models are normally parameterized using data from external measurements. This has the

advantage that data collection is relatively straightforward and can be accomplished with limited equipment. However, this simplicity may come at the expense of accuracy for certain measurements, such as branch inclination and azimuthal orientation. More recently, X-ray computed tomography techniques have been developed that can generate high-precision internal information, which could lead to improved model accuracy. Black spruce (*Picea mariana (Mill.) BSP*) is the dominant conifer in the North American boreal forest. It develops according to Rauh's model of monopodial, rhythmic growth and attains its final developmental stage after 10-15 years (Bégin and Filion 1999). After this, the basic structure of first and second order axes (trunk and branches, respectively) and third and fourth order axes (twigs) is duplicated through a process known as reiteration. The high reiterative capacity of black spruce accounts for its characteristically high phenotypic plasticity. This leads to a complex and apparently disorganised branching structure that complicates the development of functional-structural models, since the precise delineation of annual growth units can be difficult. The objectives of this study were: 1) to develop a method based on selective filters to locate annual growth units on black spruce logs using data derived from X-ray computed tomography and 2) to examine the distribution of branches around black spruce stems at the stem and growth unit levels.

Materials and methods

Measurements were taken on 33 black spruce trees from unmanaged stands in Québec, Canada. First, branch and tree characteristics were recorded following the protocol established by Colin and Houllier (1991). Sample trees were then cut into successive 2.5 m logs for X-ray scanning. Each of the resulting 107 logs were scanned at 2 mm intervals along the longitudinal axis with a 2-mm-wide X-ray beam, so that the scanned segments were contiguous. This provided accurate internal profiles for 23,040 knots (Duchateau et al. 2013c). The total number of growth units in each 2.5-m section was determined from the difference in the number of annual growth rings between discs cut from each end of the log. However, the precise limits of each annual shoot were difficult to determine, even using the X-ray data (Figure A-4). We developed an empirical method based on two filters to select the most likely location of the limits of each GU, which should correspond to the location of nodal branches produced from subterminal buds. First, the basal area of each

branch (i.e. cross-sectional surface at the bark) was calculated and summed when branches originated from the same point at the stem's pith. We then applied a series of thresholds to select basal area peaks along the main stem. Secondly, we tested thresholds of minimum GU lengths, as some of the identified peaks occurred in close proximity, presumably as a result of reiteration (Bégin and Filion 1999). Once each GU was located, we analyzed the circular branch distribution at the scale of both the tree and the growth unit. This was carried out using circular statistics and a Rayleigh test (Jammalamadaka and Sengupta 2001).

Results and Discussion

The number of GUs along the stem was significantly underestimated when only external branch measurements were used. On average, the underestimation was 2.4 GUs per 2.5-m log (SD=3.7), or around 15% of the total. For a mature tree, this would represent approximately 16 GUs, which is unsatisfactory for the development of accurate models. One possible explanation is that black spruce contains a relatively large number of branches along each growth unit, but the diameter ranges of nodal (terminal) and internodal (median) branches overlap, so the delineation of GUs based on branch basal area might be problematic.

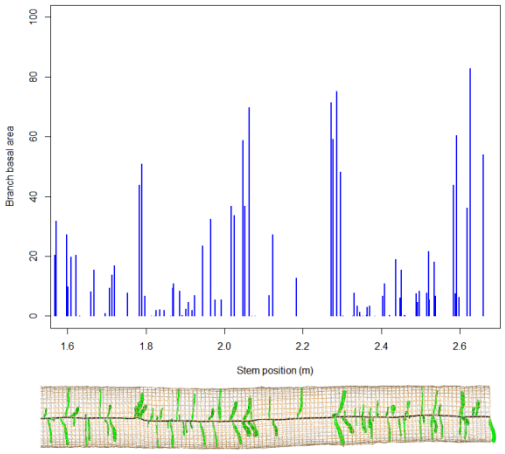

Figure A-4 Distribution of branch basal area along the stem from data extracted using the ImageJ Java plug-in 'Gourmand'.

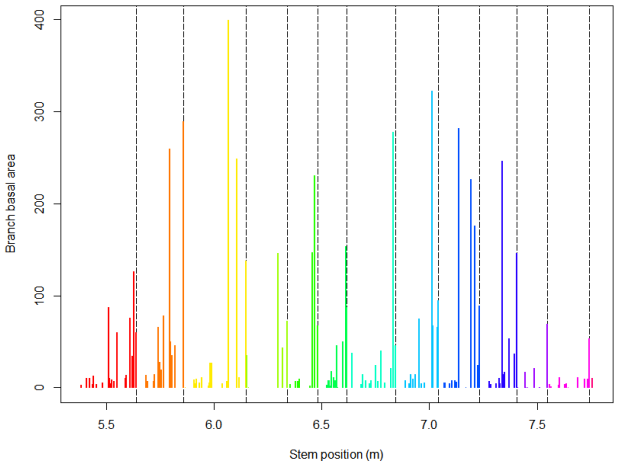

Figure A-5 Distribution of the branch basal areas along the stem and delineation of the separate growth units using our two-filter method.

For the identification of GUs using internal data, best results were obtained when 1) a GU limit was placed when the sum of branch basal areas initiating from the same point was above the 75th percentile for all branch initiation points within the log and 2) the next limit was located at a minimum distance of 7.5 cm along the main stem (Figure A-5). The utilization of the CT images coupled with this two-step method allowed us to significantly increase the accuracy of GU identification. The resulting mean bias in the number of GUs per log approached 0 (0.195). This represented a significant improvement compared to external assessment, although some variation remained (SD=2.8). The ability to identify branch initiation points at the pith of the main stem therefore allowed us to differentiate between nodal and internodal branches more accurately.

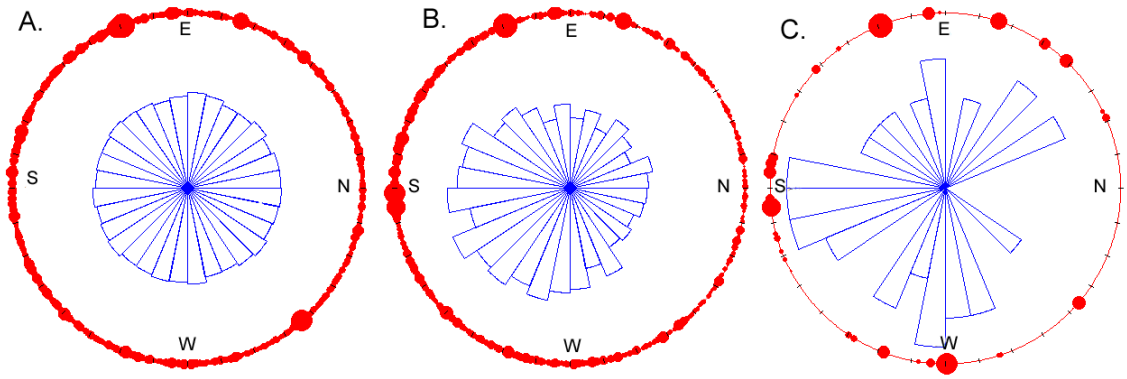

Figure A-6 Distribution of branches around the stem by diameter (in red) and by number (in blue) for **A)** all branches, **B)** the largest diameter branch per GU and **C)** the largest diameter branch per tree.

Once we had obtained the best GU selection, we studied the circular distribution of the branches at the tree and the GU levels. For all branches on one tree, the distribution was uniform (Figure A-6A). However, the largest branch per GU had a preferential orientation of 194° (SD = 65°) and the distribution was non-uniform for 18 out of 33 sample trees (Figure A-6B). The largest diameter branch in each tree had a similar mean orientation of 200° (Figure A-6C). Future work will focus on 1) the influence of inter-tree competition on branch distribution around the stem, 2) testing the applicability of the two-filter method to

other species and growing conditions, and 3) increasing data processing speed using automated knot detection and measurement algorithms (Longuetaud et al. 2012).